Novel insights into mitochondrial phospholipid homeostasis in a disease-relevant yeast model

Dissertation

der Mathematisch-Naturwissenschaftlichen Fakultät
der Eberhard Karls Universität Tübingen
zur Erlangung des Grades eines
Doktors der Naturwissenschaften
(Dr. rer. nat.)

vorgelegt von
Diana Sofia Ribeiro Duarte Antunes
aus Tomar, Portugal

Tübingen
2019

Gedruckt mit Genehmigung der Mathematisch-Naturwissenschaftlichen Fakultät
der Eberhard Karls Universität Tübingen.

Tag der mündlichen Qualifikation:	04/02/2019
Dekan:	Prof. Dr. Wolfgang Rosenstiel
1. Berichterstatter:	Prof. Dr. Doron Rapaport
2. Berichterstatter:	Prof. Dr. Gabriele Dodt

Erklärung

Ich erkläre, dass ich die zur Promotion eingereichte Arbeit mit dem Titel:

„Novel insights into mitochondrial phospholipid homeostasis in a disease-relevant yeast model“
selbstständig verfasst, nur die angegebenen Quellen und Hilfsmittel benutzt und wörtlich oder inhaltlich übernommene Stellen als solche gekennzeichnet habe. Ich erkläre, dass die Richtlinien zur Sicherung guter wissenschaftlicher Praxis der Universität Tübingen beachten wurden. Ich versichere, dass die falsche Abgabe einer Versicherung an Eides statt mit Freiheitsstrafe bis zur drei Jahren oder mit Geldstrafe bestraft wird.

Declaration

I hereby declare that I have produced the work entitled:
„Novel insights into mitochondrial phospholipid homeostasis in a disease relevant-yeast model“
Submitted for the award of a doctorate, on my own (without external help), have used only the sources and aids indicated and have marked passages included from other works, whether verbatim or in content, as such. I swear upon oath that these statements are true and that I have not concealed anything. I am aware that making a false declaration under oath is punishable by a term of imprisonment of up to three years or by a fine.

Tübingen, den 07.01.2019 .....

Contents

1. List of abbreviations

ADCK	AarF domain containing kinase
ATP	adenosine triphosphate
BCAA	branched-chain amino acid
BCAT	branched-chain amino acid transaminase
BN-PAGE	blue native polyacrylamide gel electrophoresis
BTHS	Barth syndrome
CL	cardiolipin
CoQ	coenzyme Q
DNA	deoxyribonucleic acid
EMC	ER membrane protein complex
ER	endoplasmic reticulum
ERMES	ER-mitochondria encounter structure
GFP	green fluorescent protein
HA	hemagglutinin
LC-MS	liquid chromatography coupled with mass spectrometry
IMS	intermembrane space
MAM	mitochondria-associated membrane
Mcp	mdm10 complementing protein
MCS	mitochondria contact site
MDM	mitochondrial distribution and morphology
MEF	mouse embryonic fibroblasts
MFN2	mitochondrial protein mitofusin 2
MIM	mitochondrial inner membrane
MLCL	monolyso-CL
MOM	mitochondrial outer membrane
MS	mass spectrometry
mtDNA	mitochondrial DNA
NVJ	nuclear vacuolar junctions
OXPHOS	oxidative phosphorylation
PA	phosphatidic acid
PC	phosphatidylcholine
PE	phosphatidylethanolamine

PG	phosphatidylglycerol
PI	phosphatidylinositol
PK	proteinase K
PLs	phospholipids
PS	phosphatidylserine
PVDF	polyvinylidene fluoride
ROS	reactive oxygen species
SDS-PAGE	sodium dodecyl sulfate polyacrylamide gel electrophoresis
TCA	tricarboxylic acid
TLC	thin-layer-chromatography
vCLAMP	vacuole and mitochondria patch
$\Delta\Psi$	membrane potential
WT	wild-type

2. Summary

The proper function of mitochondria critically depends on their membrane lipid composition. To ensure lipid homeostasis, *de novo* synthesis, intracellular and intraorganellar transport, remodeling, and degradation of lipids must be tightly regulated.

Several studies have emphasised the importance of the mitochondrial signature phospholipid, cardiolipin (CL) for the organelle function. The acquisition of mature CL species is catalyzed by the phospholipid acyltransferase, *Tafazzin*. The importance of CL remodeling is underscored by the fact that mutations in *Tafazzin* lead to a life-threatening genetic disorder, Barth syndrome (BTHS). Currently, the biochemical processes underlying this clinical disorder remain unclear. Deletion of the yeast homologue Taz1 results in similar phenotypes to those observed in patients suffering from BTHS, making this organism an optimal model system to study the pathomechanism of the disease. To shed light on the pathomechanism of BTHS, I searched for yeast multi-copy suppressors of the *taz1Δ* growth defect and identified the branched-chain amino acid transaminases (BCATs) *BAT1* and *BAT2* as such suppressors. Similarly, overexpression of the mitochondrial isoform BCAT2 in mammalian cells lacking *TAZ* improves their growth. Accordingly, supplying both yeast and mammalian cells lacking Tafazzin function with certain amino acids restored their growth behavior. Although elevated levels of Bat1 or Bat2 did not restore all the mitochondrial defects of BTHS, it could correct the higher respiration rate observed in *taz1Δ* cells. These findings outline that the metabolism of amino acids can influence the BTHS phenotype and has an important and disease relevant role in cells lacking Taffazzin function.

In another project, I investigated the transfer of lipids between mitochondria and vacuoles. The absence of documented mitochondrial vesicular lipid exchange suggests that membrane contact sites (MCSs) facilitate lipids transport between mitochondria and other cellular membranes. Recently, it has been demonstrated that the lack of one contact site leads to the expansion of an alternative one. Specifically, loss of the ER-mitochondria encounter structure (ERMES) can be bypassed by point mutations in the vacuolar protein Vps13, or

by overexpression of the mitochondrial Mdm10 complementing protein 1 (Mcp1). However, the mechanism by which this bypass support lipid homeostasis has remained unclear. In this work, I analyzed the membrane topology of Mcp1. My findings revealed that Mcp1 functions as a recruiter of Vps13 to mitochondria and promotes formation of vacuole-mitochondria MCS. I demonstrated that the N-terminal region of Mcp1 is exposed to the cytosol and mediates the recruitment of Vps13, thus establishing a functional mitochondria-vacuole MCS that compensate for the loss of ERMES.

Finally, in a third project of my doctoral studies I investigated the relationship between the ERMES complex and the coenzyme Q6 (CoQ6) biosynthesis system. I observed that supplementation of yeast cells lacking functional ERMES with CoQ6 could rescue the growth retardation and the altered mitochondrial morphology of these mutated cells. Based on additional results from collaborating groups, we suggest that the ERMES complex coordinates coenzyme Q biosynthesis.

3. List of publications contained in this thesis

a) Accepted papers

1. A. T., Peter, B. Herrmann, D. Antunes, D. Rapaport, K. S. Dimmer, and B. Kornmann. (2017). 'Vps13-Mcp1 interact at vacuole-mitochondria interfaces and bypass ER-mitochondria contact sites', *Journal of Cell Biology*, 216: 3219-29. DOI: 10.1083/jcb.201610055.

2. D. Antunes, A. Chowdhury, A. Aich, S. Saladi, N. Harpaz, M. Stahl, M. Schuldiner, J. Herrmann, P. Rehling, and D. Rapaport, (2018). 'Overexpression of branched-chain amino acid aminotransferases rescues the growth defects of cells lacking the Barth Syndrome related gene *TAZ1'*. *Journal of Molecular Medicine*, DOI: 10.1007/s00109-018-1728-4. (*in press)*

b) Manuscripts in revision

3. M. Eisenberg-Bord*, H. Tsui*, D. Antunes*, L. Fernández-del-Río*, C. Dunn, D. Rapaport, C. Clarke, and M. Schuldiner. (2018). 'ER-Mitochondria Encounter Structure (ERMES) coordinates coenzyme Q biosynthesis'. *Contact*. (*in revision*)
   * equal contributors.

4. Personal contribution

1. **A. T., Peter, B. Herrmann, D. Antunes, D. Rapaport, K. S. Dimmer, and B. Kornmann. (2017). 'Vps13-Mcp1 interact at vacuole-mitochondria interfaces and bypass ER-mitochondria contact sites', *Journal of Cell Biology*, 216: 3219-29. DOI: 10.1083/jcb.201610055**

I isolated mitochondria from *mcp1*Δ + pYX142-Mcp1 and *mcp1*Δ + pYX142-Mcp1-HA cells and analyzed the topology of Mcp1 via proteinase K assay (Fig. 3B). Moreover, I designed and analyzed four single point mutant variants of Mcp1 (Fig. 4E and F). I contributed to the writing of the manuscript and prepared the figures describing my experiments.

2. **D. Antunes, A. Chowdhury, A. Aich, S. Saladi, N. Harpaz, M. Stahl, M. Schuldiner, J. Herrmann, P. Rehling, and D. Rapaport, (2018). 'Overexpression of branched-chain amino acid aminotransferases rescues the growth defects of cells lacking the Barth Syndrome related gene *TAZ1'*. *Journal of Molecular Medicine*, DOI: 10.1007/s00109-018-1728-4. (*in press)***

I performed the multi-copy suppressors screen in *taz1*Δ cells and analyzed how the suppressors influenced *taz1*Δ, *gep4*Δ and *crd1*Δ cells growth in various conditions (Fig. 1A-E and Fig. S1). I investigated whether such suppressors rescue the mitochondrial defects of mitochondria lacking *TAZ1* (Fig. 2A-E). Next, I analyzed the growth and the lipid composition of *taz1*Δ cells by supplementing media with various metabolites (Fig. 3A-F, Fig. S3 and Fig. S4). Finally, I grew and collected the cells pellets to test the metabolic profile of *taz1*Δ cells (Fig. 4). I wrote the manuscript and prepared all the figures.

3. M. Eisenberg-Bord*, H. Tsui*, D. Antunes*, L. Fernández-del-Río*, C. Dunn, D. Rapaport, C. Clarke, and M. Schuldiner. (2018). 'ER-Mitochondria Encounter Structure (ERMES) coordinates coenzyme Q biosynthesis '. *Contact*, *in revision.* *, equal contributors.

I isolated mitochondria and performed blue-native (BN)-PAGE analysis in *mdm10*Δ cells (data to be included in the resubmitted manuscript). I contributed to the design of various experiments and to the writing of the manuscript. I prepared the figures presenting my experiments.

5. Introduction

5.1 Origin, structure, and function of mitochondria

Mitochondria are essential organelles of most eukaryotic cells. They evolved from a subgroup of aerobic bacteria that were incorporated by an anaerobic ancestor over 1.5 billion years ago, the so-called endosymbiotic event (Gray, 2012). Like Gram-negative bacteria, mitochondria are enclosed by two membranes that divide the organelle into four subcompartments. The mitochondrial outer membrane (MOM) separates the organelle from the surrounding cytosol, while the mitochondrial inner membrane (MIM) separates the intermembrane space (IMS) from the innermost subcompartment, the matrix. Each mitochondrial subcompartment contains a specific group of proteins with specialized functions. The MOM contains several proteins that play roles in mitochondrial fusion, fission, biogenesis, inheritance, and morphology. The MIM contains a high amount of proteins which are mostly subunits of the respiratory chain complexes or carrier proteins involved in metabolites transport across the membrane (Gutman et al., 1993; Kühlbrandt, 2015). The vast majority of mitochondrial proteins (>99%) are nuclear-encoded and are synthesized as precursors on cytosolic ribosomes before their import and assembly into mitochondria. A small number of proteins (8 in yeast and 13 in humans) are encoded by the mitochondrial genome (Neupert and Herrmann, 2007; Sickmann et al., 2003). These group of proteins, which are subunits of the respiratory chain complexes, are inserted into the MIM in a process mediated by Oxa1, a conserved membrane protein (Krüger et al., 2012; Stiller et al., 2016).

Mitochondria are highly dynamic organelles that form a branched and tubular network. This morphology is regulated by fusion and fission processes which ascertain mitochondrial DNA (mtDNA) stability and the bioenergetics function of the organelle (Hoffmann and Avers, 1973; Okamoto and Shaw, 2005; Westermann, 2010).

Mitochondria fulfil crucial roles in cellular bioenergetics, apoptosis, and metabolism of amino acids, lipids, and heme. One of the main metabolic pathways that takes place inside the organelle is the tricarboxylic acid (TCA) cycle, which provides reducing equivalents to the respiratory chain complexes

through the oxidation of acetyl-CoA (Lill et al., 1999; Scheffler, 2001). Furthermore, mitochondria are also involved in cellular signalling and aging (Bratic and Larsson, 2013; Hockenbery et al., 1990; Pizzo and Pozzan, 2007).

Taken together, all these important functions explain why mitochondrial dysfunctions can result in a variety of pathologic scenarios and have been implicated in many disorders such as diabetes mellitus, carcinogenesis, and neurodegenerative diseases (Antunes et al., 2014; Beal, 2005; Enns, 2003).

5.2 Homeostasis of mitochondrial lipids

To properly carry out all their functions, mitochondria have to maintain their own unique protein and lipid composition. Although phospholipids (PLs) comprise the most abundant lipid class of mitochondrial membranes, sphingolipids and sterols can also be found within these structures. Phosphatidylcholine (PC), phosphatidylethanolamine (PE), phosphatidylinositol (PI) and CL constitute the most abundant PLs in yeast mitochondria (Horvath and Daum, 2013; Zinser et al., 1991).

Given the nearly absent variation in the mitochondrial PL composition among different organisms or cells type, alterations in PL content have been linked to several pathological disorders such as heart failure, neurodegenerative diseases, atherosclerosis, and Barth syndrome (Chicco and Sparagna, 2007; Fruhwirth et al., 2007; Schlame and Ren, 2006). The maintenance of appropriate lipid composition relies on the capability of mitochondria to autonomously synthesize some phospholipids like CL, PE and phosphatidylglycerol (PG) from their precursors. However, other lipids, such as phosphatidic acid (PA), PI, phosphatidylserine (PS), and PC, are synthesized in other organelles, specifically in the endoplasmic reticulum (ER), from where they have to be transported to mitochondria (Daum and Vance, 1997; Horvath and Daum, 2013) (**Figure T1**).

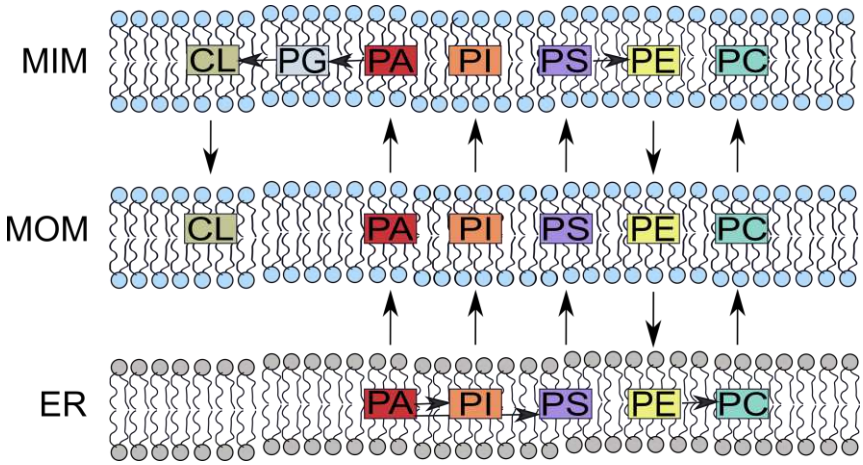

Figure T1: Phospholipid synthesis and lipid transport between ER and mitochondria. PA serves as universal phospholipid precursor, which is synthesized in the ER. Therefore, it has to be transported to mitochondria where it is required for the synthesis of PG and CL. PI and PS are also primarily made from PA but in the ER. Newly synthesized PS is transported from the ER to mitochondria and subsequently decarboxylated to PE. The latter has to be exported from mitochondria to allow its conversion to PC in the ER.

Among the mitochondrial lipids, CL constitutes the signature dimeric PL of this organelle. It exhibits a specific fatty acid composition compared to other PLs, since it predominantly harbours unsaturated fatty acyl chains (Schlame et al., 2000). Hence, in contrast to other PLs, newly synthesized CL must undergo acyl chain remodeling which replaces the pre-existing fatty acids with new ones that are organism and tissue specific (Schlame et al., 2005). This maturation is crucial for mitochondrial functionality. Indeed, defective CL remodeling is associated with a number of clinical disorders including BTHS, a rare X-linked disease characterized by skeletal myopathy, cardiomyopathy, and, in some cases, neutropenia (Barth et al., 1999).

5.2.1 ERMES complex

As previously described, PL biosynthesis in yeast is mainly taking place in the ER and mitochondria. Since the latter are not involved in vesicular lipid exchange, the transfer of lipids between mitochondria and other cellular compartments is promoted by close contacts of the membranes and via protein complexes that form bridges between the organelles involved (Kornmann et al., 2009; Tamura et al., 2014). Of note, already more than 20 years ago, lipid synthesizing enzymes were detected in mitochondria-associated membranes (MAMs) of the ER, implying a close connection of lipid synthesis and transport between the two organelles (Dimmer and Rapaport, 2017; Vance, 1990; Voelker, 1990).

In the baker's yeast *Saccharomyces cerevisiae,* a tether termed ERMES was identified as a protein complex that participates in lipid transport at contact sites between ER and mitochondria (Kornmann et al., 2009). ERMES, whose orthologues have been identified only in fungi, is composed of four subunits: two mitochondrial subunits (Mdm10 and Mdm34) embedded in the MOM, a subunit (Mmm1) anchored to the ER membrane and a soluble subunit (Mdm12). Loss of individual components of the ERMES complex results in reduced mitochondrial levels of PE and CL, suggesting the crucial role of this complex in PL exchange between ER and mitochondria (Kornmann et al., 2009; Osman et al., 2009).

Interestingly, subunits of ERMES were first identified due to their effect on mitochondrial morphology. Furthermore, ERMES loss triggers many other phenotypes such as a disturbed mitochondrial inheritance and an increased tendency to lose the mtDNA (Kornmann et al., 2009; Murley et al., 2013; Okamoto and Shaw, 2005). In addition, protein assembly in the MOM, mitophagy, and respiratory chain complexes assembly are impaired in the absence of ERMES (Klecker et al., 2014; Tan et al., 2013).

Despite the pivotal role in mitochondrial biogenesis, cells lacking functional ERMES are still viable and certain trafficking of lipids to and from mitochondria yet occurs (Kornmann et al., 2009; Nguyen et al., 2012; Voss et al., 2012). This implies the existence of alternative pathways for lipid exchange of mitochondria with either the ER or other organelles. Although the most prominent function of

the ERMES complex is its involvement in lipid homeostasis, there are still many open questions regarding its function to be addressed. Specifically, it is unclear whether other molecules are being transported via this ER- mitochondria contacts, and if additional proteins play a role in that interplay.

5.2.2 ERMES-alternative pathways

Recent studies have identified alternative tether complexes involved in lipid transport between mitochondria and other cellular organelles. The ER membrane protein complex (EMC) was identified as a second ER-mitochondria tether structure that is involved in the transport of PS from the ER to mitochondria (Lahiri et al., 2014). In addition, the vacuole and mitochondria patches (vCLAMPs) form contact sites between the mitochondria and the vacuole, mediated by the vacuolar factor Vps39. Interestingly, the simultaneous loss of ERMES and vCLAMPs is lethal in yeast cells, suggesting that the pathways are redundant. It was also shown that contact sites are highly dynamic and that the elimination of one leads to the expansion of the other (Elbaz-Alon et al., 2014; Honscher et al., 2014).

Although the ERMES complex is involved in numerous mitochondrial functions, the existence of ERMES-independent pathways for interorganellar lipid exchange implies the existence of additional players in this context. To obtain further insight into these pathways, a multi-copy suppressor screen of the growth phenotype resulting from the deletion of the ERMES subunit Mdm10 was employed. Three mitochondrial proteins, named Mcp1-3 have been identified (Sinzel et al., 2016; Tan et al., 2013). Despite the fact that all three proteins restore defects resulting from loss of ERMES, there is no physical interaction of Mcp1, Mcp2 or Mcp3 with any component of the ERMES complex. This is likely due to the involvement of these proteins in a pathway independent of the ERMES complex.

In a recent work, to which I contributed, a physical interaction between Mcp1 and the vacuolar protein Vps13 was reported (John Peter et al., 2017). Vps13 was previously described to contribute to a bypass pathway of ERMES function via its activity at vCLAMPs (Lang et al., 2015; Park et al., 2016). The

recent finding suggests that Mcp1 and Vps13 could cooperate in recruitment of lipid transport proteins serving as effectors of vCLAMPs. In this model, Mcp1 would be required to recruit Vps13 to the proximity of mitochondria, through expansion of contact sites between mitochondria and the vacuole, which are mediated by Vps39 and the vacuolar Rab GTPase Ypt7 (Elbaz-Alon et al., 2014; John Peter et al., 2017). Although Mcp1 has no orthologues in higher eukaryotes, its sequence harbours four conserved residues that are typical for an uncharacterized protein family (PF07950 family) of succinate dehydrogenases in Gram-positive bacteria. Mutations of these residues greatly decreased the activity of Mcp1 in the ERMES-bypass pathway albeit they did not totally abolish it (John Peter et al., 2017).

In contrast to Mcp1, Mcp2 has homologues in higher eukaryotes, the human ADCK1 or ADCK5, predicted kinases of the so-called AarF domain-containing kinases (ADCKs) family, with unknown function. Another member of the family, ADCK3 plays a role in coenzyme Q biosynthesis (Xie et al., 2011). To date, there is no evidence for the involvement of Mcp3 in lipid metabolism. Interestingly, there is a conserved glycine motif between Mcp3 and the mammalian mitochondrial outer membrane receptor for hypoxia-induced mitophagy FUNDC1 (Liu et al., 2012). The mammalian protein was reported to be enriched at the MAM where it promotes mitochondrial fission in a DRP1-dependent manner (Wu et al., 2016). Considering the impaired mitophagy of yeast cells lacking ERMES (Bockler and Westermann, 2014), one might speculate that Mcp3 can play a role in mitophagy.

Taken together, the molecular functions of Mcp1, Mcp2 and Mcp3 are currently unknown. The recent observations favour the hypothesis that Mcp1 acts in the same pathway together with Vps13 i.e. in tethering vacuole and mitochondria. The identification of additional pathways that can bypass ERMES might provide a more detailed understanding of the mechanism of interorganellar lipid transport in higher eukaryotes (van Meer et al., 2008).

5.3 Mitochondrial respiration and oxidative phosphorylation

Through the process of OXPHOS in the MIM, mitochondria are the main producers of ATP in eukaryotic cells. This process is facilitated by the electron flow between the respiratory chain complexes. This in turn is coupled to the generation of a proton gradient across the MIM, which ultimately leads to ATP production. The OXPHOS system is powered by reducing equivalents in the form of NADH or $FADH_2$, which are generated in different metabolic pathways such as glycolysis, fatty acid oxidation or the TCA cycle. The respiratory chain is organized in five multi-subunit enzyme complexes termed NADH dehydrogenase (complex I), succinate dehydrogenase (complex II), cytochrome C reductase (complex III), cytochrome C oxidase (complex IV) and F_1F_0-ATP synthase (complex V) (Boekema and Braun, 2007).

Complex I catalyses the oxidation of NADH to NAD^+, transfers the liberated electrons to coenzyme Q (also known as ubiquinone), and releases four protons into the IMS. In yeast, a complex formed by Nde1, Nde2, and Ndi1 substitutes for complex I. In this system, electrons are transferred from NADH to CoQ but without the transport of protons into the IMS (Matus-Ortega et al., 2015). Complex II catalyses the oxidation of succinate to fumarate in the TCA cycle. The resulting electrons are passed to CoQ, which acts as an electron carrier, mediating electron transfer to complex III. While oxidizing CoQ and in turn reducing cytochrome C, complex III releases four protons into the IMS. Complex IV is the last protein of the mitochondrial electron transport chain. This complex accepts electrons from cytochrome C and pumps four additional protons into the IMS. Finally, complex IV forms water from reduced oxygen molecules. The combined transfer of protons by the various respiratory chain complexes to the IMS generates an electrochemical gradient across the MIM. Ultimately, the proton gradient is used by complex V to produce ATP (Boekema and Braun, 2007; Kühlbrandt, 2015).

5.3.1 Coenzyme Q biosynthesis

CoQ is an essential lipid that plays a vital role in mitochondrial respiratory electron transfer and is also known as an antioxidant molecule (Genova and Lenaz, 2011). In *S. cerevisiae,* CoQ biosynthesis takes place on the matrix side of the MIM and yeast mutants lacking CoQ display a growth defect on non-fermentable carbon sources due to the respiration deficit (Awad et al., 2018; Bentinger et al., 2010). CoQ biosynthesis is mediated in yeast by the so-called CoQ synthome (or Complex Q in higher eukaryotes), which is a multisubunit complex that produces several Coq intermediates and CoQ itself (Coq3-Coq9 and Coq11) (Allan et al., 2015; Marbois et al., 2009). Studies in the last years, using human homologues of yeast proteins have started to disclose details of the CoQ biosynthesis pathway (Allan et al., 2015; He et al., 2015; Marbois et al., 2010). In yeast, the CoQ_6 precursors are derived from the isoprene biosynthetic pathway at the ER (Tran and Clarke, 2007).

Considering the known potential of contact sites to transfer molecules and metabolites between organelles (Eisenberg-Bord et al., 2016), it is tempting to postulate an additional role of ER-mitochondria contact sites in promoting the transport of CoQ6 and its intermediates or precursors between the two organelles. Indeed, it has been shown that loss of the mammalian mitochondrial protein mitofusin 2 (*MFN2*), which was reported to mediate ER-mitochondria contacts (de Brito and Scorrano, 2008; Merkwirth and Langer, 2008), results in impaired mitochondrial respiration due to decreased CoQ levels (Mourier et al., 2015). Furthermore, recent observations point to a possible role of ERMES in biosynthesis of CoQ. A human homologue of the *mdm10*Δ suppressor Mcp2 is ADCK3. This protein in turn belongs to the ADCK family, which also comprises COQ8A, an ATPase that facilitates both the assembly of the CoQ synthome and *de novo* biosynthesis of CoQ (Reidenbach et al., 2018).

5.4 Cardiolipin (CL) is required for many mitochondrial functions

In order to increase the efficiency of the electron transport, the mitochondrial respiratory complexes are stably interacting with each other and together form the so-called supercomplexes. The lipid composition of the MIM has an impact on the OXPHOS efficiency since it can affect supercomplexes assembly. It has been reported that CL is tightly associated with mitochondrial respiratory chain complexes and that its presence is required for efficient mitochondrial bioenergetics (Lange et al., 2001; Schlame et al., 2000; Zhang et al., 2002). Indeed, yeast cells lacking CL have impaired respiratory growth and decreased complex III and complex IV activities. These phenotypes cannot be complemented by any other PL or non-remodeled CL species (Baile et al., 2014; Hoffmann et al., 1994; Jiang et al., 2000; Pfeiffer et al., 2003).

In addition to its key role in maintenance of mitochondrial OXPHOS, CL has also been implicated in the biogenesis of MOM proteins (Gebert et al., 2009; Sauerwald et al., 2015). Moreover, CL supports the molecular architecture and fluidity of the membrane and several proteins, such as cytochrome C, need an electrostatic interaction with CL for their binding to the MIM. Consequently, alterations in CL can trigger downstream events in apoptosis such as the release of cytochrome C and other pro-apoptotic factors into the cytosol (Chicco and Sparagna, 2007; Iverson et al., 2004; Wenz et al., 2009). The various roles of CL in mitochondrial functions are conserved in all eukaryotes. Alterations either in the content or structure of CL represent a hallmark in a variety of diseases characterized by mitochondrial dysfunction (Chicco and Sparagna, 2007; Claypool and Koehler, 2012).

5.4.1 Relevance of CL remodeling to Barth Syndrome

While three CL remodeling pathways have been identified in higher eukaryotes, Taz1 is the only transacylase that mediates the remodeling process in yeast (Claypool and Koehler, 2012) (**Figure T2**). The importance of this process is exemplified by the loss of functional *tafazzin*, the human homologue

of *Taz1*, that leads to the life-threatening genetic disorder BTHS (Barth et al., 1999; Whited et al., 2013).

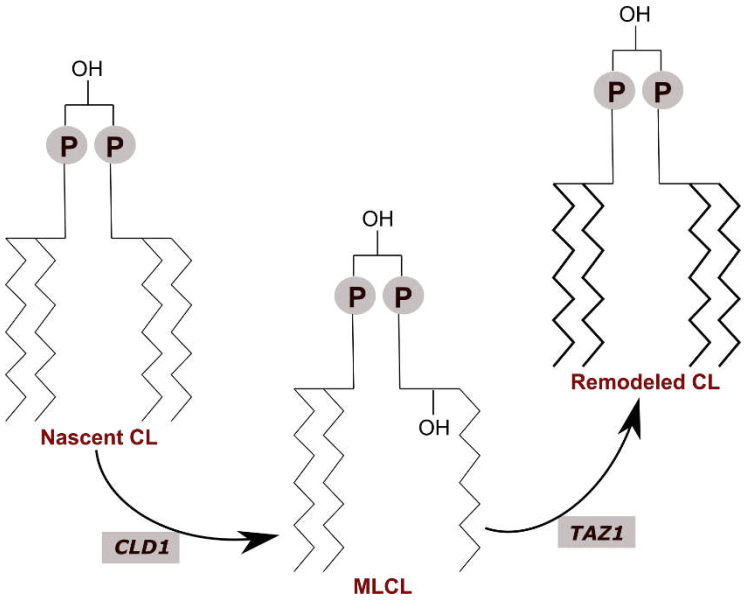

Figure T2: Schematic representation of CL remodeling in yeast. Nascent CL is deacylated by the phospholipase Cld1 forming MLCL, which is reacylated by Taz1 to form remodeled CL containing more unsaturated acyl chains (depicted in bold).

An absence of Taz1 results in a decrease of the cellular amounts of CL, an accumulation of monolyso-CL (MLCL), and aberrant CL species (Gu et al., 2004; Schlame et al., 2002). Similar alterations were also observed in fibroblasts and platelets obtained from patients with BTHS or animal models (Schlame et al., 2002; Valianpour et al., 2002; Vreken et al., 2000). Interestingly, the increased MLCL/CL ratio has been pointed out as the cause of BTHS. These findings have been supported by the rescue of the phenotypes observed in the yeast *taz1*Δ BTHS model by deleting the enzyme responsible for CL deacylation (Baile et al., 2014; Ye et al., 2014). As a result of the compromised CL levels, yeast mitochondria lacking Taz1 exhibit a decreased membrane potential and increased proton leakage (Baile et al., 2014; Ma et al., 2004). Abolishing the proton gradient across the MIM enhances the production of reactive oxygen species (ROS) which leads to oxidative damages (Chen et al., 2008). In BTHS, *tafazzin* mutations induce defective CL remodeling, which compromises the ATP production through oxidation of the respiratory intermediate NADH, leading to a decrease in the NAD^+/NADH ratio (Gonzalvez et al., 2013). As a consequence of

NADH accumulation, metabolic dysfunctions, such as inhibition of TCA cycle enzymes that use NAD^+ as a substrate, take place and the TCA cycle activity decreases (Ikon and Ryan, 2017; Vatrinet et al., 2017). Although *tafazzin* mutations have been largely implicated in BTHS, the precise role and the involvement of this protein in the pathomechanism of the disease remain unclear.

6. Research objectives

Phospholipids are essential structural components of all eukaryotes membranes. Notwithstanding their importance and wide distribution, the processes in which they take part remain ill defined. Among these processes is the lipid transport between and within organelles. Despite the increasing number of proteins identified to be involved in lipid exchange, the detailed mechanism still has to be discovered. In this thesis, I intended to obtain a deeper understanding of the processes that ensure mitochondrial phospholipid homeostasis. To this end, I focused on three main tasks:

1. To better understand the pathways of lipid transport, I investigated the process by which Mcp1 can rescue the growth phenotype of cells lacking the ERMES subunit Mdm10.

2. Despite extensive research on BTHS, the molecular basis of the disease remains uncharacterized. To shed light on the pathomechanism of this disease, which is caused by defective CL remodeling, I used yeast cells as a model system and aimed at finding multicopy suppressors of the growth retardation resulting from the absence of the CL modulating protein, Taz1.

3. To obtain a full spectrum of the functions of ERMES, I asked whether this complex is involved in regulating CoQ_6 biosynthesis in yeast cells.

7. Summary of the results

Unless otherwise specified all the figure references are referring to the figures in the articles corresponding to the current section.

7.1. Vps13-Mcp1 interact at vacuole-mitochondria interfaces and bypass ER-mitochondria contact sites (Peter et al., *Journal of Cell Biology*, 2017)

Our knowledge about ER-mitochondria contact sites is very limited. To date, the yeast ERMES complex was reported to be involved in many vital processes such as lipid transport, biogenesis of OM proteins, maintenance of mitochondrial DNA, and mitochondrial morphology and respiration (Kornmann et al., 2009; Sinzel et al., 2016; Tan et al., 2013). Yet, the main function of the complex or of its subunits is unknown.

To address this issue, a multi-copy suppressors screen of the growth defects of *mdm10Δ* cells was performed. Among other high copy suppressors of *mdm10Δ* cells, Mcp1 was identified (Tan et al., 2013).

Although the double deletion of *MCP1* and *ERMES* components is synthetic lethal, the lack of Mcp1 alone does not lead to any defect in mitochondrial function or to any clear impairment in the behaviour of yeast cells (Tan et al., 2013). The absence of such clear phenotypes of the *mcp1Δ* deletion strain makes it difficult to study the function of Mcp1.

Such observations are suggestive that Mcp1 and ERMES might function in redundant parallel pathways. In fact, it has been recently shown that a vacuolar protein Vps13 acts as an ERMES suppressor probably by enhancing the formation of vCLAMPs (Lang et al., 2015). Additionally, Mcp1 was observed to be required for this Vps13 suppressor function, behaving as Vps39, a known component of vCLAMPs (Lang et al., 2015).

According to these recent findings, Mcp1 might function in the same pathway as Vps13 and Vps39. Thus, we aimed to investigate the ERMES-independent pathway in which Mcp1 may be involved. To obtain further insights into the molecular function of Mcp1, I searched for potential physical interaction partners of this mitochondrial protein.

To that end, I employed immunoprecipitation experiments assays using

lysates from *mcp1Δ* yeast cells expressing plasmid-encoded HA-tagged Mcp1. Bound proteins were analyzed by immunodecoration and gel staining followed by mass spectrometry (MS). Specifically, MS analysis revealed that a ~370 kDa band corresponds to Vps13 whereas another band migrating at ~35 kDa represents HA-Mcp1 itself (Figure T3, data not included in the manuscript). Reciprocal immunoprecipitation experiments have been performed with tagged Vps13. However, it was not possible to confirm this interaction, probably due to technical problems. I anticipated that the fact that Vps13 is the fifth largest protein in the yeast proteome and dynamically localizes to different membrane contact sites (vCLAMPs and NVJs), combined with an apparent low steady-state levels of Mcp1 might be responsible for the difficult detection of this interaction.

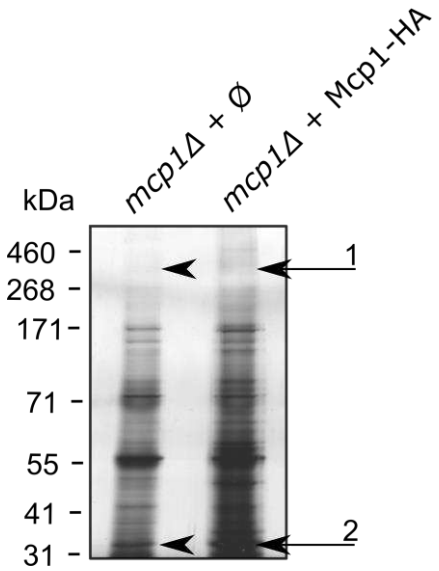

Figure T3: Mcp1 interacts with Vps13.
Whole cell lysate from *mcp1Δ* cells transformed with an empty plasmid (Ø) or with a plasmid encoding Mcp1-HA were subjected to anti-HA immunoprecipitation and analyzed by SDS-PAGE and silver staining. The arrows depict the retrieved bands which were analyzed by LC-MS/MS (#1, Vps13; #2, Mcp1-HA).

Bioinformatics analysis of Mcp1's sequence predicts a total of five transmembrane domains. However, Mcp1 topology has not been experimentally assessed and such knowledge is fundamental to understand how the Mcp1-Vps13 interaction might occur. In order to obtain further insight into the topology of Mcp1, I treated mitochondria isolated from cells overexpressing either Mcp1 or its C-terminally HA-tagged version with proteinase K (PK). Proteolytic fragments were detected by Western blotting with either an anti-HA antibody to detect the

C-terminal region of the protein or an antibody raised against the N-terminal domain of Mcp1 (Fig. 3B). Interestingly, using low concentrations of PK and both versions of Mcp1, a proteolytic fragment of ~20 kDa was identified with the anti-Mcp1 antibody. These findings suggest cleavage at the level of loop 2 and that the N-terminal domain is exposed to the cytosol (Fig. 3B and C). Of note, at higher PK concentrations, a proteolytic fragment of ~ 12 kDa is observed (Fig. 3B, fragment II). According to its size, this fragment corresponds to a cleavage immediately after the second transmembrane domain, excluding loop 2 (Fig. 3C).

Surprisingly, the N-terminal fragment remained protease resistant. This indicates that either the N-terminal is tightly folded or the epitope was too close to the membrane. In accordance with this, the localization of the HA-tag at the C-terminal of Mcp1 and the detection of Mcp1-HA fragments even at high concentrations of PK further confirm the N-out, C-in topology. Accordingly, at different concentrations of externally added PK, it was possible to detect with the anti-HA antibody a double fragment of ~ 17 kDa in size (Fig. 3B, fragment IIIa and IIIb). The detected fragments probably correspond to a fragment containing the transmembrane domains three to five with different cleavage levels in loop 2 (Fig. 3C, fragment III).

Based on the aforementioned results I suggest a Mcp1 topology where the N-terminal domain is exposed to the cytosol whereas the C-terminal is facing the intermembrane space. Such a topology suggests that the N-terminal of Mcp1 (aa 1-61) and/or loop 2 (aa 122-173) could potentially interact with Vps13. Although loop 4 is equally exposed to the cytosol, it might be too short to act as a binding site.

Homology analysis based on the sequence of Mcp1 proposed similarity to quinol fumarate reductase diheme cytochrome B subunit C of the proteobacterium *Wolinella succinogenes*. Thus, suggesting that beyond the recruitment of Vps13, Mcp1 might have an additional role as a heme binding protein.

To investigate whether heme binding is an important feature of Mcp1, the likely heme-binding histidines and other residues that are conserved among Mcp1 and other members of an uncharacterized protein family (PF07950 family) were mutated to the neutral amino acid alanine. Next, in collaboration with the Kormann's group, we addressed the capacity of the Mcp1 mutants to rescue the

growth defects of ERMES mutants and to recruit Vps13 to mitochondria (Fig. 4E-F). In fact, mutating the presumptive heme-binding domains histidine residues (H187A and H237A) led to a lost rescue of the ERMES growth defects (Fig. 4E), independently of the ability to recruit Vps13 to mitochondria (Fig. 4F). While mutating other conserved residues (P195A and G241A) resulted on variable effects on ERMES rescue but did not affect Vps13 recruitment (Fig. 4E-F).

Collectively, the conserved presumptive heme-binding domains in Mcp1 appear to be essential for the rescue effect of the growth defects of ERMES mutants but do not appear to be related to Vps13-Mcp1 interaction on mitochondria.

7.2 Overexpression of branched-chain amino acid aminotransferases rescues the growth defects of cells lacking the Barth Syndrome related gene *TAZ1* (Antunes et al., *Journal of Molecular Medicine*, 2018)

Tafazzin is a mitochondrial protein involved in the metabolism of CL, functioning as a phospholipid-lysophospholipid transacylase. Mutations in the *tafazzin* gene are associated with Barth syndrome (BTHS). BTHS is a rare X-linked disease characterized by skeletal myopathy and cardiomyopathy, and in some cases neutropenia. The *tafazzin* gene is highly conserved from yeast to human. Deletion of the yeast orthologue *TAZ1* results in a decrease in the total cellular amounts of CL, increased levels of monolyso-CL (MLCL), and compromised functions of mitochondria (Ye et al. 2014; Baile et al. 2014). Similar alterations were also observed in fibroblasts and platelets obtained from either patients with BTHS or animal models (Valianpour et al. 2002; Vreken et al. 2000; Schlame et al. 2002). Despite extensive research, the molecular basis of BTHS remains uncharacterized.

To gain insight into the pathomechanism of BTHS, I performed a screen for multi-copy suppressors of the *taz1Δ* growth defect using a yeast genomic library cloned into a high copy number (2μ) yeast expression vector. The deletion of *TAZ1* leads to a strong growth defect on synthetic medium containing ethanol

as the sole carbon source (SE) (Fig. 1A). Initially, I verified that the growth defect can be reversed upon overexpression of Taz1 from a plasmid (Fig. 1A), suggesting that the absence of Taz1 is the primary reason for this defect.

To ensure complete coverage of all yeast genes, I screened 55,000 colonies and identified genomic segments harbouring *CRG1, COX24, HMX1,* and *BAT1* as suppressors of *taz1Δ* growth defect. However, among these candidates only *BAT1* genomically overexpression in *taz1Δ* cells could rescue the *taz1Δ* growth defect (Fig. 1B-D). *BAT1* encodes for a mitochondrial branched-chain amino acid transaminase (Kispal et al., 1996). Yeast cells contain in addition to Bat1 also its cytosolic homologous protein Bat2.

Therefore, I asked whether the cytosolic branched-chain amino acid transaminase isoform also has a growth defect rescue capacity, similarly to its mitochondrial homologue. Using complementation growth tests, I observed that overexpression of *BAT2* could also complement the impaired growth of *taz1Δ* cells, although the rescue conferred by *BAT2* was weaker than that observed with *BAT1* (Fig. 1D). Such a difference could result from different protein expression among the isoforms or simply from their diverse localisations and/or function. To investigate whether the observed effects could be explained by altered protein expression, I performed western blotting analysis and verified that indeed Bat1 and Bat2 are detected in higher levels in the overexpressing strains. Given the high sequence homology between Bat1 and Bat2, the antibody raised against Bat1 also recognises Bat2. Hence, it is difficult to draw a conclusion on whether Bat1 and Bat2 are expressed at similar levels. Notably, Bat1 expression levels are decreased in *bat2*∆ cells (Fig. S1) This observation might be explained by the synergetic function of these dual distributed enzymes.

To test whether the observed compensation can be also extended to the loss of CL, I analyzed the growth of cells deficient for CL upon the deletion of key enzymes in its biosynthesis pathway, *GEP4* and *CRD1*. BCATs overexpression did not rescue of the growth defects of cells lacking any of the CL biosynthetic enzymes (Fig. 1E). These results indicate that enhanced metabolism of amino acids can compensate for defects specifically related to CL remodeling but not to its absence.

In accordance with the stabilizing role of CL in the electron transport chain supercomplexes, mitochondria lacking yeast Tafazzin display a defective

assembly of the respiratory chain complexes (Bazan et al., 2013; McKenzie et al., 2006; Zhang et al., 2005) and consequently reduced membrane potential (*ΔΨ*) (Brandner et al., 2005). To examine the effect of BCATs overexpression on these mitochondrial defects of *taz1Δ* cells, I performed blue native (BN)-PAGE analysis. Importantly, this analysis showed that genomically overexpressed *BAT1* or *BAT2* did not affect the complexes stability (Fig. 2A-B). Similarly, using the membrane potential-sensitive dye 3,3'-diprophylthiadicarbocyanine iodide ($DiSC_3(5)$) I determined the *ΔΨ* of mitochondria isolated from *taz1Δ* cells overexpressing either *BAT1* or *BAT2*, and did not observe any improvement upon such overexpression (Fig. 2C).

As a major consequence for the loss of the phospholipid-lysophospholipid transacylase function, mitochondria from *taz1Δ* cells exhibit a decrease in the amount of CL and accumulation of MLCL (Xu et al., 2016). Therefore, I decided to investigate the effect of *BAT1*/2 overexpression on *taz1Δ* mitochondrial PL profile. Hence, I performed thin layer chromatography (TLC). However, *BAT1* or *BAT2* overexpression in these cells did not rescue this altered PL profile (Fig. 2D). This suggests that recovery of the mutant cells defective growth does not depend on a rescue of lipid homeostasis. In line with this notion, I further investigated the effect of BCATs on the steady state levels of various mitochondrial proteins residing in all sub-compartments of the organelle and found no alteration of the proteins levels upon *BAT1*/2 overexpression in *taz1Δ* cells (Fig. 2E).

Next, I sought to investigate whether amino acids metabolism is relevant for the growth deficit observed of cells lacking Taz1. Bat1/2 catalyze the conversion of branched-chain amino acids (BCAAs) and α-ketoglutarate into branched chain α-keto acids and glutamate. The products that result from BCATs activity are in turn used as TCA cycle substrates. To test the involvement of BCAAs on the *taz1Δ* cells growth defect, I analyzed by drop dilution assay the effect of supplementing SE medium with these amino acids. I observed a significantly improvement of the growth of the mutated cells upon valine supplementation (Fig. 3A). This enhancement is especially noticeable upon addition of an effective valine concentration of 6.4 mM (Fig. 3A). However, the addition of the two other BCAAs, leucine (Fig. S3A) or isoleucine (Fig. S3D) was unable to abrogate the observed growth deficit of *taz1Δ* cells. Similar to the

situation upon BCAAs supplementation, the overexpression in *taz1Δ* cells of the *LEU2* gene, encoding a key enzyme in the biosynthesis pathway of leucine, did not improve the growth of these cells (Fig. S3B).

Since the BCATs enzymes can catalyze the conversion between keto acids and amino acids in both directions, I assessed the growth of *taz1Δ* cells when the corresponding keto acid form of leucine, alpha-ketoisocaproic acid (KIC), was supplemented to the medium. Nonetheless, the growth of the mutated cells did not improve upon its addition to the solid medium (Fig. S3C). Interestingly, previous studies have shown that amino acids supplemented in the medium can be used by the cells as carbon source, contributing to the cellular oxidative energy supply via the TCA cycle (Hothersall and Ahmed, 2013; Kiebish et al., 2013). Therefore, I wanted to investigate whether the supplementation with amino acids that are easily converted to TCA cycle substrates could rescue the defects of *taz1Δ* cells. To this end, the amino acids aspartate, glutamate or histidine were added to the ethanol-containing plates and the growth of the mutated cells was monitored. Of note, the impaired growth of *taz1Δ* cells was largely or partially rescued upon supplementation with aspartate or glutamate (Fig. 3B and D, respectively). Additionally, supplementing the mutant cells with either valine or aspartate did not alter the MLCL/CL ratio of mitochondria of *taz1Δ* cells (Fig. 3C). Interestingly, addition of histidine to the medium could fully restore the growth deficit of *taz1Δ* cells (Fig. 3E). These findings demonstrate that Bat1/2-mediated rescue of *Taz1*-depleted cells might be explained by elevated cellular levels of some amino acids. Since I cannot exclude the impaired transport of amino acids from the vacuole to the cytosol as the cause of *taz1Δ* cells growth defect, I investigate whether the overexpression of two vacuolar amino acid transporters *AVT1* and *AVT4* in the mutated cells could rescue such impaired growth. In yeast cells, under nutrient-rich growth, approximately 50% of the total amino acids are stored in the vacuole (Kawano-Kawada et al., 2018). Therefore, in conditions such as under nutrient starvation, these amino acids should be rapidly excreted to the cytosol in order to be used for *de novo* protein synthesis. However, overexpression of both amino acid transporters did not improve the growth of *taz1Δ* cells (Fig. 3F). This demonstrates that elevated amino acids transport is not sufficient or related to, the growth rescue guaranteed by certain amino acids supplementation in the mutant cells.

Next, I sought to investigate whether the direct supplementation of the SE media with TCA cycle metabolites could improve the growth of cells lacking Taz1. Surprisingly, I did not observe any rescue of the growth defect in those cells (Fig. S4A-E). These findings might suggest that the TCA-cycle products prevenient from BCATs overexpression are not sufficient to improve the growth defect of *taz1Δ* cells and that some other BCATs-related metabolites might be involved in this scenario.

In conclusion, my findings indicate that the overexpression of BCATs and enhanced metabolism of certain amino acids like valine have an important and disease relevant role in cells lacking Taz1 function.

7.3 ER-Mitochondria Encounter Structure (ERMES) coordinates coenzyme Q biosynthesis (Eisenberg-Bord et al., *Contact*, 2018, *in revision*)

CoQ is a redox lipophilic molecule responsible for electron transfer between the mitochondrial respiratory chain complexes whose deficiency causes pathologic disorders. To date, comprehensive information on CoQ biosynthesis and/or relevance is still missing. Biosynthesis of CoQ is facilitated by the CoQ synthome consisting of several *COQ* gene products, CoQ itself, and CoQ intermediates. The above-mentioned process is not completely characterized and several players with unclear molecular functions remain unidentified (Allan et al., 2015; Awad et al., 2018).

In *S. cerevisiae*, CoQ biosynthesis takes place in the mitochondria matrix and yeast CoQ mutants display a growth defect on non-fermentable carbon sources due to the respiration deficit (Kawamukai, 2016). Although some human Coq deficiencies can be relieved upon CoQ dietary supplementation, the uptake and incorporation of this highly hydrophobic molecule is mostly ineffective (Hernández-Camacho et al., 2018).

Interestingly, a study in yeast has shown that CoQ mutants with defective production of CoQ_6 (yeast CoQ) were rescued upon exogenously added CoQ_6 (Santos-Ocaña et al., 2002). This observation raises an intriguing possibility that

respiratory defective mutants might benefit from CoQ_6 supplementation to their growth media.

Specifically, I asked whether exogenous addition of CoQ_6 could rescue mitochondrial defects of *ERMES* mutant cells, such as yeast cells lacking the ERMES component *MDM10*. As previously mentioned, the deletion of *MDM10* leads to alterations in mitochondrial distribution, morphogenesis, and membrane potential. Mutant cells bear a strong growth defect on non-fermentable carbon sources (Sinzel et al., 2016; Tan et al., 2013).

Thus, I analyzed the effect of adding exogenously CoQ_6 to *mdm10Δ* cells grown on non-fermentable carbon source. Growth analysis indicated that this supplementation did rescue the growth defect of *MDM10* mutant suggesting that CoQ_6 is indeed taken-up by *mdm10Δ* cells (Figure T4A below, data not included in the manuscript). Next, I analyzed the effect of exogenously added CoQ_6 on the mitochondrial morphology defects that are observed upon loss of Mdm10. Fluorescence microscopy of *mdm10Δ* cells using a membrane potential independent dye (MitoTracker Green FM) revealed that CoQ_6 supplemented to the growth media could rescue the mitochondrial morphology phenotype of these mutated cells, leading to a WT-like tubular network shape in 50% of the mutated cells (Figure T4B-C below, data not included in the manuscript).

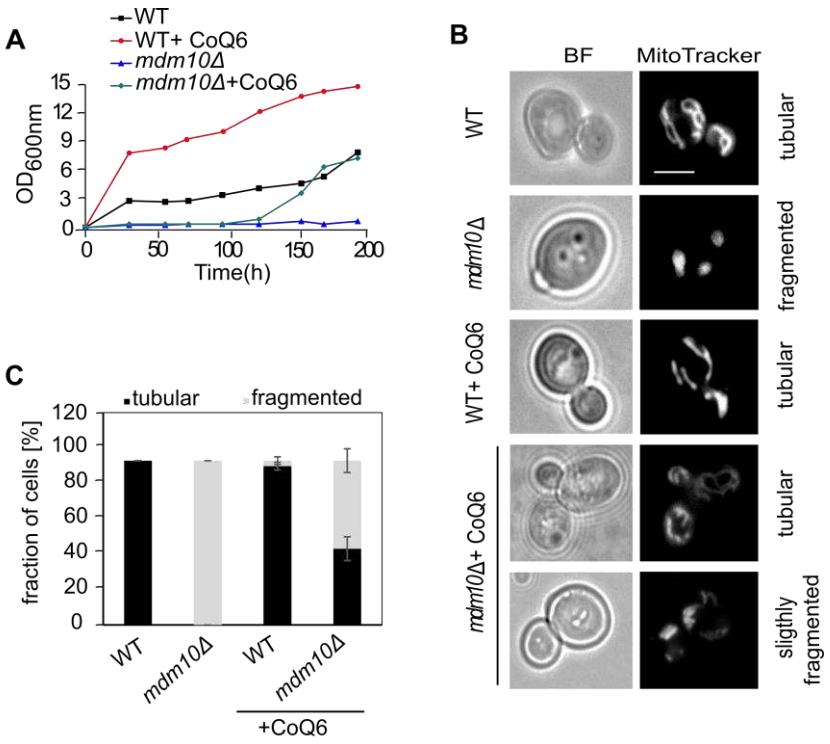

Figure T4. Supplementation of YPE medium with CoQ_6 affects mitochondrial morphogenesis of *mdm10Δ* cells. (A) Supplementation of YPE medium with CoQ_6 rescues the growth phenotype of *mdm10Δ* cells. The indicated cells were incubated in YPE liquid medium in the presence or absence of 30 µm exogenous CoQ_6 and grown for 7 days. Growth was inferred (OD_{600}) at the indicated times, Average values of six biological independent experiments are shown. **(B)** CoQ_6 partially restores the mitochondria morphology defect in *mdm10Δ* cells. Cells described in (A) were grown to mid-logarithmic phase on YPE medium, stained with Mitotracker Green FM and then analyzed by fluorescence microscopy. Typical images from three biological independent experiments are shown (scale bar = 5 µm). **(C)** Analysis of the cells described in B. Average values with standard deviation bars of three biological independent experiments with at least 100 cells per experiment are shown.

Taking together, ubiquinone can partially restore the mitochondria morphology defects of the ERMES mutant *mdm10*Δ.

Recently, analysis of human homologues of yeast proteins have started to disclose details of the CoQ biosynthesis pathway (Allan et al., 2015; He et al., 2015; Marbois et al., 2010). Although CoQ is present in several cellular compartments, its biosynthesis takes place on the matrix side of the MIM (Tran and Clarke, 2007), which implies the need of CoQ's exchange between cellular compartments. Due to the known potential of contact sites to transfer molecules and metabolites between two organelles (Eisenberg-Bord et al., 2016), it is tempting to speculate an additional role of ERMES in CoQ biosynthesis pathway. However, strong evidence for such connection is still to be obtain.

In Eisenberg-Bord et al., (2018) it was shown that loss of ERMES leads to defective assembly of the CoQ synthome. To exclude the possibility that defective assembly of mitochondrial protein complexes is a general outcome of losing ERMES function, I performed BN-PAGE analysis of isolated mitochondria of *mdm10*Δ cells. This analysis showed that the monomer and dimer forms of ATPase synthase complex were not altered in the mutated cells (Figure T5 below, data to be included in the resubmitted manuscript).

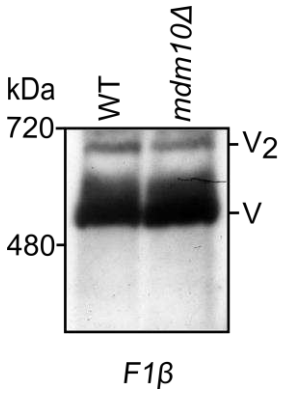

Figure T5. The assembly of the ATP synthase complex (complex V) is not altered in mitochondria lacking Mdm10. Mitochondria isolated from the indicated strains were lysed with 1% digitonin and subjected to a 6-14% BN-PAGE. Proteins were analyzed by immunodetection with antibodies against F1β (subunit of complex V). The monomeric and dimeric forms of complex V are indicated as V and V2, respectively.

Collectively, the results described in Eisenberg-Bord et al. (2018) suggest that CoQ_6 biosynthesis is coordinated with the ER-mitochondria contact site. Currently, the mechanism that mediates this process remains unclear.

8. Discussion

8.1. Vps13-Mcp1 interact at vacuole-mitochondria interfaces and bypass ER-mitochondria contact sites

The yeast mitochondrial outer membrane protein Mcp1 was identified as a high-copy suppressor of the growth phenotype of *mdm10Δ* cells. Overexpression of Mcp1 in *mdm10Δ* cells can restore typical ERMES defects (Tan *et al*., 2013). ERMES components are functionally involved in a broad spectrum of cellular processes, making it difficult to unravel the direct effect on lipid homeostasis. Taking advantage of the identified suppressors for ERMES defects, it is possible to study direct, and indirect effects derived from ERMES deletion (Dimmer and Rapaport, 2017; Lang et al., 2015; Tan et al., 2013).

Mcp1 is not conserved in higher eukaryotes and loss of this protein does not result in any observable mitochondrial defect, suggesting that Mcp1 is part of an ERMES-independent pathway, which becomes crucial only when ERMES is deleted. In fact, it has been shown that the vacuolar protein Vps13 acts as an ERMES suppressor probably by enhancing the formation of mitochondria-vacuolar contacts and that Mcp1 is required for the Vps13 dominant mutant suppression function (Lang et al., 2015).

In this study, I could identify by mass spectrometry analysis the vacuolar protein Vps13 as one of Mcp1 interaction partners. This is in agreement with a previous report that Mcp1 and a Vps13 dominant mutant cooperate to bypass ERMES defects (Lang et al., 2015). In fact, co-immunoprecipitation experiments performed by my collaboration partners using Mcp1-HA and a GFP-tagged version of Vps13 with a point mutation (L1627S), which enhances the protein activity (Fig. 3A), could provide further evidence for the physical interaction between the mitochondrial Mcp1 protein and Vps13 (John Peter et al., 2017).

Furthermore, I have demonstrated that the N-terminal of Mcp1 is exposed to the cytosol, whereas the C-terminal faces the IMS. Unexpectedly, the N-terminal fragment of the protein is protease resistant, which suggests that this domain is tightly folded. These results confirmed a Mcp1 topology where the N-terminal domain is exposed to the cytosol whereas the C-terminal region is facing the

intermembrane space. In fact, upon the expression of the N-terminal of Mcp1 (aa 1-61) it could be observed a strong recruitment of Vps13 to mitochondria. These observations demonstrate that Mcp1 recruits Vps13 to mitochondria and its N-terminal mediates the recruitment (John Peter et al., 2017).

It is surprising that even though Mcp1 is not conserved, we could demonstrate that the overexpression of the N-terminal fragment of Mcp1 was sufficient to recruit Vps13 to mitochondria. Of note, Mcp1 is predicted to fold into a heme-binding five-helix bundle, as found in quinol-fumarate reductases. On the same line, overexpressing Mcp1 variants that carry single mutations in the putative heme-binding domain failed to suppress the *ERMES*Δ growth defects without affecting the recruitment of Vps13 to mitochondria (John Peter et al., 2017). Given the involvement of ERMES in lipid transport and the ability of Mcp1 and Vps13 to induce the formation vacuole-mitochondria contact sites, it is plausible that both proteins are directly involved in lipid exchange.

Interestingly, it has been recently reported the co-existence of another vacuole-mitochondria contact site, which is functionally distinct from the vCLAMP formed by Vps13 and Mcp1 (González Montoro et al., 2018). Accordingly, the vacuolar effector Vps39 binds the Rab Ypt7 and tether vacuoles with the TOM complex, via the Tom40 receptor, and thus establishes a vCLAMP. However, in contrast to the Vps13-Mcp1 complex, the afore-mentioned vCLAMP cannot function in the ERMES bypass pathway, which requires vesicular trafficking to the vacuole. This suggests that the vacuole might be the donor organelle for the lipid supplying pathway in which Vps13 functions (González Montoro et al., 2018).

Moreover, the structure of the N-terminal region of Vps13 ($Vps13_{crystal;}$ aa 1-335) has recently been resolved and a hydrophobic cavity has been identified, which may form an extended lipid-binding surface formed by several $Vps13_{crystal}$-like domains present in the full-length Vps13 (Kumar et al., 2018). In the same study, it was demonstrated that the purified yeast N-terminal domain of Vps13 binds approximately ten glycerophospholipids molecules, suggesting that Vps13 might be able to accommodate and transfer several lipid molecules at once (Kumar et al., 2018).

Moreover, recently a PxP motif, comprised of highly conserved prolines flanked by hydrophobic amino acids, was identified in the N-terminal domain of Mcp1. This motif was suggested to be the binding and recruitment site for Vps13.

This motif is not only involved in recruiting Vps13 to mitochondria but also to other membranes that can form vacuole contact sites (Bean et al., 2018). The cellular localization of Vps13 is mediated by the PxP motif present in its effectors. Specifically, the recruitment of Vps13 to mitochondria by Mcp1, to prespore membrane by Spo71, to endosomal and vacuolar membranes by Ypt35, and possibly more (Bean et al., 2018).

In conclusion, our study revealed that Mcp1 functions in the same pathway as Vps13 and recruits the latter to mitochondria, mediating the association of vacuole to mitochondria. In contrast to Mcp1, Vps13 is highly conserved with four homologs in humans (Vps13A-D). This suggests that in metazoans probably another mitochondrial protein is functioning as Mcp1 by recruiting Vps13 to mitochondria. In a more general way, further studies are needed to determine whether there is a functional ERMES orthologue in higher eukaryotes or if its function is taken over by other inter-organelle contact sites.

8.2. Overexpression of branched-chain amino acid aminotransferases rescues the growth defects of cells lacking the Barth Syndrome related gene *TAZ1*

TAZ1 encodes the yeast orthologue of *tafazzin* whose mutations are the genetic origin of BTHS (Bione et al., 1996). Although the involvement of *taffazin* in this syndrome has been known for many years, it is still unclear why the absence of CL remodeling causes the associated clinical phenotypes. I sought to shed light on the cellular mechanisms that might be involved in the outcome of BTHS, using yeast as a model system. Yeast cells lacking Taz1 display a severe growth defect on synthetic medium using ethanol as the sole carbon source. Hence, I anticipated that the overexpression of a protein, which is relevant to this clinical disorder, would result in a rescue of the growth phenotype that could easily be screened for.

Interestingly, *taz1Δ* mutant cells grow normally on non-fermentable carbon sources like glycerol or acetate suggesting that compromised respiration

is not the primary defect of these cells. In fact, my collaboration partners demonstrated that these cells have increased respiration when compared to WT. These observations suggest that the higher oxygen consumption rate in *taz1Δ* mitochondria could be an attempt to compensate their compromised respiratory function (Fig. S2A). Interestingly, the overexpression of *BAT1* or *BAT2* in *taz1Δ* cells reverts the oxygen consumption to WT levels (Fig. S2A).

Furthermore, yeast mutants acquire an ethanol-tolerance dependent on their lipid composition and unsaturation degree (Chi and Arneborg, 1999). Thus, the sensitivity of the *taz1Δ* mutant to ethanol is most likely caused by the decreased CL levels and altered acyl composition of this crucial dimeric PL. Ethanol stress leads to inactivation of some mitochondrial enzymes upon increased production of reactive oxygen species (ROS) ultimately causing mitochondrial damage (Costa et al., 1997; Du and Takagi, 2007; Jimenez and Benitez, 1988). Indeed, the levels of carbonylation of proteins in *taz1Δ* cells grown in ethanol have been shown to be double than those of cells grown on glucose (Chen et al., 2008). This suggests that the various mitochondrial defects observed in *taz1Δ* mutant cells exacerbate their ethanol sensitivity.

In my work, I identified the branched-chain amino acid (BCAA) transaminase (BCAT) Bat1 and Bat2, mitochondrial and cytosolic proteins, respectively, as suppressors of the growth defects of yeast cells lacking *TAZ1* Along this line, supplying *taz1Δ* cells with the BCAA valine or aspartate, which is a product of a transamination reaction as well, improved their growth on ethanol without affecting their lipid composition. This observation is surprising since although both BCATs were reported previously to affect directly or indirectly several cellular processes, none has been linked to the pathogenesis of BTHS so far. Additionally, Bat1*,* but not Bat2*,* was identified as a high-copy suppressor of a temperature-sensitive mutation in *ATM1,* encoding a mitochondrial ABC transporter (Kispal et al., 1996).

Surprisingly, overexpression of *BAT1* or *BAT2* did not reverse the respiratory chain complexes assembly defects, the reduced membrane potential of mitochondria, or altered mitochondrial lipid profiles, i.e. the decreased CL and increased MLCL levels. Hence, I can hypothesize that the rescued *taz1* mutant growth defects exerted by BCATs is not related to the primary mitochondrial defects of losing Taz1 function, but rather to secondary defects characteristic of

these cells. In fact, both BCATs yeast homologs have been implicated to be critical for the activation of TORC1 signalling, a process that is in turn is coordinated by the TCA cycle flux (Kingsbury et al., 2015). Indeed, liquid chromatography coupled with mass spectrometry (LC-MS) analysis performed by my collaboration partners verified that the TCA metabolites and some amino acids levels are decreased in *taz1Δ* cells and their levels are restored upon overexpression of Bat1/2. In fact, *BAT1* overexpression in *taz1Δ* cells restored the decreased levels of most of the TCA cycle metabolites and of the beneficial amino acids valine and histidine.

Remarkably, the growth defect rescue only occurred upon supplementation with one out of three of the BCAAs. This data is consistent with a recent study in which it has been reported that the levels of both remaining BCAAs, leucine or isoleucine, were not affected by disruption of *BAT1* or *BAT2* (Takpho et al., 2018). This observation suggests that the mitochondrial biosynthesis of valine is more prominent than its cytosolic synthesis, and can also explain why the growth rescue by *BAT1* overexpression was better than with its cytosolic homologue.

Although I assessed the protein expression of each BCAT individually, due to their high sequence homology, which hinders their individual detection, I cannot exclude that these isoforms are differently expressed.

Finally, to corroborate in a mammalian model the findings obtained with a yeast model of BTHS, my collaboration partners tested the effects of human BCATs homologs and supplementation with valine on the proliferation of *TAZ*$^{-/-}$ cells. They could show that the mitochondrial *BAT* homolog, but not the cytosolic one, enhanced significantly the proliferation of MEF cells lacking *TAZ*. Additionally, valine supplementation resulted in an increased proliferation of *TAZ* mutant mammalian cells. Hence, the observed growth defect rescue with the two different BCAT isoforms and with valine supplementation is consistent in both yeast and mammalian cells.

Previous studies reported beneficial effects of amino acids in several analogous contexts. For example, dietary supplementation of BCAAs has been shown to revert structural and functional mitochondrial damages in rodents with alcoholic liver disease (Tedesco et al., 2018). Furthermore, a link between impaired CL remodeling and amino acids metabolism is further supported in a

TAZ knock-down mouse model in which the increased MLCL/CL ratio led to a substrate shift via *de novo* amino acid biosynthesis as well as amino acid usage by the TCA cycle (Kiebish et al., 2013).

Currently, the pathomechanism of BTHS is not clear and although the molecular pathway behind these observations remains obscure, these findings could clearly open up a new and previously unknown direction to learn more about the mechanism of BTHS. One possibility is that BCATs provide substrates to the TCA cycle, and aspartate can be deaminated to produce oxaloacetate, therefore also feeding the cycle. However, since it is hard to determine how much of the externally added metabolites are actually transported across the cell wall, plasma membrane and into the mitochondrial matrix, we cannot exclude that differences in rescue ability reflect variations in the effective transport of the different molecules, Alternatively, supplementation of certain amino acids can enhance cellular growth indirectly by their induction of the mTOR signalling pathway.

Collectively, these results also hint to a potential use of branched-chain amino acids as a therapeutic avenue to treat patients with Barth syndrome.

8.3. ER-Mitochondria Encounter Structure (ERMES) coordinates coenzyme Q biosynthesis

The absence of vesicular lipid exchange among mitochondria and other cellular compartments proposes that the exchange of lipids between the ER, where most PLs biosynthesis takes place, and mitochondria must occur via inter-organelle close contacts (Dimmer and Rapaport, 2017; Kornmann et al., 2009). While the subunits and respective localization of the ER-mitochondria encounter structure (ERMES) complex, and its function as a multi-protein tether that mediates PL transfer is well defined, additional roles of ERMES are less explored (Lahiri et al., 2014b). It is still puzzling why the loss of a functional ERMES complex leads to so many unrelated phenotypes in yeast cells. Although the ERMES complex is not conserved in higher eukaryotes, several proteins have been described as potential tethers between ER and mitochondria in metazoans.

Interestingly, in similarity to the situation in yeast, such tether proteins in higher eukaryotes are also involved in different physiological processes. for a prominent example is the mitochondrial protein mitofusin Mfn2, which is involved in ER-mitochondria contacts, and whose deletion displays decreased CoQ levels, ultimately leading to defective respiration (de Brito and Scorrano, 2008; Mourier et al., 2015). Additionally, the ATPase Coq8A that is involved in both the assembly of the high molecular mass multisubunit complex (CoQ synthome) and in *de novo* biosynthesis of CoQ, belongs to the family of ADCKs. Interestingly, the human homologues of the Mdm10 complementing protein, Mcp2 belong also to this family (Reidenbach et al., 2018). These findings are in line with our observation that loss of functional ERMES complex leads to destabilization of the yeast CoQ synthome.

Our data show that ERMES seem to be located above specialized matrix niches where the CoQ synthome is enriched, suggesting a spatially regulated process. Naturally, we cannot exclude the possibility that this observation might be an indirect consequence of the modified PL metabolism or altered mitochondrial function in ERMES mutants (Sinzel et al., 2016; Tan et al., 2013).

To date, there is no evidence for a direct interaction between ERMES and CoQ synthome subunits. Nevertheless, work done by our collaboration partners demonstrated that Coq10 is involved in the apparent coordination of the CoQ synthome by the ERMES complex, suggesting a direct role yet unclear mechanism by which this tether mediates CoQ biosynthesis (Eisenberg-Bord et al., 2018). Although Coq10 is not part of the CoQ synthome, it has been reported to chaperone CoQ_6 and late-stage CoQ_6-intermediates from the location where they are synthesized to the sites where they exerts their function (Allan et al., 2013; Barros et al., 2005). Furthermore, in the yeast genome both *COQ10* and *MDM12* genes are adjacent, suggesting that they might share a promoter (Cherry et al., 2012). Indeed, yeast gene expression microarray analysis have demonstrated that the both genes are co-expressed (Hibbs et al., 2007Hibbs et al., 2007). Hence, it is tempting to speculate that the transcriptional co-regulation between *COQ10* and *MDM12* might be the basis for the coordination of the levels of Coq10 polypeptide and the ERMES complex to assist a better positioning of the CoQ synthome at the proximity of the ER-mitochondria contact site.

In fact, it was demonstrated that in the absence of a functional ERMES

complex the mRNA levels of the *COQ* genes and the cellular levels of CoQ_6 were increased. Surprisingly, the steady state levels of the proteins encoded by the aforementioned mRNAs were unaltered in the mutant cells and the mitochondrial levels of CoQ_6 were reduced (Eisenberg-Bord et al., 2018). These findings suggest a scenario where mitochondria have a defective leakage of CoQ_6, which is followed by a compensatory signalling to the nucleus to upregulate transcription of CoQ genes. Such communication between mitochondria and nucleus to cope with cellular alterations has been previously described (Eisenberg-Bord and Schuldiner, 2017).

In conclusion, our study revealed that ERMES complex and coenzyme Q biosynthesis are intimately connected, however the mechanism by which this occurs is still unknown. Future detailed studies on the interplay between CoQ_6 biosynthesis and the ER-mitochondria contact site will allow identifying possible alternative factors that have evolved to serve similar functions in eukaryotes.

9. References

Allan, C.M., A.M. Awad, J.S. Johnson, D.I. Shirasaki, C. Wang, C.E. Blaby-Haas, S.S. Merchant, J.A. Loo, and C.F. Clarke. 2015. Identification of Coq11, a new coenzyme Q biosynthetic protein in the CoQ-synthome in Saccharomyces cerevisiae. *The Journal of biological chemistry*. 290:7517-7534.

Allan, C.M., S. Hill, S. Morvaridi, R. Saiki, J.S. Johnson, W.S. Liau, K. Hirano, T. Kawashima, Z. Ji, J.A. Loo, J.N. Shepherd, and C.F. Clarke. 2013. A conserved START domain coenzyme Q-binding polypeptide is required for efficient Q biosynthesis, respiratory electron transport, and antioxidant function in Saccharomyces cerevisiae. *Biochimica et biophysica acta*. 1831:776-791.

Antunes, D., A.I. Padrao, E. Maciel, D. Santinha, P. Oliveira, R. Vitorino, D. Moreira-Goncalves, B. Colaco, M.J. Pires, C. Nunes, L.L. Santos, F. Amado, J.A. Duarte, M.R. Domingues, and R. Ferreira. 2014. Molecular insights into mitochondrial dysfunction in cancer-related muscle wasting. *Biochimica et biophysica acta*. 1841:896-905.

Awad, Agape M., Michelle C. Bradley, L. Fernández-del-Río, A. Nag, H.S. Tsui, and Catherine F. Clarke. 2018. Coenzyme Q₁₀ deficiencies: pathways in yeast and humans. *Essays In Biochemistry*. 62:361.

Baile, M.G., M. Sathappa, Y.W. Lu, E. Pryce, K. Whited, J.M. McCaffery, X. Han, N.N. Alder, and S.M. Claypool. 2014. Unremodeled and remodeled cardiolipin are functionally indistinguishable in yeast. *The Journal of biological chemistry*. 289:1768-1778.

Barros, M.H., A. Johnson, P. Gin, B.N. Marbois, C.F. Clarke, and A. Tzagoloff. 2005. The Saccharomyces cerevisiae COQ10 gene encodes a START domain protein required for function of coenzyme Q in respiration. *The Journal of biological chemistry*. 280:42627-42635.

Barth, P.G., R.J. Wanders, and P. Vreken. 1999. X-linked cardioskeletal myopathy and neutropenia (Barth syndrome)-MIM 302060. *The Journal of pediatrics*. 135:273-276.

Bazan, S., E. Mileykovskaya, V.K. Mallampalli, P. Heacock, G.C. Sparagna, and W. Dowhan. 2013. Cardiolipin-dependent reconstitution of respiratory supercomplexes from purified Saccharomyces cerevisiae complexes III and IV. *The Journal of biological chemistry*. 288:401-411.

Beal, M.F. 2005. Mitochondria take center stage in aging and neurodegeneration. *Annals of neurology*. 58:495-505.

Bean, B.D.M., S.K. Dziurdzik, K.L. Kolehmainen, C.M.S. Fowler, W.K. Kwong, L.I. Grad, M. Davey, C. Schluter, and E. Conibear. 2018. Competitive organelle-specific adaptors recruit Vps13 to membrane contact sites. *The Journal of Cell Biology*. 217:3593-3607

Bentinger, M., M. Tekle, and G. Dallner. 2010. Coenzyme Q – Biosynthesis and functions. *Biochemical and Biophysical Research Communications*. 396:74-79.

Bione, S., P. D'Adamo, E. Maestrini, A.K. Gedeon, P.A. Bolhuis, and D. Toniolo. 1996. A novel X-linked gene, G4.5. is responsible for Barth syndrome. *Nature genetics*. 12:385-389.

Bockler, S., and B. Westermann. 2014. Mitochondrial ER contacts are crucial for mitophagy in yeast. *Developmental cell*. 28:450-458.

Boekema, E.J., and H.P. Braun. 2007. Supramolecular structure of the mitochondrial oxidative phosphorylation system. *The Journal of biological chemistry*. 282:1-4.

Brandner, K., D.U. Mick, A.E. Frazier, R.D. Taylor, C. Meisinger, and P. Rehling. 2005. Taz1, an outer mitochondrial membrane protein, affects stability and assembly of inner membrane protein complexes: implications for Barth Syndrome. *Molecular biology of the cell*. 16:5202-5214.

Bratic, A., and N.G. Larsson. 2013. The role of mitochondria in aging. *The Journal of clinical investigation*. 123:951-957.

Chen, S., Q. He, and M.L. Greenberg. 2008. Loss of tafazzin in yeast leads to increased oxidative stress during respiratory growth. *Molecular Microb*iology 68:1061-1072.

Cherry, J.M., E.L. Hong, C. Amundsen, R. Balakrishnan, G. Binkley, E.T. Chan, K.R. Christie, M.C. Costanzo, S.S. Dwight, S.R. Engel, D.G. Fisk, J.E. Hirschman, B.C. Hitz, K. Karra, C.J. Krieger, S.R. Miyasato, R.S. Nash, J. Park, M.S. Skrzypek, M. Simison, S. Weng, and E.D. Wong. 2012.

Saccharomyces Genome Database: the genomics resource of budding yeast. *Nucleic acids research*. 40:D700-705.

Chi, Z., and N. Arneborg. 1999. Relationship between lipid composition, frequency of ethanol-induced respiratory deficient mutants, and ethanol tolerance in Saccharomyces cerevisiae. *Journal of applied microbiology*. 86:1047-1052.

Chicco, A.J., and G.C. Sparagna. 2007. Role of cardiolipin alterations in mitochondrial dysfunction and disease. *American Journal of Physiology-Cell Physiology*. 292:C33-44.

Claypool, S.M., and C.M. Koehler. 2012. The Complexity of Cardiolipin in Health and Disease. *Trends in Biochemical Sciences*. 37:32-41.

Costa, V., M.A. Amorim, E. Reis, A. Quintanilha, and P. Moradas-Ferreira. 1997. Mitochondrial superoxide dismutase is essential for ethanol tolerance of Saccharomyces cerevisiae in the post-diauxic phase. *Microbiology (Reading, England)*. 143 (Pt 5):1649-1656.

Daum, G., and J.E. Vance. 1997. Import of lipids into mitochondria. *Progress in lipid research*. 36:103-130.

de Brito, O.M., and L. Scorrano. 2008. Mitofusin 2 tethers endoplasmic reticulum to mitochondria. *Nature*. 456:605-610.

Dimmer, K.S., and D. Rapaport. 2017. Mitochondrial contact sites as platforms for phospholipid exchange. *Biochimica et biophysica acta*. 1862:69-80.

Du, X., and H. Takagi. 2007. N-Acetyltransferase Mpr1 confers ethanol tolerance on Saccharomyces cerevisiae by reducing reactive oxygen species. *Applied Microbiology and Biotechnology*. 75:1343-1351.

Eisenberg-Bord, M., and M. Schuldiner. 2017. Ground control to major TOM: mitochondria-nucleus communication. *The FEBS journal*. 284:196-210.

Eisenberg-Bord, M., N. Shai, M. Schuldiner, and M. Bohnert. 2016. A Tether Is a Tether Is a Tether: Tethering at Membrane Contact Sites. *Developmental cell*. 39:395-409.

Elbaz-Alon, Y., E. Rosenfeld-Gur, V. Shinder, A.H. Futerman, T. Geiger, and M. Schuldiner. 2014. A dynamic interface between vacuoles and mitochondria in yeast. *Developmental Cell*. 30:95-102.

Enns, G.M. 2003. The contribution of mitochondria to common disorders. *Molecular Genetics and Metabolism*. 80:11-26.

Fruhwirth, G.O., A. Loidl, and A. Hermetter. 2007. Oxidized phospholipids: from molecular properties to disease. *Biochimica et biophysica acta*. 1772:718-736.

Gebert, N., A.S. Joshi, S. Kutik, T. Becker, M. McKenzie, X.L. Guan, V.P. Mooga, D.A. Stroud, G. Kulkarni, M.R. Wenk, P. Rehling, C. Meisinger, M.T. Ryan, N. Wiedemann, M.L. Greenberg, and N. Pfanner. 2009. Mitochondrial cardiolipin involved in outer-membrane protein biogenesis: implications for Barth syndrome. *Current biology : CB*. 19:2133-2139.

Genova, M.L., and G. Lenaz. 2011. New developments on the functions of coenzyme Q in mitochondria. *BioFactors (Oxford, England)*. 37:330-354.

González Montoro, A., K. Auffarth, C. Hönscher, M. Bohnert, T. Becker, B. Warscheid, F. Reggiori, M. van der Laan, F. Fröhlich, and C. Ungermann. 2018. Vps39 Interacts with Tom40 to Establish One of Two Functionally Distinct Vacuole-Mitochondria Contact Sites. *Developmental cell*. 45:621-636.e627.

Gonzalvez, F., M. D'Aurelio, M. Boutant, A. Moustapha, J.P. Puech, T. Landes, L. Arnaune-Pelloquin, G. Vial, N. Taleux, C. Slomianny, R.J. Wanders, R.H. Houtkooper, P. Bellenguer, I.M. Moller, E. Gottlieb, F.M. Vaz, G. Manfredi, and P.X. Petit. 2013. Barth syndrome: cellular compensation of mitochondrial dysfunction and apoptosis inhibition due to changes in cardiolipin remodeling linked to tafazzin (TAZ) gene mutation. *Biochimica et biophysica acta*. 1832:1194-1206.

Gray, M.W. 2012. Mitochondrial evolution. *Cold Spring Harbor perspectives in biology*. 4:a011403.

Gutman, M., A.B. Kotlyar, N. Borovok, and E. Nachliel. 1993. Reaction of bulk protons with a mitochondrial inner membrane preparation: time-resolved measurements and their analysis. *Biochemistry*. 32:2942-2946.

He, C.H., D.S. Black, T.P. Nguyen, C. Wang, C. Srinivasan, and C.F. Clarke. 2015. Yeast Coq9 controls deamination of coenzyme Q intermediates that derive from para-aminobenzoic acid. *Biochimica et biophysica acta*. 1851:1227-1239.

Hernández-Camacho, J.D., M. Bernier, G. López-Lluch, and P. Navas. 2018. Coenzyme Q(10) Supplementation in Aging and Disease. *Frontiers in physiology*. 9:44-44.

Hibbs, M.A., D.C. Hess, C.L. Myers, C. Huttenhower, K. Li, and O.G. Troyanskaya. 2007. Exploring the functional landscape of gene expression: directed search of large microarray compendia. *Bioinformatics (Oxford, England)*. 23:2692-2699.

Hockenbery, D., G. Nunez, C. Milliman, R.D. Schreiber, and S.J. Korsmeyer. 1990. Bcl-2 is an inner mitochondrial membrane protein that blocks programmed cell death. *Nature*. 348:334-336.

Hoffmann, B., A. Stockl, M. Schlame, K. Beyer, and M. Klingenberg. 1994. The reconstituted ADP/ATP carrier activity has an absolute requirement for cardiolipin as shown in cysteine mutants. *The Journal of biological chemistry*. 269:1940-1944.

Hoffmann, H.-P., and C.J. Avers. 1973. Mitochondrion of Yeast: Ultrastructural Evidence for One Giant, Branched Organelle per Cell. *Science*. 181:749-751.

Honscher, C., M. Mari, K. Auffarth, M. Bohnert, J. Griffith, W. Geerts, M. van der Laan, M. Cabrera, F. Reggiori, and C. Ungermann. 2014. Cellular metabolism regulates contact sites between vacuoles and mitochondria. *Developmental Cell*. 30:86-94.

Horvath, S.E., and G. Daum. 2013. Lipids of mitochondria. *Progress in lipid research*. 52:590-614.

Hothersall, J.S., and A. Ahmed. 2013. Metabolic Fate of the Increased Yeast Amino Acid Uptake Subsequent to Catabolite Derepression. *Journal of Amino Acids*. 2013:7.

Ikon, N., and R.O. Ryan. 2017. Barth Syndrome: Connecting Cardiolipin to Cardiomyopathy. *Lipids*. 52:99-108.

Iverson, S.L., M. Enoksson, V. Gogvadze, M. Ott, and S. Orrenius. 2004. Cardiolipin Is Not Required for Bax-mediated Cytochrome c Release from Yeast Mitochondria. *Journal of Biological Chemistry*. 279:1100-1107.

Jiang, F., M.T. Ryan, M. Schlame, M. Zhao, Z. Gu, M. Klingenberg, N. Pfanner, and M.L. Greenberg. 2000. Absence of cardiolipin in the crd1 null mutant results in decreased mitochondrial membrane potential and reduced mitochondrial function. *Journal of Biology Chemistry*. 275:22387-22394.

Jimenez, J., and T. Benitez. 1988. Yeast cell viability under conditions of high temperature and ethanol concentrations depends on the mitochondrial genome. *Current genetics*. 13:461-469.

John Peter, A.T., B. Herrmann, D. Antunes, D. Rapaport, K.S. Dimmer, and B. Kornmann. 2017. Vps13-Mcp1 interact at vacuole-mitochondria interfaces and bypass ER-mitochondria contact sites. *Journal of Cell Biology*. 216: 3219-3229.

Kawano-Kawada, M., Y. Kakinuma, and T. Sekito. 2018. Transport of Amino Acids across the Vacuolar Membrane of Yeast: Its Mechanism and Physiological Role. *Biological & pharmaceutical bulletin*. 41:1496-1501.

Kiebish, M.A., K. Yang, X. Liu, D.J. Mancuso, S. Guan, Z. Zhao, H.F. Sims, R. Cerqua, W.T. Cade, X. Han, and R.W. Gross. 2013. Dysfunctional cardiac mitochondrial bioenergetic, lipidomic, and signaling in a murine model of Barth syndrome. *Journal of Lipid Research*. 54:1312-1325.

Kingsbury, J.M., N.D. Sen, and M.E. Cardenas. 2015. Branched-Chain Aminotransferases Control TORC1 Signaling in Saccharomyces cerevisiae. *PLoS genetics*. 11:e1005714.

Kispal, G., H. Steiner, D.A. Court, B. Rolinski, and R. Lill. 1996. Mitochondrial and cytosolic branched-chain amino acid transaminases from yeast, homologs of the myc oncogene-regulated Eca39 protein. *The Journal of biological chemistry*. 271:24458-24464.

Klecker, T., S. Bockler, and B. Westermann. 2014. Making connections: interorganelle contacts orchestrate mitochondrial behavior. *Trends in cell biology*. 24:537-545.

Kornmann, B., E. Currie, S.R. Collins, M. Schuldiner, J. Nunnari, J.S. Weissman, and P. Walter. 2009. An ER-mitochondria tethering complex revealed by a synthetic biology screen. *Science*. 325:477-481.

Krüger, V., M. Deckers, M. Hildenbeutel, M. van der Laan, M. Hellmers, C. Dreker, M. Preuss, J.M. Herrmann, P. Rehling, R. Wagner, and M. Meinecke. 2012. The Mitochondrial Oxidase Assembly Protein1 (Oxa1) Insertase Forms a Membrane Pore in Lipid Bilayers. *Journal of Biological Chemistry*. 287:33314-33326.

Kühlbrandt, W. 2015. Structure and function of mitochondrial membrane protein complexes. *BMC Biology*. 13:89.

Kumar, N., M. Leonzino, W. Hancock-Cerutti, F.A. Horenkamp, P. Li, J.A. Lees, H. Wheeler, K.M. Reinisch, and P. De Camilli. 2018. VPS13A and VPS13C are lipid transport proteins differentially localized at ER contact sites. *Journal of Cell Biology*. 217:3625-3639.

Lahiri, S., J.T. Chao, S. Tavassoli, A.K. Wong, V. Choudhary, B.P. Young, C.J. Loewen, and W.A. Prinz. 2014. A conserved endoplasmic reticulum membrane protein complex (EMC) facilitates phospholipid transfer from the ER to mitochondria. *PLoS Biology*. 12:e1001969.

Lang, A.B., A.T.J. Peter, P. Walter, and B. Kornmann. 2015. ER–mitochondrial junctions can be bypassed by dominant mutations in the endosomal protein Vps13. *The Journal of Cell Biology*. 210:883-890.

Lange, C., J.H. Nett, B.L. Trumpower, and C. Hunte. 2001. Specific roles of protein-phospholipid interactions in the yeast cytochrome bc1 complex structure. *EMBO Journal*. 20:6591-6600.

Lill, R., K. Diekert, A. Kaut, H. Lange, W. Pelzer, C. Prohl, and G. Kispal. 1999. The essential role of mitochondria in the biogenesis of cellular iron-sulfur proteins. *Biological chemistry*. 380:1157-1166.

Liu, L., D. Feng, G. Chen, M. Chen, Q. Zheng, P. Song, Q. Ma, C. Zhu, R. Wang, W. Qi, L. Huang, P. Xue, B. Li, X. Wang, H. Jin, J. Wang, F. Yang, P. Liu, Y. Zhu, S. Sui, and Q. Chen. 2012. Mitochondrial outer-membrane protein FUNDC1 mediates hypoxia-induced mitophagy in mammalian cells. *Nature cell biology*. 14:177-185.

Ma, L., F.M. Vaz, Z. Gu, R.J.A. Wanders, and M.L. Greenberg. 2004. The Human TAZ Gene Complements Mitochondrial Dysfunction in the Yeast taz1Δ Mutant: IMPLICATIONS FOR BARTH SYNDROME. *Journal of Biological Chemistry*. 279:44394-44399.

Marbois, B., P. Gin, M. Gulmezian, and C.F. Clarke. 2009. The Yeast Coq4 Polypeptide Organizes a Mitochondrial Protein Complex Essential for Coenzyme Q Biosynthesis. *Biochimica et biophysica acta*. 1791:69-75.

Marbois, B., L.X. Xie, S. Choi, K. Hirano, K. Hyman, and C.F. Clarke. 2010. para-Aminobenzoic acid is a precursor in coenzyme Q6 biosynthesis in Saccharomyces cerevisiae. *The Journal of biological chemistry*. 285:27827-27838.

Matus-Ortega, M.G., C.A. Cárdenas-Monroy, O. Flores-Herrera, G. Mendoza-Hernández, M. Miranda, B. González-Pedrajo, H. Vázquez-Meza, and J.P. Pardo. 2015. New complexes containing the internal alternative NADH dehydrogenase (Ndi1) in mitochondria of Saccharomyces cerevisiae. *Yeast*. 32:629-641.

McKenzie, M., M. Lazarou, D.R. Thorburn, and M.T. Ryan. 2006. Mitochondrial respiratory chain supercomplexes are destabilized in Barth Syndrome patients. *Journal of molecular biology*. 361:462-469.

Merkwirth, C., and T. Langer. 2008. Mitofusin 2 builds a bridge between ER and mitochondria. *Cell*. 135:1165-1167.

Mourier, A., E. Motori, T. Brandt, M. Lagouge, I. Atanassov, A. Galinier, G. Rappl, S. Brodesser, K. Hultenby, C. Dieterich, and N.G. Larsson. 2015. Mitofusin 2 is required to maintain mitochondrial coenzyme Q levels. *Journal of Cell Biology*. 208:429-442.

Murley, A., L.L. Lackner, C. Osman, M. West, G.K. Voeltz, P. Walter, and J. Nunnari. 2013. ER-associated mitochondrial division links the distribution of mitochondria and mitochondrial DNA in yeast. *eLife*. 2:e00422.

Neupert, W., and J.M. Herrmann. 2007. Translocation of proteins into mitochondria. *Annual Review of Biochemistry*. 76:723-749.

Nguyen, T.T., A. Lewandowska, J.Y. Choi, D.F. Markgraf, M. Junker, M. Bilgin, C.S. Ejsing, D.R. Voelker, T.A. Rapoport, and J.M. Shaw. 2012. Gem1 and ERMES do not directly affect phosphatidylserine transport from ER to mitochondria or mitochondrial inheritance. *Traffic*. 13:880-890.

Okamoto, K., and J.M. Shaw. 2005. Mitochondrial morphology and dynamics in yeast and multicellular eukaryotes. *Annual review of genetics*. 39:503-536.

Osman, C., M. Haag, C. Potting, J. Rodenfels, P.V. Dip, F.T. Wieland, B. Brugger, B. Westermann, and T. Langer. 2009. The genetic interactome of prohibitins: coordinated control of cardiolipin and phosphatidylethanolamine by conserved regulators in mitochondria. *Journal of Cell Biology*. 184:583-596.

Park, J.S., M.K. Thorsness, R. Policastro, L.L. McGoldrick, N.M. Hollingsworth, P.E. Thorsness, and A.M. Neiman. 2016. Yeast Vps13 promotes mitochondrial function and is localized at membrane contact sites. *Molecular biology of the cell*. 27:2435-2449.

Pfeiffer, K., V. Gohil, R.A. Stuart, C. Hunte, U. Brandt, M.L. Greenberg, and H. Schagger. 2003. Cardiolipin stabilizes respiratory chain supercomplexes. *The Journal of biological chemistry*. 278:52873-52880.

Pizzo, P., and T. Pozzan. 2007. Mitochondria-endoplasmic reticulum choreography: structure and signaling dynamics. *Trends in cell biology*. 17:511-517.

Reidenbach, A.G., Z.A. Kemmerer, D. Aydin, A. Jochem, M.T. McDevitt, P.D. Hutchins, J.L. Stark, J.A. Stefely, T. Reddy, A.S. Hebert, E.M. Wilkerson, I.E. Johnson, C.A. Bingman, J.L. Markley, J.J. Coon, M. Dal Peraro, and D.J. Pagliarini. 2018. Conserved Lipid and Small-Molecule Modulation of COQ8 Reveals Regulation of the Ancient Kinase-like UbiB Family. *Cell chemical biology*. 25:154-165.e111.

Sauerwald, J., T. Jores, M. Eisenberg-Bord, S.G. Chuartzman, M. Schuldiner, and D. Rapaport. 2015. Genome-Wide Screens in Saccharomyces cerevisiae Highlight a Role for Cardiolipin in Biogenesis of Mitochondrial Outer Membrane Multispan Proteins. *Molecular and cellular biology*. 35:3200-3211.

Scheffler, I.E. 2001. A century of mitochondrial research: achievements and perspectives. *Mitochondrion*. 1:3-31.

Schlame, M., and M. Ren. 2006. Barth syndrome, a human disorder of cardiolipin metabolism. *FEBS letters*. 580:5450-5455.

Schlame, M., M. Ren, Y. Xu, M.L. Greenberg, and I. Haller. 2005. Molecular symmetry in mitochondrial cardiolipins. *Chemistry and physics of lipids*. 138:38-49.

Schlame, M., D. Rua, and M.L. Greenberg. 2000. The biosynthesis and functional role of cardiolipin. *Progress in lipid research*. 39:257-288.

Schlame, M., J.A. Towbin, P.M. Heerdt, R. Jehle, S. DiMauro, and T.J. Blanck. 2002. Deficiency of tetralinoleoyl-cardiolipin in Barth syndrome. *Annals of neurology*. 51:634-637.

Sickmann, A., J. Reinders, Y. Wagner, C. Joppich, R. Zahedi, H.E. Meyer, B. Schonfisch, I. Perschil, A. Chacinska, B. Guiard, P. Rehling, N. Pfanner, and C. Meisinger. 2003. The proteome of Saccharomyces cerevisiae mitochondria. *Proceedings of the National Academy of Sciences of the United States of America*. 100:13207-13212.

Sinzel, M., T. Tan, P. Wendling, H. Kalbacher, C. Özbalci, X. Chelius, B. Westermann, B. Brügger, D. Rapaport, and K.S. Dimmer. 2016. Mcp3 is a novel mitochondrial outer membrane protein that follows a unique IMP-dependent biogenesis pathway. *EMBO reports*. 17:965-981.

Stiller, Sebastian B., J. Höpker, S. Oeljeklaus, C. Schütze, Sandra G. Schrempp, J. Vent-Schmidt, Susanne E. Horvath, Ann E. Frazier, N. Gebert, M. van der Laan, M. Bohnert, B. Warscheid, N. Pfanner, and N. Wiedemann. 2016. Mitochondrial OXA Translocase Plays a Major Role in Biogenesis of Inner-Membrane Proteins. *Cell Metabolism*. 23:901-908.

Takpho, N., D. Watanabe, and H. Takagi. 2018. Valine biosynthesis in Saccharomyces cerevisiae is regulated by the mitochondrial branched-chain amino acid aminotransferase Bat1. *Microbial cell (Graz, Austria)*. 5:293-299.

Tamura, Y., H. Sesaki, and T. Endo. 2014. Phospholipid transport via mitochondria. *Traffic (Copenhagen, Denmark)*. 15:933-945.

Tan, T., C. Özbalci, B. Brügger, D. Rapaport, and K.S. Dimmer. 2013. Mcp1 and Mcp2, two novel proteins involved in mitochondrial lipid homeostasis. *Journal of Cell Science*. 126:3563-3574.

Tedesco, L., G. Corsetti, C. Ruocco, M. Ragni, F. Rossi, M.O. Carruba, A. Valerio, and E. Nisoli. 2018. A specific amino acid formula prevents alcoholic liver disease in rodents. *American journal of physiology. Gastrointestinal and liver physiology*. 314: g566-g582.

Tran, U.C., and C.F. Clarke. 2007. Endogenous Synthesis of Coenzyme Q in Eukaryotes. *Mitochondrion*. 7:S62-S71.

Valianpour, F., R.J. Wanders, H. Overmars, P. Vreken, A.H. Van Gennip, F. Baas, B. Plecko, R. Santer, K. Becker, and P.G. Barth. 2002. Cardiolipin deficiency in X-linked cardioskeletal myopathy and neutropenia (Barth syndrome, MIM 302060): a study in cultured skin fibroblasts. *The Journal of pediatrics*. 141:729-733.

van Meer, G., D.R. Voelker, and G.W. Feigenson. 2008. Membrane lipids: where they are and how they behave. *Nature reviews. Molecular cell biology*. 9:112-124.

Vance, J.E. 1990. Phospholipid synthesis in a membrane fraction associated with mitochondria. *Journal of Biology Chemistry*. 265:7248-7256.

Vatrinet, R., G. Leone, M. De Luise, G. Girolimetti, M. Vidone, G. Gasparre, and A.M. Porcelli. 2017. The α-ketoglutarate dehydrogenase complex in cancer metabolic plasticity. *Cancer & Metabolism*. 5:3.

Voelker, D.R. 1990. Lipid transport pathways in mammalian cells. *Experientia*. 46:569-579.

Voss, C., S. Lahiri, B.P. Young, C.J. Loewen, and W.A. Prinz. 2012. ER-shaping proteins facilitate lipid exchange between the ER and mitochondria in S. cerevisiae. *Journal of Cell Science*. 125:4791-4799.

Vreken, P., F. Valianpour, L.G. Nijtmans, L.A. Grivell, B. Plecko, R.J. Wanders, and P.G. Barth. 2000. Defective remodeling of cardiolipin and phosphatidylglycerol in Barth syndrome. *Biochemical and biophysical research communications*. 279:378-382.

Wenz, T., R. Hielscher, P. Hellwig, H. Schägger, S. Richers, and C. Hunte. 2009. Role of phospholipids in respiratory cytochrome bc1 complex catalysis and supercomplex formation. *Biochimica et Biophysica Acta (BBA) - Bioenergetics*. 1787:609-616.

Westermann, B. 2010. Mitochondrial fusion and fission in cell life and death. *Nature reviews. Molecular cell biology*. 11:872-884.

Whited, K., M.G. Baile, P. Currier, and S.M. Claypool. 2013. Seven functional classes of Barth syndrome mutation. *Human molecular genetics*. 22:483-492.

Wu, W., C. Lin, K. Wu, L. Jiang, X. Wang, W. Li, H. Zhuang, X. Zhang, H. Chen, S. Li, Y. Yang, Y. Lu, J. Wang, R. Zhu, L. Zhang, S. Sui, N. Tan, B. Zhao, J. Zhang, L. Li, and D. Feng. 2016. FUNDC1 regulates mitochondrial dynamics at the ER–mitochondrial contact site under hypoxic conditions. *The EMBO Journal*. 35:1368-1384.

Xie, L.X., E.J. Hsieh, S. Watanabe, C.M. Allan, J.Y. Chen, U.C. Tran, and C.F. Clarke. 2011. Expression of the human atypical kinase ADCK3 rescues coenzyme Q biosynthesis and phosphorylation of Coq polypeptides in yeast coq8 mutants. *Biochimica et Biophysica Acta (BBA) - Molecular and Cell Biology of Lipids*. 1811:348-360.

Xu, Y., C.K. Phoon, B. Berno, K. D'Souza, E. Hoedt, G. Zhang, T.A. Neubert, R.M. Epand, M. Ren, and M. Schlame. 2016. Loss of protein association

causes cardiolipin degradation in Barth syndrome. *Nature chemical biology*. 12:641-647.

Ye, C., W. Lou, Y. Li, I.A. Chatzispyrou, M. Huttemann, I. Lee, R.H. Houtkooper, F.M. Vaz, S. Chen, and M.L. Greenberg. 2014. Deletion of the cardiolipin-specific phospholipase Cld1 rescues growth and life span defects in the tafazzin mutant: implications for Barth syndrome. *The Journal of biological chemistry*. 289:3114-3125.

Zhang, M., E. Mileykovskaya, and W. Dowhan. 2002. Gluing the respiratory chain together. Cardiolipin is required for supercomplex formation in the inner mitochondrial membrane. *The Journal of biological chemistry*. 277:43553-43556.

Zhang, M., E. Mileykovskaya, and W. Dowhan. 2005. Cardiolipin is essential for organization of complexes III and IV into a supercomplex in intact yeast mitochondria. *The Journal of biological chemistry*. 280:29403-29408.

Zinser, E., C.D. Sperka-Gottlieb, E.V. Fasch, S.D. Kohlwein, F. Paltauf, and G. Daum. 1991. Phospholipid synthesis and lipid composition of subcellular membranes in the unicellular eukaryote Saccharomyces cerevisiae. *Journal of bacteriology*. 173:2026-2034.

10. Acknowledgements

Firstly, I would like to express my sincere gratitude to my advisor Prof. Dr. Doron Rapaport for the opportunity to do research in his lab. For his continuous support, for his patience and immense knowledge. His concise guidance encouraged me in my research endeavors providing me insightful values to develop as a researcher. I would like to extend my gratitude to my thesis advisory committee, Prof. Dr. Ralf-Peter Jansen and Prof. Dr. Tassula Proikas-Cezanne for their valuable suggestions. Furthermore, I would like to thank Prof. Dr. Gabriele Dodt for her time and to be part of my PhD committee. Special thanks also go to Prof. Dr. Maya Schuldiner for her warm welcome in her lab, for all the scientific insights and the intensive support.

I am extremely fortunate for the helpful discussions and the pleasant time with a fantastic set of lab colleagues. To Elena, for her excellent technical guidance and for teaching me so many German words. To Daniela, for sharing late experiments, 'southern european english' and for being Dianiela! To Janani, for being my big sister in Tübingen and for always correcting my English. To Tobias, for his great suggestions throughout my PhD, for being always available and happy to help, and for his nice jokes, specially the stupid ones. To Ravi, for his constant enthusiasm, and for organizing so many enjoyable times with great food, and chats. To Bogdan, for always looking after my plants even when I am at home. To Moni, for all the sugar rush. To Kai, for countless scientific help and for being Nikolaus. To all the current and former lab members for the great working atmosphere: Layla, for all the healthy-oriented support and also nice conversations, Klaudia, for all the heavy squats and more, Jialin, for all the optimism you bring, Fenja, for all the laughs and for always singing in the lab, and Anasuya for being jolly and dedicated. Also to Thomas and Hoda.

Special thanks go to my Tübinger-crew Francesco and Prateek, not only for walking along this journey from the day 1, but specially for the support during the cloudy days. Thanks also to Inês, João, Aarón, Kushal, Ursula and many others! Finally, from my heart to my parents and sister for believing even when I didn't. My dearest aunt Helena for all the complicity and support.

11. Appendix

a) Accepted papers

1. A. T., Peter, B. Herrmann, D. Antunes, D. Rapaport, K. S. Dimmer, and B. Kornmann. (2017). Vps13-Mcp1 interact at vacuole-mitochondria interfaces and bypass ER-mitochondria contact sites. *Journal of Cell Biology*, 216: 3219-29.

 doi:10.1083/jcb.201610055

2. D. Antunes, A. Chowdhury, A. Aich, S. Saladi, N. Harpaz, M. Stahl, M. Schuldiner, J. Herrmann, P. Rehling, and D. Rapaport, (2018). Overexpression of branched-chain amino acid aminotransferases rescues the growth defects of cells lacking the Barth Syndrome related gene *TAZ1*. *Journal of Molecular Medicine*. (*in press*)

 doi: 10.1007/s00109-018-172

b) Manuscripts in revision

3. M. Eisenberg-Bord*, H. Tsui*, D. Antunes*, L. Fernández-del-Río*, C. Dunn, D. Rapaport, C. Clarke, and M. Schuldiner. (2018). ER-Mitochondria Encounter Structure (ERMES) coordinates coenzyme Q biosynthesis. *Contact*. (*in revision*)
   * equal contributors

Vps13-Mcp1 interact at vacuole–mitochondria interfaces and bypass ER–mitochondria contact sites

Arun T. John Peter,[1] Beatrice Herrmann,[1] Diana Antunes,[2] Doron Rapaport,[2] Kai Stefan Dimmer,[2] and Benoît Kornmann[1]

[1]ETH Zürich, Institute of Biochemistry, Zürich, Switzerland
[2]Interfaculty Institute of Biochemistry, University of Tübingen, Tübingen, Germany

Membrane contact sites between endoplasmic reticulum (ER) and mitochondria, mediated by the ER–mitochondria encounter structure (ERMES) complex, are critical for mitochondrial homeostasis and cell growth. Defects in ERMES can, however, be bypassed by point mutations in the endosomal protein Vps13 or by overexpression of the mitochondrial protein Mcp1. How this bypass operates remains unclear. Here we show that the mitochondrial outer membrane protein Mcp1 functions in the same pathway as Vps13 by recruiting it to mitochondria and promoting its association to vacuole–mitochondria contacts. Our findings support a model in which Mcp1 and Vps13 work as functional effectors of vacuole–mitochondria contact sites, while tethering is mediated by other factors, including Vps39. Tethered and functionally active vacuole–mitochondria interfaces then compensate for the loss of ERMES-mediated ER–mitochondria contact sites.

Introduction

In eukaryotic cells, exchange of membrane lipids between organelles is critical for sustaining their biogenesis and function. How lipids are exchanged with organelles that are not part of the vesicular transport network, such as mitochondria, remains unclear. Recent research stresses the importance of membrane contact sites (MCSs), zones of close proximity (10–30 nm) between two organellar membranes, as a means of nonvesicular lipid exchange between organelles (Helle et al., 2013; Phillips and Voeltz, 2016). In yeast and other fungi, an MCS between the ER and mitochondria is constituted by the ER–mitochondria encounter structure (ERMES). This protein complex consists of an ER transmembrane protein, Mmm1; a mitochondrial outer membrane protein, Mdm10; and two peripheral membrane proteins, Mdm12 and Mdm34 (Kornmann et al., 2009; Ellenrieder et al., 2016). ERMES tethers the ER to mitochondria, and three of its four core components bind lipid molecules through a tubular lipid–binding domain. Tubular lipid domains can extract lipid molecules from a membrane, shelter them from the cytosol, and deliver them to another membrane, thus acting as membrane lipid transporters (Kopec et al., 2010; Schauder et al., 2014; AhYoung et al., 2015; Jeong et al., 2016).

Despite this seemingly crucial role in mitochondrial membrane biogenesis, ERMES deficiency is not lethal and does not completely block lipid delivery to mitochondria (Kornmann et al., 2009). This is likely due to the existence of redundant pathways. One such pathway involves the formation of an MCS between the mitochondria and the vacuole. This MCS can be readily evidenced by the overexpression of the vacuolar fusion factor Vps39, which leads to the formation of extensive vacuole and mitochondria patches (vCLAMPs; Elbaz-Alon et al., 2014; Hönscher et al., 2014). The tethering of these two organelles is mediated by Vps39, the vacuolar Rab GTPase Ypt7, and a hypothetical mitochondrial factor. Simultaneous inactivation of ERMES and Vps39 is lethal and strongly reduces mitochondrial lipid import (Elbaz-Alon et al., 2014).

Therefore, a likely role for the ER–mitochondria MCSs is to deliver lipids to mitochondria from the ER, a function that is shared by vacuole–mitochondria MCSs. However, the compensation by redundant pathways is only partial because mutations that impair ERMES lead to a host of mitochondrial phenotypes. This suggests that redundant pathways are able to provide lipids to the mitochondria but are probably insufficient to completely compensate for the loss of ERMES.

Interestingly, the phenotypes associated with ERMES deficiency can be reverted by the overexpression of two mitochondrial proteins, Mcp1 and Mcp2, or by single amino acid substitutions in Vps13 (Tan et al., 2013; Lang et al., 2015; Park et al., 2016). Both Mcp1 and Mcp2 are integral membrane proteins that reside on the outer and inner mitochondrial membrane, respectively, and their molecular functions remain unclear. Vps13 is a conserved ∼360-kD protein that localizes to endosomes, to vacuole–mitochondria and mitochondria–endosome contact sites, and, upon glucose starvation, to the nuclear–vacuole junctions (Lang et al., 2015; Park et al., 2016). *MCP1*, *MCP2*, and

Correspondence to Benoît Kornmann: benoit.kornmann@bc.biol.ethz.ch

Abbreviations used: ERMES, ER–mitochondria encounter structure; MCS, membrane contact site; PH, Pleckstrin homology; PI3K, phosphatidylinositol-3 kinase; PK, proteinase K; SD, synthetic dextrose; ts, temperature-sensitive; vCLAMP, vacuole and mitochondria patch.

The Rockefeller University Press
J. Cell Biol. Vol. 216 No. 10 3219–3229
https://doi.org/10.1083/jcb.201610055

VPS13 are all synthetically lethal with the loss of ERMES, indicating that they function in ERMES-redundant pathways.

Together, this suggests that ERMES-redundant pathways can be boosted to render ERMES entirely dispensable. Yet whether Mcp1, Mcp2, and Vps13 function at mitochondria–vacuole contacts is unclear. The fact that *VPS13* suppressor allele can exert its suppressive functions only in the presence of Vps39 and Mcp1, but independent of Mcp2 (Lang et al., 2015), suggests that Vps13, Mcp1, and Vps39 might constitute one coherent unit to mediate the tethering and function of vacuole–mitochondria MCSs and ensure cell survival in the absence of the ERMES complex. Here we investigate the relationship among Mcp1, Vps13, and Vps39. We show that Mcp1 recruits Vps13 to mitochondria and vCLAMPs and that this recruitment underlies the functionality of vacuole–mitochondria contacts in the ERMES bypass pathway. Our data support a model in which Vps39 and its binding partners establish tethering between mitochondria and vacuole, whereas Mcp1 and Vps13 participate in the functional output of mitochondria–vacuole contact sites to restore cellular growth and homeostasis.

Results

To address in an unbiased manner how Vps13 is involved in bypassing ERMES function, we inspected two published genetic interaction datasets (Costanzo et al., 2010; Hoppins et al., 2011). Synthetic genetic screens involve the creation of double-deletion strains, monitoring their growth, and computing genetic interaction scores. A highly powerful way to analyze genetic interaction data is to compute correlations between profiles of genetic interactions (Collins et al., 2010) in which strong positive correlations are typically indicative of a common function. According to Costanzo et al. (2010), the gene that best correlated with *VPS13* was *VPS38*, and the second best was *VPS30* (Fig. 1 A). In the dataset of Hoppins et al. (2011), which did not contain *VPS38*, the best-correlated gene was *VPS30* (Fig. 1 A). Both Vps30 and Vps38 are part of the phosphatidylinositol-3 kinase (PI3K) complex II, together with Vps34 (Kihara et al., 2001), which was absent from both datasets. The PI3K complex II is important for vacuolar protein sorting and is targeted to endosomes and vacuole by Vps38 (Obara et al., 2006). The link between Vps38/Vps30 and Vps13 in protein sorting along the endocytic pathway is further supported by a recent study showing that Vps13 is necessary for transport between trans-Golgi and late endosomes (De et al., 2017). Moreover, a hidden Markov model–based homology prediction uncovered a putative Pleckstrin homology (PH)–like domain at the extreme C terminus of Vps13 (Fig. 1 B and Alignments S1–S3; Söding et al., 2005; Fidler et al., 2016). The strong correlation with PI3K complex II subunits along with the presence of a PH-like domain at the C terminus of Vps13 suggests a nexus between Vps13 and the endocytic pathway via phosphatidylinositol-3-phosphate. Indeed, Vps13 localizes to Vps38-positive early endosomes (Huh et al., 2003; Fig. 2 A).

We hypothesized that Vps38 may recruit Vps13 to the endosomes either by itself or via phosphatidylinositol-3-phosphate. To directly test this idea, we deleted *vps38* in a strain expressing a functional GFP-tagged Vps13 (Vps13^GFP; Lang et al., 2015). To our surprise, Vps13 remained on FM4-64-positive, defective endosomes found in *vps38Δ* cells (Fig. 1 C; Luo and Chang, 1997). This observation suggested that Vps13 requires

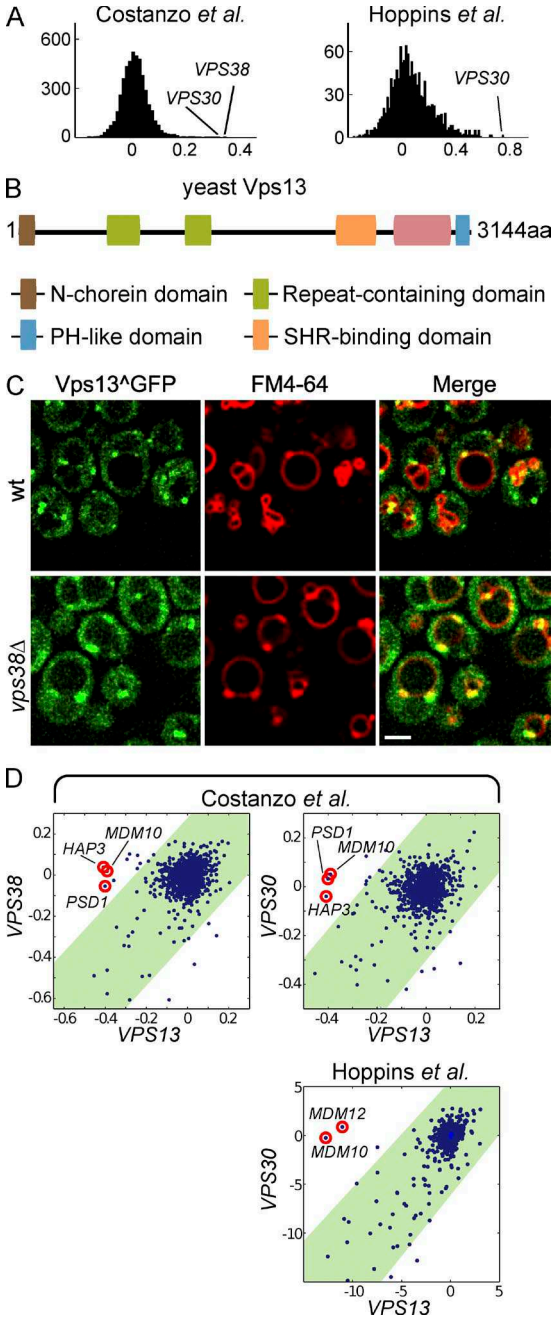

Figure 1. **The function of Vps13 on endosomes is unlinked to its function in ERMES suppression.** (A) Correlation analysis of the genetic interactions of *VPS13*. Correlation coefficients were calculated for the genetic interaction profile of *VPS13* and all genes present in the Costanzo et al. (2010) dataset (left) and Hoppins et al. (2011) dataset (right). (B) Domain architecture of yeast Vps13. Repeat-containing domains are mapped according to Velayos-Baeza et al. (2004). Predictions were made using a hidden Markov model–based homology search (HHPred; Söding et al., 2005). A PH-like domain was detected at the C terminus (3,037–3,133 aa) when searched against the Protein Data Bank. (C) Vps13 remains on endosomes in *vps38Δ* cells. Localization of GFP-tagged endogenous Vps13 in WT and *vps38Δ* cells. Vacuoles and endosomes are stained with FM4-64. Bar, 2 µm. (D) Genetic interaction profile of *VPS13* (x axis) plotted against *VPS38 and VPS30* (y axis; left and middle) using data from Costanzo et al. (2010). (Right) The profile of *VPS13* versus *VPS30* using data from Hoppins et al. (2011). The correlation in the genetic interaction profiles of *VPS13* with that of both *VPS30* and *VPS38* is highlighted by the green area. Genes encoding ERMES members as well as *PSD1* and *HAP3* are circled in red when present.

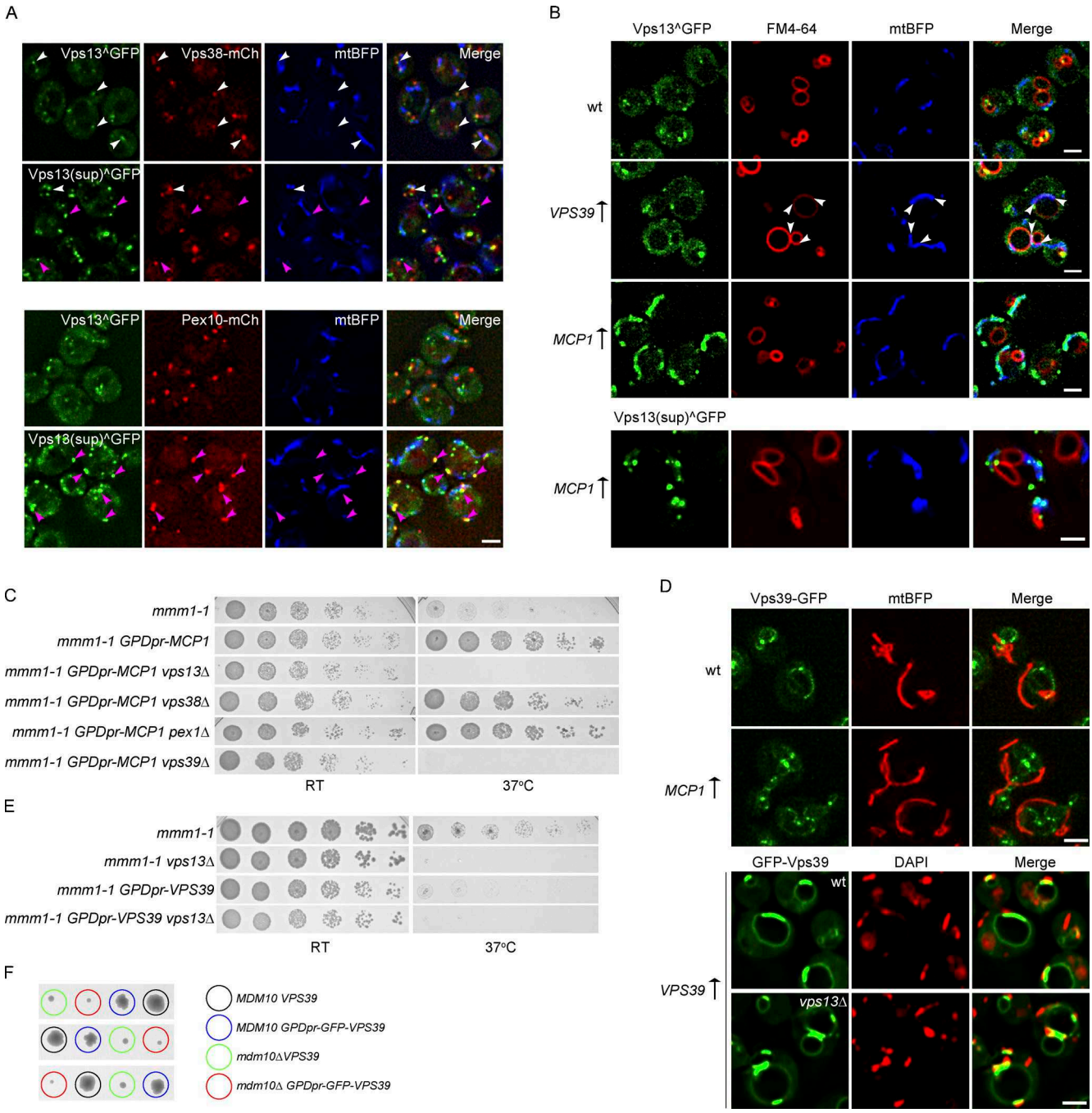

Figure 2. **Relationship between Vps13 and suppressors of ERMES defects.** (A, top) Localization of internally GFP-tagged Vps13 (WT or suppressor; Vps13 bearing the internal GFP tag that retains its functionality is depicted as Vps13^GFP) with mCherry-tagged Vps38 expressed from endogenous promoters. Mitochondria are marked by a plasmid-encoded, matrix-targeted BFP (mtBFP). White and pink arrowheads mark Vps13 foci that do or do not colocalize with Vps38, respectively. (Bottom) Localization of GFP-tagged Vps13 (WT or suppressor) with mCherry-tagged Pex10 expressed from endogenous promoters. Pink arrowheads point at Vps13 foci that colocalize with peroxisomes marked by Pex10-mCherry. Bar, 2 µm. (B) Localization of endogenous Vps13 under normal conditions or upon overexpression of Vps39 or Mcp1 (*VPS39*↑ and *MCP1*↑, respectively). Vacuoles are stained with FM4-64. Bars, 2 µm. Arrowheads indicate vacuole–mitochondria patches (vCLAMPs). The Vps13 suppressor version is expressed from a low-copy plasmid, under the control of its native promoter. (C) Mcp1-mediated growth rescue requires both Vps13 and Vps39. The ts strain *mmm1-1* with the indicated genotypes was spotted as serial dilutions on yeast extract peptone dextrose plates and grown either at RT or 37°C. (D, top) Maximum intensity projection of five Z-sections showing the localization of endogenous GFP-tagged Vps39 (green) in WT and Mcp1-overexpressing cells. Mitochondria are marked by mtBFP (shown in red). (Bottom) WT or *vps13Δ* cells expressing GFP-tagged Vps39, from the strong GPD promoter, were stained with DAPI to visualize mitochondrial DNA (shown in red). Bars, 2 µm. (E) Vps39 overexpression does not rescue temperature-induced dysfunction of ERMES subunit Mmm1. Strains with the indicated genotype were spotted as in C. (F) Tetrad dissection of sporulated *MDM10/mdm10Δ VPS39/GPDpr-GFP-VPS39* diploids. Genotype of individual spores is indicated with color-coded circles.

neither Vps38 nor phosphatidylinositol-3-phosphate, made by PI3K complex II, to localize to endosomes. Furthermore, the analyses of genetic interaction datasets also showed that despite the strong similarity in the genetic interaction profiles of *VPS13*, *VPS38*, and *VPS30*, several genes had synthetic genetic interactions with *VPS13* only (Fig. 1 D). These genes encode members of the ERMES complex (*MDM10* and *MDM12*) and other factors associated with mitochondrial function, including *PSD1*, encoding phosphatidylserine decarboxylase, which makes phosphatidylethanolamine from phosphatidylserine at the inner mitochondrial membrane, and HAP3, a transcriptional regulator of respiratory gene expression (Mattoon et al., 1990). Collectively, we conclude that Vps13 functions in the endocytic pathway in a way that correlates with PI3K complex II but that this function is probably separable from its role in substituting the functions of the ERMES complex.

Because Vps13 function in the ERMES bypass pathway appeared disconnected to its role at the endosome, we reasoned that the ability of Vps13 to suppress ERMES function might be linked to an alternative subcellular localization. We colocalized Vps13 with different organellar markers in various ERMES-suppressing conditions. We assessed Vps13 localization when it bore a suppressing mutation (L1627S), when vacuole–mitochondria MCSs were exacerbated into vCLAMPs by Vps39 overexpression, and upon Mcp1 overexpression. As expected, in normal conditions, a majority (60 ± 1.7%, mean ± SEM) of the Vps13 foci colocalized with the endosomal marker Vps38 (Fig. 2 A, top). In contrast, a much smaller fraction (17.5 ± 0.8%) of Vps13 bearing the suppressor mutation localized to Vps38-positive foci. To address the localization of remaining foci, we performed colocalization with different organellar markers (not depicted) and found that these foci mostly corresponded to peroxisomes (Fig. 2 A, bottom). Indeed, in contrast to 6.8 ± 1.6% of WT Vps13 foci, 41.1 ± 1.23% of the Vps13 suppressor foci localized to Pex10-positive peroxisomes. We also observed that Pex10-positive peroxisomes only seldom (0.43 ± 0.28%) colocalized with Vps38-positive endosomes (Fig. S1). Upon Vps39 overexpression, there was no change in the localization of Vps13 (Fig. 2 B, *VPS39*↑), even though large vCLAMPs, indicative of vCLAMP formation, could be seen (arrowheads). Intriguingly, when Mcp1 was overexpressed, Vps13 relocalized to mitochondria. The relocalization was also observed for the suppressor allele, but in a more dotted fashion (Fig. 2 B, *MCP1*↑). Thus, whereas a suppressor mutation induces the relocalization of Vps13 to peroxisomes, Mcp1 overexpression induces the relocalization of both the Vps13 WT and suppressor mutant to mitochondria. Of note, vCLAMP induction has largely no effect on Vps13 localization.

As the ability of Mcp1 to suppress ERMES defects was in line with the dramatic localization phenotype of Vps13, we tested whether Mcp1 overexpression required *VPS13* to bypass ERMES function. To this end, we used the *mmm1-1* temperature-sensitive (ts) strain, which manifests the typical slow-growth phenotype of ERMES mutants at the restrictive temperature only. Overexpression of Mcp1 in this strain rescued the growth phenotype at 37°C, in accordance with published data (Tan et al., 2013). However, deletion of *vps13* completely abolished the ability of *MCP1* overexpression to rescue the loss of *MMM1* function (Fig. 2 C), suggesting that Vps13 recruitment to mitochondria is a critical event in the ERMES bypass pathway.

We also found that Vps38 was necessary neither for the Vps13- nor for the Mcp1-mediated rescue (Fig. 2 C and Fig. S2), confirming our earlier conclusion that Vps38 is not linked to the function of Vps13 in rescuing the loss of ERMES. (Fig. 1 D).

Our colocalization analysis also suggested that peroxisomes could be involved in the bypass pathway (Fig. 2 A). To test this genetically, we deleted pex1 in the *mmm1-1* ts strain overexpressing Mcp1. Cells lacking *PEX1*, a critical factor for peroxisomal biogenesis, lack functional peroxisomes and harbor only peroxisomal "ghosts" that do not have any matrix proteins (Knoops et al., 2015). Interestingly, Mcp1 overexpression rescued loss of *MMM1* function even in the absence of *pex1* (Fig. 2 C), indicating that functional peroxisomes are not necessary to bypass ERMES functions. Therefore, it is possible that the localization of the suppressor mutant to peroxisomes is an epiphenomenon unrelated to ERMES suppression.

Finally, we found that Vps39 was necessary for Mcp1 to rescue the *mmm1-1* growth defect (Fig. 2 C). This is consistent with the fact that Vps39 is also necessary for suppressor alleles of Vps13 to exert their suppressive function (Lang et al., 2015). However, Mcp1 overexpression, like the expression of Vps13 suppressor alleles (Lang et al., 2015), did not lead to visible Vps39-mediated vCLAMP formation (Fig. 2 D, top), and vCLAMP formation upon Vps39 overexpression was not dependent on the presence of Vps13 (Fig. 2 D, bottom). We then wondered if Vps39 overexpression-mediated vCLAMP formation was sufficient to rescue the loss of ERMES function. Because of the rapidity of suppressor accumulation in haploid strains bearing ERMES mutations, we used either a *mmm1-1* ts mutant or tetrad-dissected heterozygous diploid strains. Surprisingly, we found that vCLAMP formation mediated by Vps39 overexpression rescued neither the growth defect of a ts *mmm1-1* strain (Fig. 2 E) nor, contrary to published literature (Hönscher et al., 2014), of an *mdm10Δ* strain (Fig. 2 F). Actually, WT, *mdm10Δ*, and *mmm1-1* cells, overexpressing *VPS39* from the strong GPD promoter, grew slower than cells expressing *VPS39* from its endogenous promoter. Collectively, these results indicate that vCLAMPs induced by Vps39 overexpression are not sufficient by themselves to compensate for the loss of ERMES.

Because overexpression of Mcp1 clearly shifted most of the Vps13 signal to mitochondria, we wondered if Mcp1 might be a limiting binding partner for Vps13 on mitochondria. To address this, we coimmunoprecipitated HA-tagged Mcp1 together with either the WT or suppressor (L1627S) GFP-tagged Vps13, expressed from their endogenous promoters. We found that both the WT and suppressor versions interacted with Mcp1 (Fig. 3 A). Mcp1 is a membrane protein with five predicted transmembrane domains. Only short regions that stick out of the membrane could potentially interact with Vps13 (Fig. 3 C). To assess which part of Mcp1 interacted with Vps13, we first assessed Mcp1 topology by exposing purified mitochondria overexpressing C-terminally HA-tagged Mcp1 to increasing amounts of proteinase K (PK). We then detected protected fragments by Western blotting, using either an anti-HA antibody to detect the C terminus or an antibody raised against the N terminus of Mcp1 (aa 20–40). At small amounts of PK, both antibodies detected the appearance of fragments of 20 kD (Fig. 3 B), indicating cleavage at the level of loop 2 and an N-out, C-in conformation for Mcp1 (Fig. 3 C). Interestingly, the N-terminal fragment remained protease resistant even at large PK concentrations, suggesting either that the epitope was too close to the membrane to be accessible to PK or that this domain is tightly folded. An N-out, C-in conformation indicated that two domains could potentially interact with Vps13, namely, the

N terminus (aa 1–61) and loop 2 (aa 122–173), whereas loop 4 appeared too short to serve as a binding site. To assess if any of these fragments was binding to Vps13, we adopted a relocalization approach in which we targeted these two segments of Mcp1 to the ER (Fig. 3 D) and asked if Vps13 follows any of these segments. Strikingly, expressing the N terminus fused to an ER-targeted red fluorescent protein (mCherry–Ubc6) led to the recruitment of Vps13 to the ER. The same effect was not observed for the fusion protein containing loop 2 (Fig. 3 D). Thus, the N-terminal fragment (1–61 aa) of Mcp1 was sufficient for the binding of Vps13 and its recruitment to a foreign organelle.

Suppressor mutations identified in Vps13 all cluster to the repeat-containing domains (Lang et al., 2015; Park et al., 2016). We wondered if these domains or any other region was involved in Mcp1-mediated recruitment. To this aim, we performed a series of N- and C-terminal truncations on the endogenous Vps13 and asked if the truncated versions were still able to localize to mitochondria upon Mcp1 overexpression. Vps13 C-terminally truncated up to aa 2,599 was robustly recruited to mitochondria. Shorter truncations remained, however, mostly cytoplasmic (Fig. 3, E and F). Short N-terminal truncations destabilized the protein, such that their localization was difficult to assess. However, a larger deletion up to aa 2,247 was recruited to the mitochondria. Even though, in this case, the fluorescence levels were low, the mitochondrial localization was evident only in MCP1 overexpression conditions (Fig. 3 E, bottom). Thus, the Mcp1-binding region (aa 2,247–2,599) of Vps13 does not overlap with the region harboring suppressor mutations, in agreement with the fact that the suppressor mutation does not act by increasing Vps13/Mcp1 interaction (Fig. 3 A). Dominant suppressor mutations therefore probably act by relieving an inhibitory activity in Vps13 (Lang et al., 2015), without affecting its mitochondrial recruitment.

Having established the key elements of Mcp1-Vps13 interaction, we asked if the only function of Mcp1 in the ERM ES-bypass pathway is to recruit Vps13 to mitochondria. To test this, we constructed a minimal mitochondrial recruiting fragment by fusing aa 1–61 of Mcp1 to an outer mitochondrial membrane-targeted red fluorescent protein (mCherry–Fis1) and asked whether its expression could suppress the phenotype of the *mmm1-1* ts strain at the restrictive temperature. The expression of this construct, but not of mCherry–Fis1 alone, led to the strong recruitment of Vps13 to mitochondria (Fig. 4 A). However, the growth phenotype was not rescued at 37°C upon the loss of functional Mmm1 (Fig. 4 B). This was not due to a failure of Mcp1 (1–61 aa) to recruit Vps13 onto mitochondria in ERMES mutant conditions, as Vps13 was recruited to mitochondria even at the restrictive temperature (Fig. 4 A, right). In fact, *mmm1-1* ts strain expressing the Mcp1 (1–61 aa) construct grew worse than the nonexpressing parent, indicating that the nonfunctional fragment likely titrated Vps13 away from the functional, full-length Mcp1 (Fig. 4 B). We conclude that Vps13 recruitment to mitochondria is necessary but not sufficient to rescue the loss of ERMES function. Thus, full-length Mcp1, in addition to recruiting Vps13, plays an active role in the ERMES bypass pathway. Indeed, a hidden Markov model homology analysis (HHPred) suggested that Mcp1 might fold as a five-helix bundle, as in succinate dehydrogenase and quinol–fumarate reductases (Alignment S4), pointing to a role beyond the mere recruitment of Vps13. We used homology modeling to construct a model of MCP1. The homology started at aa 45 of Mcp1, that is, close to the first transmembrane region, and extended until the end of the protein. In the model, four histidines (H72, H114, H187, and H237) constituted two putative heme-binding domains (Fig. 4 C), as in the quinol fumarate reductase from *Wolinella succinogenes*, which served as a template for homology modeling. Mcp1 is conserved within a subgroup of ascomycetes. Therefore, to address if heme binding is a conserved feature of Mcp1, we aligned *MCP1* in several fungi. Although the homology was generally good within transmembrane domains, the presumptive heme-binding histidines were among the completely conserved amino acids, suggesting that heme binding is an important feature of Mcp1 (Fig. 4 D). Indeed, mutating histidine residues in either presumptive heme-binding domains (H187A and H237A, respectively) severely blunted the ability of Mcp1 to rescue ERMES defects when overexpressed (Fig. 4 E), without affecting Vps13 recruitment to mitochondria (Fig. 4 F). Mutating other conserved residues (P195A and G241A) yielded variable outcomes on ERMES rescue but did not affect Vps13 recruitment, as expected.

In summary, Vps13 and Mcp1 interact either directly or indirectly on the mitochondrial surface. This interaction is necessary for the ERMES bypass pathway, but merely bringing Vps13 to mitochondria is not sufficient, and presumptive heme-binding domains are important for the ERMES-rescue phenomenon.

How does this bypass work? It is logical that an MCS can be bypassed by another MCS, and in this case, vacuole–mitochondria contacts might serve as an alternative MCS. Indeed, both Vps13- and Mcp1-mediated suppression require Vps39 (Lang et al., 2015; Fig. 2 C). However, two observations challenge the idea that vacuole–mitochondria contacts are involved in ERMES suppression. First, vCLAMP formation through Vps39 overexpression does not alter Vps13 localization (Fig. 2 B). Conversely, neither the Vps13 suppressor alleles nor Mcp1 overexpression induces the formation of vCLAMPs (Lang et al., 2015; Fig. 2 D).

In an effort to resolve this paradox, we co-overexpressed Vps39 and Mcp1 in cells expressing Vps13^GFP. In this case, Vps13 was not only recruited to mitochondria by Mcp1 but was robustly enriched at Vps39 overexpression-mediated vCLAMPs (Fig. 5 A).

Discussion

Here we show that Mcp1 and Vps13 interact at vacuole–mitochondria interfaces and require Vps39 function in the ERMES-bypass pathway. What is the relationship among these three factors? Unlike the overexpression of Mcp1 or the expression of the Vps13 suppressor, the overexpression of Vps39, despite causing the formation of vCLAMPs, is incapable of reverting ERMES growth phenotype (Fig. 2, E and F), in contrast to previously reported findings (Hönscher et al., 2014). In contrast, Mcp1- and Vps13-mediated ERMES rescue happens in conditions in which vacuole–mitochondria contacts are not enlarged into vCLAMPs. These results indicate that the amount and activity of Vps13 targeted to mitochondria, but not the enhanced surface of contact between the organelles, are limiting for the output of the bypass pathway.

Vps13 is enriched at vCLAMPs only when both Vps39 and Mcp1 are co-overexpressed. This suggests that when Vps39 overexpression mediates vCLAMP formation, Vps13 fails to accumulate there, because Mcp1 is limiting for its recruitment to mitochondria. Conversely, when Mcp1 overexpression

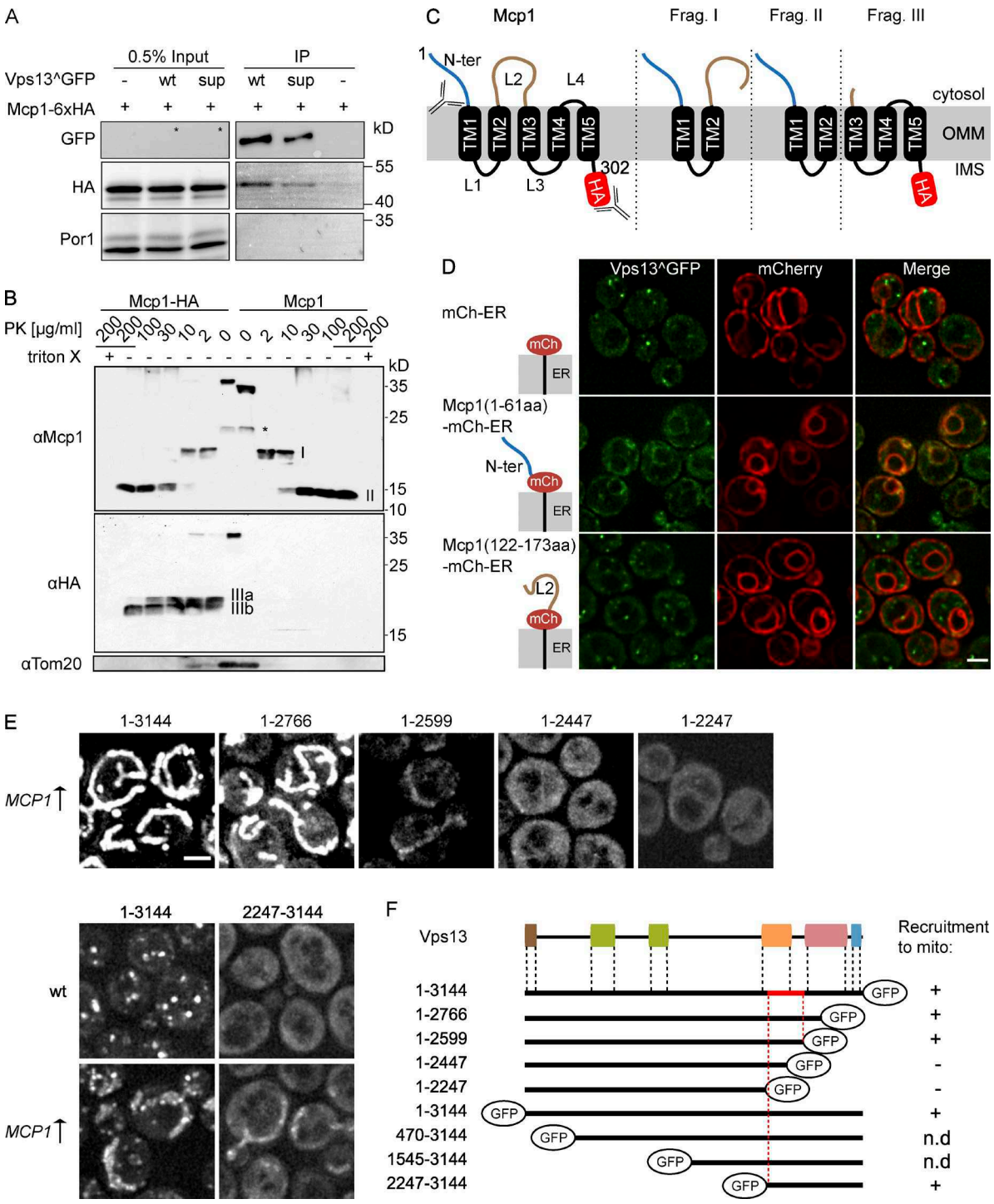

Figure 3. **Mcp1 recruits Vps13 to mitochondria.** (A) Cells expressing Vps13^GFP (WT or suppressor) along with HA-tagged Mcp1 were subjected to immunoprecipitation (IP) using GFP–TrapA beads. Eluates from the beads were analyzed by SDS-PAGE and Western blotting using antibodies against GFP, HA, or yeast porin, Por1 (negative control). Note that the GFP antibody did not detect endogenous Vps13 in whole-cell lysates (asterisks). (B) PK accessibility assay. Isolated mitochondria were incubated in presence of the indicated amounts of PK and then subjected to Western blotting with the indicated antibodies. Proteolytic fragments I, II, and III are indicated. Asterisk denotes uncharacterized PK-independent fragment. (C) Topology of Mcp1 and proteolytic fragments on the outer mitochondrial membrane (OMM). Mcp1 bears five transmembrane (TM) helices (TM1–TM5) and four loops (L1–L4). The cytosol-exposed N terminus (aa 1–61) and L2 (aa 122–173) are shown in blue and brown, respectively. IMS, intermembrane space. (D) Localization of endogenous Vps13 (green) with ER-targeted mCherry alone or fused to the indicated Mcp1 fragments, expressed from a plasmid. (E) Mapping the Mcp1-binding region of Vps13. (Top) Localization of full-length Vps13 and the indicated truncations C-terminally tagged with GFP, upon Mcp1 overexpression. (Bottom) Localization of full-length Vps13 and the indicated truncated version N-terminally tagged with GFP, under normal conditions and Mcp1 overexpression. The expression of the N-terminal truncations was driven by the CYC1 promoter. All truncations were performed genomically. (F) Schematic representation of C-terminal and N-terminal truncations and their mitochondrial recruitment upon Mcp1 overexpression. The region of interaction with Mcp1 lies between aa 2,247 and 2,599. n.d., not determined. Bars, 2 µm.

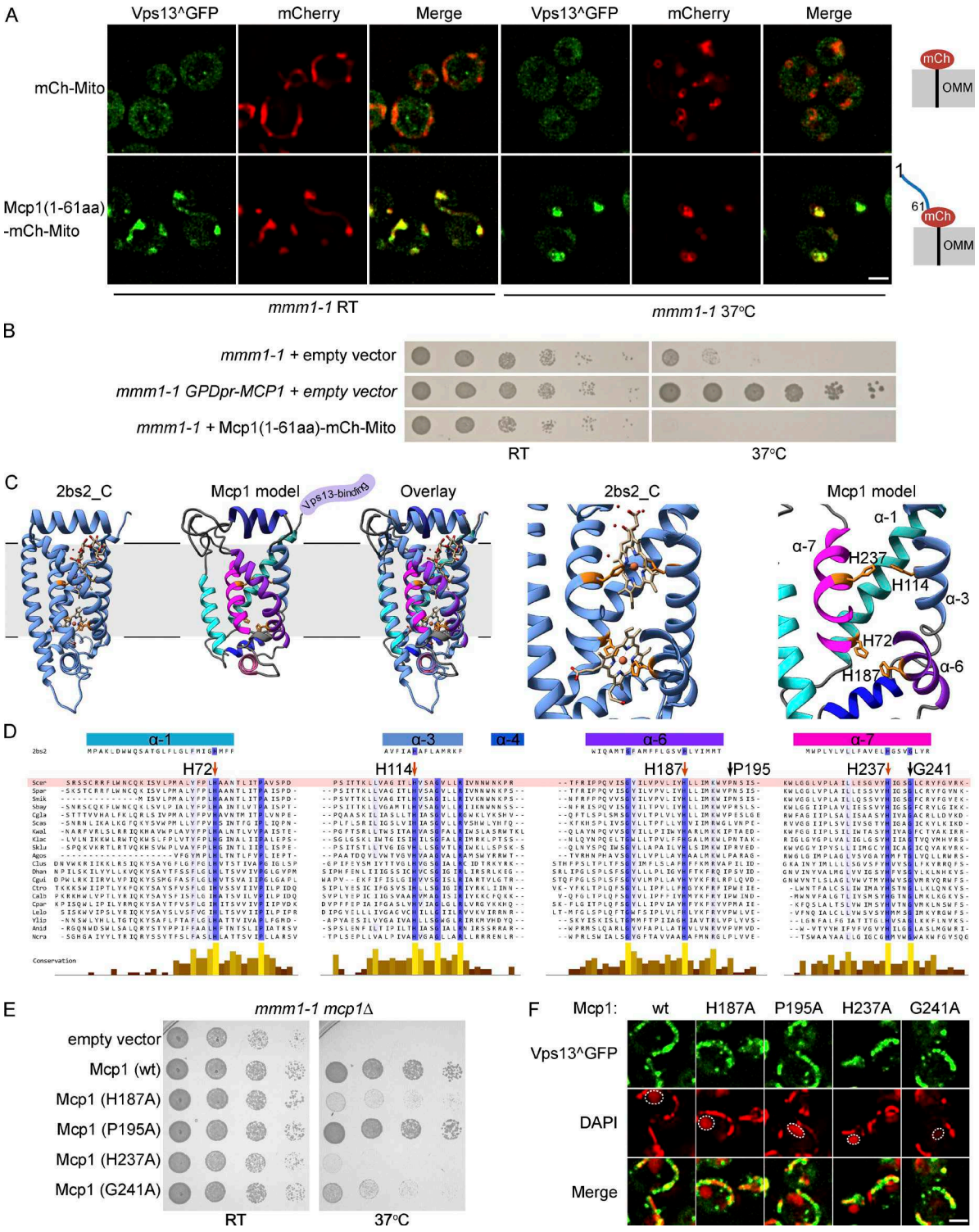

Figure 4. **Mcp1 has additional functions besides recruiting Vps13.** (A) Cells coexpressing Vps13^GFP and either mitochondria-targeted mCherry alone or mCherry fused to the Mcp1 fragment 1–61 were grown at RT (left). To inactivate Mmm1, cells were shifted to 37°C for 2 h and imaged (right). Note the altered mitochondrial morphology at the restrictive temperature. OMM, outer mitochondrial membrane. (B) The *mmm1-1* ts strains carrying an empty vector or the vector bearing the Mcp1 fragment 1–61 were spotted as serial dilutions on SD-HIS plates and grown for 2 d either at RT or 37°C. The *mmm1-1* ts strain with Mcp1 overexpression along with empty vector served as a positive control for growth rescue at the restrictive temperature. (C, top) The structure of the membrane-spanning component of the fumarate quinol reductase from *W. succinogenes* (left; Protein Data Bank 2BS2) was used for homology modeling of Mcp1. (Right) Magnification of the heme-binding sites in the fumarate quinol reductase and their predicted location in Mcp1. (D) Alignment of Mcp1 α-helices 1, 3, 6, and 7 in different ascomycetes orthologues. (E) *mmm1-1* ts *mcp1Δ* cells transformed with plasmids overexpressing WT or mutant Mcp1 were spotted as serial dilutions and grown at either RT or 37°C. (F) Live cells expressing Vps13^GFP and overexpressing indicated mutants of Mcp1 were counterstained with DAPI to reveal mitochondria and nuclei (dashed lines). Bars, 2 µm.

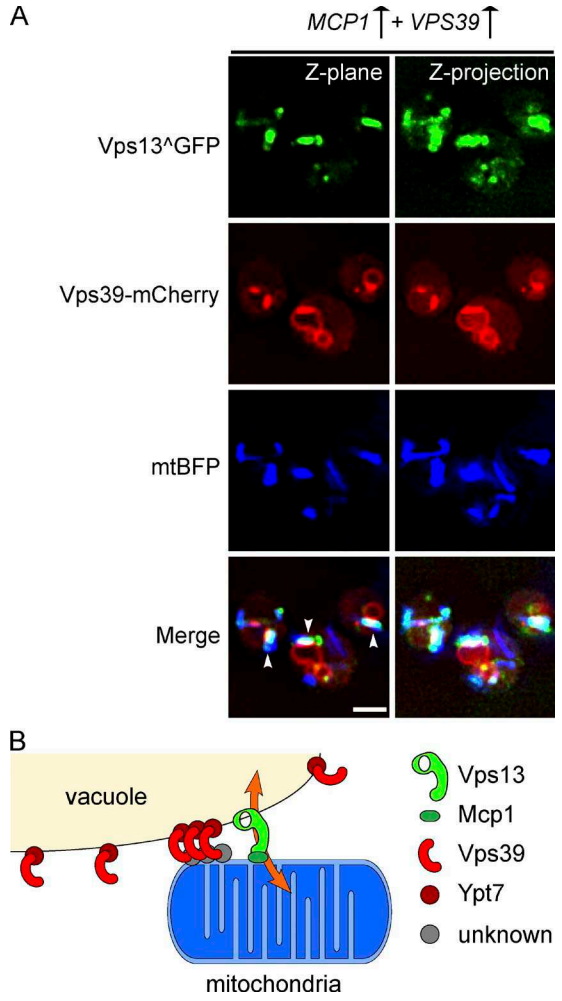

Figure 5. **Recruitment of Vps13 to vCLAMPs upon Vps39 and Mcp1 co-overexpression.** (A) Vps39 is genomically tagged with mCherry at its C terminus. Mitochondria are marked by a plasmid-encoded, matrix-targeted BFP (mtBFP). A single Z-section and a maximum intensity projection of five Z-sections are shown. White arrowheads point at vCLAMPs. Bar, 2 µm. (B) Proposed model for the mechanism of the ERMES-bypass pathway. The recruitment of the vCLAMP factor Vps39 by the Rab GTPase Ypt7 anchors the vacuole to mitochondria via a yet unknown mitochondrial factor. This anchoring facilitates the recruitment of Vps13 to vacuole–mitochondria contacts sites by the outer mitochondrial membrane protein Mcp1. These two proteins potentially act in tandem to function as effectors of vacuole–mitochondria contacts.

recruits Vps13 to mitochondria, Vps13 is not visibly enriched at vacuole–mitochondria contacts, because the surface of contact between both organelles is limiting.

A model that reconciles our observations is that Vps39 acts as a vacuole–mitochondria tether, while Vps13 and Mcp1 act as physiological effectors of vacuole–mitochondria MCSs function, which can compensate for the absence of ERMES (Fig. 5 B). In this case, the tethering and physiological output of vacuole–mitochondria MCSs would be performed by separate factors. Such a division of labor between tethers and effectors at MCSs is novel, as most MCS proteins described so far harbor both tethering and physiological effector activities. For instance, ERMES has an important tethering activity but also harbors lipid exchange proteins (Kornmann et al., 2009; Ah-Young et al., 2015; Jeong et al., 2016). The same is true for extended synaptotagmins, which both tether the ER to the plasma membrane and transport lipids (Manford et al., 2012; Schauder et al., 2014; Saheki et al., 2016).

Consistent with biochemical tethering activity, Vps39 is a known member of the homotypic fusion and protein sorting complex, which is involved in the tethering of late endosomes and vacuoles (Bröcker et al., 2012). By contrast, Vps13 is known to function at MCSs that are tethered by other factors, for instance, nuclear–vacuole junctions tethered by Nvj1 and Vac8 (Pan et al., 2000).

Our elucidation of the mechanism of suppression by the Mcp1-Vps13-Vps39 module supports previous findings (Elbaz-Alon et al., 2014; Hönscher et al., 2014) and firmly establishes vacuole as a critical organelle involved in restoring mitochondrial homeostasis upon the loss of ER–mitochondria contacts. Although endosome–mitochondria (Park et al., 2016) and peroxisome–mitochondria contacts might play a role in ERMES compensation, our data suggest that neither a fully functional endocytic pathway nor functional peroxisomes are required for this purpose (Fig. 2 C).

Because a core function of ERMES appears to be lipid exchange and because Mcp1 and Vps13 serve as effectors of vacuole–mitochondria contacts, it is tempting to speculate that these two proteins are directly involved in lipid transport. Unlike well-characterized lipid transport proteins that localize to organelle contact sites, Vps13 does not seem to harbor any known lipid transport domains based on sequence alignments. However, because only low-resolution structures of Vps13 are available (De et al., 2017), it cannot be excluded that Vps13 harbors a yet uncharacterized lipid transport domain. In the case of Mcp1, our data point to an important role for the membrane-embedded part of Mcp1. This segment likely folds as a heme-binding five-helix bundle, as in quinol–fumarate reductases. This domain might be involved in lipid extraction from and/or lipid insertion into the outer mitochondrial membrane. Whether heme binding serves oxidoreductive roles is unknown. Because Mcp1 is present only in a subset of ascomycetes, and because the five-helix bundle of Mcp1 resembles that found in the succinate dehydrogenases of gram-positive bacteria, it appears that Mcp1 is the result of a recent horizontal gene transfer. It is thus possible that heme binding serves only a structural role in Mcp1. Consistent with this idea, overexpressing a mutant protein presumably incapable of binding heme did severely blunt, but did not entirely abrogate, the activity of Mcp1 in the ERMES-bypass pathway (Fig. 4 E). Of note, succinate dehydrogenases and fumarate reductases use quinols and quinones as electron donors and acceptors and bind these lipids in dedicated cavities at the interface with the lipid bilayer. This lipid-binding ability might be exploited in the ERMES bypass pathway to favor the desorption of phospholipids from the membrane. Alternatively, it is conceivable that Mcp1 and Vps13 cooperate to recruit lipid transport proteins that are yet to be identified.

Could the ERMES bypass pathway be conserved in metazoans? Like ERMES subunits, Mcp1 is not conserved. However, Vps13 is highly conserved with four paralogs, Vps13A-D, in humans. Mutations in these genes are associated with different neurological disorders (Ueno et al., 2001; Kolehmainen et al., 2003; Tomiyasu et al., 2011). In particular, mutation in VPS13C, associated with a form of Parkinson's disease, is linked to mitochondrial dysfunction (Lesage et al., 2016). Given that a short amino acid stretch alone is sufficient to recruit Vps13 to mitochondria, it is conceivable that Mcp1 function has been

substituted by another mitochondrial protein in metazoans, despite low sequence conservation. Therefore, by shedding light on the mechanism of Vps13 recruitment and its function in vacuole/lysosome–mitochondria contact sites, our study has taken an important step toward understanding the function of the mitochondrial pool of Vps13 in health and disease.

Materials and methods

Yeast strains and plasmids

Strains used in this study are listed in Table S1. Genomic integration of PCR fragments was performed by homologous recombination (Puig et al., 1998; Janke et al., 2004; Gauss et al., 2005). Gene deletions were confirmed by colony PCR. Plasmids and primers used in the study are listed in Tables S2 and S3, respectively. mCherry was targeted to the ER by C-terminal fusion of aa 230–250 of Ubc6. Targeting to mitochondria was achieved by C-terminal fusion of aa 132–155 of Fis1. Plasmids bearing MCP1 fragments with mCherry targeted to the ER or mitochondria were constructed using the Gibson Assembly cloning kit (New England Biolabs). To generate the plasmid bearing GFP-tagged Vps13 after aa 499, the pSOI1 plasmid (Brickner and Fuller, 1997) bearing the full-length VPS13 sequence was digested and gap-repaired in a yeast strain bearing the GFP-tagged *VPS13* in the genome (Lang et al., 2015).

Growth assay

Cells were grown in yeast extract peptone dextrose or minimal medium to mid-log phase, diluted to 0.25 OD_{600}, spotted on appropriate plates, and grown at RT or 37°C. Fivefold serial dilutions were made, with the first spot in each row corresponding to 2.5 µl of 0.25 OD_{600}.

PK accessibility assay

Mitochondria were isolated from yeast cells expressing either Mcp1-HA or Mcp1 by differential centrifugation as described before (Daum et al., 1982). Mitochondria (50 µg) were treated with increasing amounts (2–200 µg/ml) of PK in the absence or presence of 1% Triton X-100. Samples were analyzed using SDS-PAGE followed by Western blot analysis with antibodies against Mcp1, the HA tag, or the indicated mitochondrial proteins.

GFP immunoprecipitation

Approximately 1,500 OD units of cells grown overnight in yeast extract peptone dextrose were resuspended in 2 ml TNG buffer (50 mM Tris, pH 7.4, 100 mM NaCl, and 5% glycerol) together with protease inhibitors pepstatin and aprotinin at a final concentration of 1 µg/ml. Glass beads were added, and cells were lysed using a Disrupter Genie (Scientific Industries) for 10 min at 4°C. The lysate was centrifuged at 13,000 *g* for 5 min, and the supernatant was collected. To the pellet, 700 µl of TNG buffer with 1% NP-40 was added, resuspended, and left on a nutator at 4°C for 30 min. After centrifugation, the supernatants were pooled, and the protein amount was estimated. 20 µl GFP–TrapA beads (ChromoTek) were added and left on a nutator at 4°C for 4 h. After washing the beads (50 mM Tris, pH 7.4, 400 mM NaCl, and 5% glycerol), bound proteins were eluted with 1× Laemmli buffer with incubation at 42°C for 15 min.

Fluorescence microscopy

Cells were grown to mid-log phase in complete synthetic dextrose (SD) medium or SD–uracil (for selection for mitochondrial blue fluorescent protein plasmid) or SD–uracil–leucine (for selection of mitochondrial blue fluorescent protein and the Vps13^GFP plasmids). Images were acquired using a DeltaVision MPX microscope (Applied Precision) equipped with a 100× 1.40 NA oil UplanS-Apo objective lens (Olympus), a multicolor illumination light source, and a CoolSNAPHQ2 camera (Roper Scientific). Image acquisition was done at RT. Images were deconvolved with SoftWoRx software using the manufacturer's parameters. Images were processed further using FIJI ImageJ bundle and assembled on Adobe Illustrator CS6. A single Z-section is depicted in the figures unless otherwise mentioned. For vacuolar staining, cells were pulsed with FM4-64 (Molecular Probes) at a concentration of 5 µg/ml for 20 min in the dark at 30°C. After washing, cells were chased for another 20 min in medium without FM4-64 and imaged subsequently. Quantification of colocalization was performed automatically in ImageJ (see the scripts in the online supplemental material).

Bioinformatics analyses

Hidden Markov model homology searches were performed using HHpred software (Söding et al., 2005). Homology modeling was performed using the Swiss-Model server (Biasini et al., 2014). 3D protein structures were rendered using tCHIMERA software (Pettersen et al., 2004).

Online supplemental material

Fig. S1 shows that Pex10 and Vps38 do not colocalize. Fig. S2 shows that the Vps13 suppressor rescues loss of ERMES function in the absence of Vps38. Yeast strains, plasmids, and primers used in the study are listed in Tables S1, S2, and S3, respectively. Alignments S1 and S2 show homology search results for Vps13 (1–3,000 aa) and Vps13 (1,501–3,144 aa), searched against the Pfam database and yeast proteome, respectively. Alignments S3 and S4 show the results for the C terminus of Vps13 (3,030–3,144 aa) and full-length Mcp1, respectively, searched against the Protein Data Bank. All homology alignments were generated using the HHPred server. Scripts S1, S2, and S3 are ImageJ macros used to calculate the percentage of colocalization between Vps13^GFP/Pex10-mCherry foci, Vps13^GFP/Vps38-mCherry foci, and Pex10-GFP/Vps38-mCherry foci, respectively.

Acknowledgments

We are thankful to the Kornmann laboratory members for discussions and helpful suggestions. Imaging was done at the ETH Zürich ScopeM facility.

This work was supported by Schweizerischer Nationalfonds zur Förderung der Wissenschaftlichen Forschung (grant PP00P3_133651) and the H2020 European Research Council (ERC-2013-StG 337906-OrgaNet) to B. Kornmann. D. Antunes was supported by the International Max Planck Research Schools "From Molecules to Organisms" (Tuebingen, Germany).

The authors declare no competing financial interests.

Author contributions: A.T. John Peter and B. Kornmann conceived and designed the experiments. A.T. John Peter performed the experiments, except the experiments in Fig. 3, D and E (designed and performed by B. Hermann and A.T. John Peter); Fig. 3 B (designed by D. Antunes, D. Rapaport, and K.S. Dimmer and performed by D. Antunes); and Fig. 4, E and F (designed by D. Antunes, D. Rapaport, and K.S. Dimmer and performed by D. Antunes and A.T. John Peter). A.T. John Peter and B. Kornmann wrote the paper with input from D. Antunes and D. Rapaport.

Submitted: 17 October 2016
Revised: 26 June 2017
Accepted: 25 July 2017

References

AhYoung, A.P., J. Jiang, J. Zhang, X. Khoi Dang, J.A. Loo, Z.H. Zhou, and P.F. Egea. 2015. Conserved SMP domains of the ERMES complex bind phospholipids and mediate tether assembly. *Proc. Natl. Acad. Sci. USA*. 112:E3179–E3188. http://dx.doi.org/10.1073/pnas.1422363112

Biasini, M., S. Bienert, A. Waterhouse, K. Arnold, G. Studer, T. Schmidt, F. Kiefer, T. Gallo Cassarino, M. Bertoni, L. Bordoli, and T. Schwede. 2014. SWISS-MODEL: Modelling protein tertiary and quaternary structure using evolutionary information. *Nucleic Acids Res.* 42:W252–W258. http://dx.doi.org/10.1093/nar/gku340

Brickner, J.H., and R.S. Fuller. 1997. SOI1 encodes a novel, conserved protein that promotes TGN-endosomal cycling of Kex2p and other membrane proteins by modulating the function of two TGN localization signals. *J. Cell Biol.* 139:23–36. http://dx.doi.org/10.1083/jcb.139.1.23

Bröcker, C., A. Kuhlee, C. Gatsogiannis, H.J. Balderhaar, C. Hönscher, S. Engelbrecht-Vandré, C. Ungermann, and S. Raunser. 2012. Molecular architecture of the multisubunit homotypic fusion and vacuole protein sorting (HOPS) tethering complex. *Proc. Natl. Acad. Sci. USA*. 109:1991–1996. http://dx.doi.org/10.1073/pnas.1117797109

Collins, S.R., A. Roguev, and N.J. Krogan. 2010. Quantitative genetic interaction mapping using the E-MAP approach. *Methods Enzymol.* 470:205–231. http://dx.doi.org/10.1016/S0076-6879(10)70009-4

Costanzo, M., A. Baryshnikova, J. Bellay, Y. Kim, E.D. Spear, C.S. Sevier, H. Ding, J.L.Y. Koh, K. Toufighi, S. Mostafavi, et al. 2010. The genetic landscape of a cell. *Science.* 327:425–431. http://dx.doi.org/10.1126/science.1180823

Daum, G., P.C. Böhni, and G. Schatz. 1982. Import of proteins into mitochondria. Cytochrome b2 and cytochrome c peroxidase are located in the intermembrane space of yeast mitochondria. *J. Biol. Chem.* 257:13028–13033.

De, M., A.N. Oleskie, M. Ayyash, S. Dutta, L. Mancour, M.E. Abazeed, E.J. Brace, G. Skiniotis, and R.S. Fuller. 2017. The Vps13p-Cdc31p complex is directly required for TGN late endosome transport and TGN homotypic fusion. *J. Cell Biol.* 216:425–439. http://dx.doi.org/10.1083/jcb.201606078

Elbaz-Alon, Y., E. Rosenfeld-Gur, V. Shinder, A.H. Futerman, T. Geiger, and M. Schuldiner. 2014. A dynamic interface between vacuoles and mitochondria in yeast. *Dev. Cell.* 30:95–102. http://dx.doi.org/10.1016/j.devcel.2014.06.007

Ellenrieder, L., Ł. Opaliński, L. Becker, V. Krüger, O. Mirus, S.P. Straub, K. Ebell, N. Flinner, S.B. Stiller, B. Guiard, et al. 2016. Separating mitochondrial protein assembly and endoplasmic reticulum tethering by selective coupling of Mdm10. *Nat. Commun.* 7:13021. http://dx.doi.org/10.1038/ncomms13021

Fidler, D.R., S.E. Murphy, K. Courtis, P. Antonoudiou, R. El-Tohamy, J. Ient, and T.P. Levine. 2016. Using HHsearch to tackle proteins of unknown function: A pilot study with PH domains. *Traffic.* 17:1214–1226. http://dx.doi.org/10.1111/tra.12432

Gauss, R., M. Trautwein, T. Sommer, and A. Spang. 2005. New modules for the repeated internal and N-terminal epitope tagging of genes in Saccharomyces cerevisiae. *Yeast*. 22:1–12. http://dx.doi.org/10.1002/yea.1187

Helle, S.C.J., G. Kanfer, K. Kolar, A. Lang, A.H. Michel, and B. Kornmann. 2013. Organization and function of membrane contact sites. *Biochim. Biophys. Acta.* 1833:2526–2541. http://dx.doi.org/10.1016/j.bbamcr.2013.01.028

Hönscher, C., M. Mari, K. Auffarth, M. Bohnert, J. Griffith, W. Geerts, M. van der Laan, M. Cabrera, F. Reggiori, and C. Ungermann. 2014. Cellular metabolism regulates contact sites between vacuoles and mitochondria. *Dev. Cell.* 30:86–94. http://dx.doi.org/10.1016/j.devcel.2014.06.006

Hoppins, S., S.R. Collins, A. Cassidy-Stone, E. Hummel, R.M. Devay, L.L. Lackner, B. Westermann, M. Schuldiner, J.S. Weissman, and J. Nunnari. 2011. A mitochondrial-focused genetic interaction map reveals a scaffold-like complex required for inner membrane organization in mitochondria. *J. Cell Biol.* 195:323–340. http://dx.doi.org/10.1083/jcb.201107053

Huh, W.-K., J.V. Falvo, L.C. Gerke, A.S. Carroll, R.W. Howson, J.S. Weissman, and E.K. O'Shea. 2003. Global analysis of protein localization in budding yeast. *Nature.* 425:686–691. http://dx.doi.org/10.1038/nature02026

Janke, C., M.M. Magiera, N. Rathfelder, C. Taxis, S. Reber, H. Maekawa, A. Moreno-Borchart, G. Doenges, E. Schwob, E. Schiebel, and M. Knop. 2004. A versatile toolbox for PCR-based tagging of yeast genes: New fluorescent proteins, more markers and promoter substitution cassettes. *Yeast*. 21:947–962. http://dx.doi.org/10.1002/yea.1142

Jeong, H., J. Park, and C. Lee. 2016. Crystal structure of Mdm12 reveals the architecture and dynamic organization of the ERMES complex. *EMBO Rep.* 17:1857–1871. http://dx.doi.org/10.15252/embr.201642706

Kihara, A., T. Noda, N. Ishihara, and Y. Ohsumi. 2001. Two distinct Vps34 phosphatidylinositol 3-kinase complexes function in autophagy and carboxypeptidase Y sorting in *Saccharomyces cerevisiae*. *J. Cell Biol.* 152:519–530. http://dx.doi.org/10.1083/jcb.152.3.519

Knoops, K., R. de Boer, A. Kram, and I.J. van der Klei. 2015. Yeast pex1 cells contain peroxisomal ghosts that import matrix proteins upon reintroduction of Pex1. *J. Cell Biol.* 211:955–962. http://dx.doi.org/10.1083/jcb.201506059

Kolehmainen, J., G.C.M. Black, A. Saarinen, K. Chandler, J. Clayton-Smith, A.-L. Träskelin, R. Perveen, S. Kivitie-Kallio, R. Norio, M. Warburg, et al. 2003. Cohen syndrome is caused by mutations in a novel gene, COH1, encoding a transmembrane protein with a presumed role in vesicle-mediated sorting and intracellular protein transport. *Am. J. Hum. Genet.* 72:1359–1369. http://dx.doi.org/10.1086/375454

Kopec, K.O., V. Alva, and A.N. Lupas. 2010. Homology of SMP domains to the TULIP superfamily of lipid-binding proteins provides a structural basis for lipid exchange between ER and mitochondria. *Bioinformatics.* 26:1927–1931. http://dx.doi.org/10.1093/bioinformatics/btq326

Kornmann, B., E. Currie, S.R. Collins, M. Schuldiner, J. Nunnari, J.S. Weissman, and P. Walter. 2009. An ER-mitochondria tethering complex revealed by a synthetic biology screen. *Science.* 325:477–481. http://dx.doi.org/10.1126/science.1175088

Lang, A.B., A.T. John Peter, P. Walter, and B. Kornmann. 2015. ER-mitochondrial junctions can be bypassed by dominant mutations in the endosomal protein Vps13. *J. Cell Biol.* 210:883–890. http://dx.doi.org/10.1083/jcb.201502105

Lesage, S., V. Drouet, E. Majounie, V. Deramecourt, M. Jacoupy, A. Nicolas, F. Cormier-Dequaire, S.M. Hassoun, C. Pujol, S. Ciura, et al. International Parkinson's Disease Genomics Consortium (IPDGC). 2016. Loss of VPS13C function in autosomal-recessive parkinsonism causes mitochondrial dysfunction and increases PINK1/Parkin-dependent mitophagy. *Am. J. Hum. Genet.* 98:500–513. http://dx.doi.org/10.1016/j.ajhg.2016.01.014

Luo, W., and A. Chang. 1997. Novel genes involved in endosomal traffic in yeast revealed by suppression of a targeting-defective plasma membrane ATPase mutant. *J. Cell Biol.* 138:731–746. http://dx.doi.org/10.1083/jcb.138.4.731

Manford, A.G., C.J. Stefan, H.L. Yuan, J.A. Macgurn, and S.D. Emr. 2012. ER-to-plasma membrane tethering proteins regulate cell signaling and ER morphology. *Dev. Cell.* 23:1129–1140. http://dx.doi.org/10.1016/j.devcel.2012.11.004

Mattoon, J.R., E. Caravajal, and D. Guthrie. 1990. Effects of hap mutations on heme and cytochrome formation in yeast. *Curr. Genet.* 17:179–183. http://dx.doi.org/10.1007/BF00312865

Obara, K., T. Sekito, and Y. Ohsumi. 2006. Assortment of phosphatidylinositol 3-kinase complexes—Atg14p directs association of complex I to the pre-autophagosomal structure in *Saccharomyces cerevisiae*. *Mol. Biol. Cell.* 17:1527–1539. http://dx.doi.org/10.1091/mbc.E05-09-0841

Pan, X., P. Roberts, Y. Chen, E. Kvam, N. Shulga, K. Huang, S. Lemmon, and D.S. Goldfarb. 2000. Nucleus-vacuole junctions in *Saccharomyces cerevisiae* are formed through the direct interaction of Vac8p with Nvj1p. *Mol. Biol. Cell.* 11:2445–2457. http://dx.doi.org/10.1091/mbc.11.7.2445

Park, J.-S., M.K. Thorsness, R. Policastro, L.L. McGoldrick, N.M. Hollingsworth, P.E. Thorsness, and A.M. Neiman. 2016. Yeast Vps13 promotes mitochondrial function and is localized at membrane contact sites. *Mol. Biol. Cell.* 27:2435–2449. http://dx.doi.org/10.1091/mbc.E16-02-0112

Pettersen, E.F., T.D. Goddard, C.C. Huang, G.S. Couch, D.M. Greenblatt, E.C. Meng, and T.E. Ferrin. 2004. UCSF Chimera—a visualization system for exploratory research and analysis. *J. Comput. Chem.* 25:1605–1612. http://dx.doi.org/10.1002/jcc.20084

Phillips, M.J., and G.K. Voeltz. 2016. Structure and function of ER membrane contact sites with other organelles. *Nat. Rev. Mol. Cell Biol.* 17:69–82. http://dx.doi.org/10.1038/nrm.2015.8

Puig, O., B. Rutz, B.G. Luukkonen, S. Kandels-Lewis, E. Bragado-Nilsson, and B. Séraphin. 1998. New constructs and strategies for efficient PCR-based gene manipulations in yeast. *Yeast*. 14:1139–1146. http://dx.doi.org/10.1002/(SICI)1097-0061(19980915)14:12<1139::AID-YEA306>3.0.CO;2-B

Saheki, Y., X. Bian, C.M. Schauder, Y. Sawaki, M.A. Surma, C. Klose, F. Pincet, K.M. Reinisch, and P. De Camilli. 2016. Control of plasma membrane lipid homeostasis by the extended synaptotagmins. *Nat. Cell Biol.* 18:504–515. http://dx.doi.org/10.1038/ncb3339

Schauder, C.M., X. Wu, Y. Saheki, P. Narayanaswamy, F. Torta, M.R. Wenk, P. De Camilli, and K.M. Reinisch. 2014. Structure of a lipid-bound extended synaptotagmin indicates a role in lipid transfer. *Nature.* 510:552–555. http://dx.doi.org/10.1038/nature13269

Söding, J., A. Biegert, and A.N. Lupas. 2005. The HHpred interactive server for protein homology detection and structure prediction. *Nucleic Acids Res.* 33(Web Server):W244–W248. http://dx.doi.org/10.1093/nar/gki408

Tan, T., C. Ozbalci, B. Brügger, D. Rapaport, and K.S. Dimmer. 2013. Mcp1 and Mcp2, two novel proteins involved in mitochondrial lipid homeostasis. *J. Cell Sci.* 126:3563–3574. http://dx.doi.org/10.1242/jcs.121244

Tomiyasu, A., M. Nakamura, M. Ichiba, S. Ueno, S. Saiki, M. Morimoto, J. Kobal, Y. Kageyama, T. Inui, K. Wakabayashi, et al. 2011. Novel pathogenic mutations and copy number variations in the VPS13A gene in patients with chorea-acanthocytosis. *Am. J. Med. Genet. B. Neuropsychiatr. Genet.* 156B:620–631. http://dx.doi.org/10.1002/ajmg.b.31206

Ueno, S., Y. Maruki, M. Nakamura, Y. Tomemori, K. Kamae, H. Tanabe, Y. Yamashita, S. Matsuda, S. Kaneko, and A. Sano. 2001. The gene encoding a newly discovered protein, chorein, is mutated in chorea-acanthocytosis. *Nat. Genet.* 28:121–122. http://dx.doi.org/10.1038/88825

Velayos-Baeza, A., A. Vettori, R.R. Copley, C. Dobson-Stone, and A.P. Monaco. 2004. Analysis of the human VPS13 gene family. *Genomics*. 84:536–549. http://dx.doi.org/10.1016/j.ygeno.2004.04.012

Overexpression of branched-chain amino acid aminotransferases rescues the growth defects of cells lacking the Barth Syndrome related gene *TAZ1*

Diana Antunes[1], Arpita Chowdhury[2], Abhishek Aich[2], Sreedivya Saladi[3], Nofar Harpaz[4], Mark Stahl[5], Maya Schuldiner[4], Johannes M. Herrmann[3], Peter Rehling[2,6,7], Doron Rapaport[1,*]

[1] Interfaculty Institute of Biochemistry, University of Tübingen, 72076 Tübingen, Germany
[2] Department of Cellular Biochemistry, University Medical Center Göttingen, 37073 Göttingen, Germany
[3] Cell Biology, University of Kaiserslautern, 67663 Kaiserslautern, Germany
[4] Department of Molecular Genetics, Weizmann Institute of Science, 7610001 Rehovot, Israel
[5] Center for Plant Molecular Biology (ZMBP), University of Tübingen, 72076 Tübingen, Germany.
[6] Göttingen Centre for Molecular Biosciences, Georg-August-University, Göttingen, Germany
[7] Max Planck Institute for Biophysical Chemistry, D-37077, Göttingen, Germany

[*] Author for correspondence: doron.rapaport@uni-tuebingen.de, Tel. +0049-7071-2974184, OrchidID: 0000-0003-3136-1207

Abstract

The yeast protein Taz1 is the orthologue of human *Tafazzin*, a phospholipid acyltransferase involved in cardiolipin (CL) remodeling via a monolyso CL (MLCL) intermediate. Mutations in *Tafazzin* lead to Barth syndrome (BTHS), a metabolic and neuromuscular disorder that primarily affects the heart, muscles, and immune system. Similar to observations in fibroblasts and platelets from patients with BTHS or from animal models, abolishing yeast Taz1 results in decreased total CL amounts, increased levels of MLCL, and mitochondrial dysfunction. However, the biochemical mechanisms underlying the mitochondrial dysfunction in BTHS remain unclear. To better understand the pathomechanism of BTHS, we searched for multi-copy suppressors of the *taz1Δ* growth defect in yeast cells. We identified the branched-chain amino acid transaminases (BCATs) Bat1 and Bat2 as such suppressors. Similarly, overexpression of the mitochondrial isoform BCAT2 in mammalian cells lacking *TAZ* improves their growth. Elevated levels of Bat1 or Bat2 did not restore the reduced membrane potential, altered stability of respiratory complexes, or the defective accumulation of MLCL species in yeast *taz1Δ* cells. Importantly, supplying yeast or mammalian cells lacking *TAZ1* with certain amino acids restored their growth behavior. Hence, our findings suggest that the metabolism of amino acids has an important and disease relevant role in cells lacking Taz1 function.

Keywords: Barth syndrome / cardiolipin / mitochondria / *Tafazzin* / *TAZ1* /

Introduction

Mitochondria are essential organelles that fulfil crucial roles in cellular bioenergetics, apoptosis, and metabolism of amino acids, lipids, nucleic acids, and heme. To properly carry out all these functions, mitochondria have to maintain their unique protein and lipid composition. Of the mitochondrial lipids, cardiolipin (CL) comprises the signature dimeric phospholipid (PL) for this organelle. CL interacts with several inner membrane (IM) protein complexes affecting the structure and activity of respiratory supercomplexes and ultimately the oxidative generation of ATP (Pfeiffer et al., 2003; Zhang et al., 2005). In addition, CL has been implicated in the biogenesis of outer membrane proteins (Gebert et al., 2009; Sauerwald et al., 2015).

After its initial synthesis, CL undergoes acyl chain remodeling that replaces the pre-existing fatty acids with other ones, which are organism and tissue specific (Schlame et al., 2005). This reaction is catalysed by the enzyme *TAZ* (*Tafazzin)* that encodes a phospholipid transacylase, which is highly conserved from yeast to human. Mutations in the *tafazzin* gene are associated with a number of clinical disorders including Barth syndrome (BTHS).

BTHS is a rare X-linked disease characterized by skeletal myopathy and cardiomyopathy, and in some cases neutropenia. Although three CL remodeling pathways have been identified in higher eukaryotes, *TAZ1* is the only transacylase that mediates such remodeling in yeast cells (Claypool and Koehler, 2012). Loss of Taz1 leads to a decrease in the total cellular amounts of CL, accumulation of monolyso-cardiolipin (MLCL, CL lacking one acyl chain), and aberrant CL species (Gu et al., 2004). Similar alterations were also observed in fibroblasts and platelets obtained from either patients with BTHS or animal models (Schlame et al., 2002; Valianpour et al., 2002; Vreken et al., 2000). Despite the aforementioned CL-related disturbances, it was reported that the major phenotypes of yeast cells lacking *TAZ1* are mainly due to the increased ratio MLCL/CL rather than the absence of modified CL (Baile et al., 2014; Ye et al., 2014). In addition to the altered CL composition, a multitude of various mitochondrial defects is observed in cells lacking *TAZ1*. Mitochondria of yeast *taz1Δ* cells also exhibit a decreased membrane potential and increased proton leak (Baile et al., 2013). Such a hampered proton-motive force across the IM aggravates mitochondria function and the organelles are then prone to oxidative damage by the increased production of reactive oxygen species (ROS).

One of the main metabolic pathways that takes place inside mitochondria is the tricarboxylic acid (TCA) cycle, which is crucial for providing reductive equivalents to the respiratory chain complexes. In cells defective for *TAZ1*, the ATP production via oxidation of NADH is

compromised, resulting in a decreased NAD^+/NADH ratio (Gonzalvez et al., 2013). As a consequence of the NADH accumulation, metabolic dysfunctions such as inhibition of TCA cycle enzymes that require NAD^+ occur and subsequently, the TCA cycle activity halts (Ikon and Ryan, 2017; Vatrinet et al., 2017).

Although *TAZ* mutations have been clearly implicated in BTHS, the precise role and the involvement of this protein in the pathomechanism of the disease has remained elusive. To address this issue, we screened for multi-copy suppressors of the *taz1Δ* growth defect in yeast cells and identified the branched-chain amino acid transaminases (BCATs), Bat1 and Bat2, as such suppressors. Accordingly, we found that altered metabolism of amino acids likely play an important and disease relevant role in human cells lacking *TAZ*. Collectively, our findings provide insights to the pathomechanism of the TAZ-mediated Barth syndrome.

Results

Identification of multi-copy suppressors for impaired growth of *taz1Δ* cells

Yeast cells provide a reliable model system to study the pathomechanism of BTHS. The deletion of *TAZ1* does not lead to observable growth defects on synthetic medium containing a fermentable carbon source like glucose (SD) or non-fermentable ones like glycerol or acetate (SG or SA, respectively). In contrast, cells lacking *Taz1* grow poorly when ethanol is the sole carbon source (Fig. 1A, SE-Leu). This growth defect can be reversed upon expression of *TAZ1* from a plasmid (Fig. 1A), suggesting that the absence of Taz1 is the primary reason for this defect. To better understand the molecular mechanisms involved in this phenotype, we searched for gene targets whose overexpression suppress the growth defect of *taz1Δ* cells. For this purpose, we transformed *taz1Δ* cells with a yeast genomic library cloned in a high copy number (2μ based) yeast expression vector (Stettler et al., 1993; Tan et al., 2013). Transformants were initially grown on selective medium lacking uracil (SD-Ura) to select for those containing the plasmid and then replica-platted several times on plates containing ethanol (SE-Ura), condition where *taz1Δ* cells do not grow. Clones able to grow on ethanol as the sole carbon source were considered as those harbouring potential suppressors (Fig. 1B). To ensure saturation, we screened 55,000 colonies and identified several clones that exhibited rescue of the growth defect.

One of the identified clones contained the *TAZ1* open reading frame (ORF) (data not shown), confirming the validity of the screen. The remaining plasmids harboured DNA fragments mostly co-encoding for *CRG1*, *COX24*, *HMX1*, and *BAT1* (Fig. 1B, #16 and #29). *CRG1* encodes for a methyltransferase involved in lipid homeostasis, Cox24 is a translation modulator of *COX1* mRNA, and Hmx1 is an ER heme oxygenase, whereas *BAT1* encodes for a mitochondrial branched-chain amino acid transaminase (BCAT) (Kispal et al., 1996). To verify the potential of these genes to complement the growth defect, they were genomically overexpressed in *taz1Δ* cells under the control of the strong GPD promoter. Growth assessments of the four initial candidates demonstrated that only *BAT1* overexpression was able to reproducibly rescue the *taz1Δ* growth defect (Fig. 1C, D). Since Bat1 has a highly homologous protein, Bat2, which shares the same function but is located in the cytosol (Kispal et al., 1996), we analysed whether the overexpression of *BAT2* can also complement the growth defect of *taz1Δ* cells. Indeed, the overexpression of *BAT2* rescues the growth defect of *taz1Δ* cells, though not as efficient as the overexpression of *BAT1* (Fig. 1D).

Western blotting analysis verified that indeed Bat1 and Bat2 are detected in higher levels in the overexpressing strains. Given the high sequence homology between Bat1 and Bat2, the antibody raised against Bat1 also recognises Bat2. Interestingly, it appears that Bat1 levels are decreased in *bat2Δ* cells (Fig. S1).

The rescue of the growth defect of *taz1Δ* cells by *BAT1* or *BAT2* overexpression suggests a functional compensation related to the defective CL remodeling process. To address whether the observed compensation can be also extended to the loss of CL, we analysed the growth of cells deficient for CL due to deletion of key enzymes in its biosynthesis pathway, *GEP4* and *CRD1*. These mutant cells have a severe growth defect when incubated at elevated temperatures on non-fermentable carbon sources. In contrast to the situation with *taz1Δ* cells, we did not observe rescue of the growth defects of cells lacking CL biosynthetic enzymes upon BCATs overexpression (Fig. 1E). These results indicate that enhanced metabolism of amino acids can compensate for defects specifically related to CL remodeling but not to its absence.

BCATs-mediated rescue of the retarded growth of *taz1Δ* cells is not associated with repair of mitochondrial defects in these cells

CL is known to stabilize the electron transport chain supercomplexes (Bazan et al., 2013; McKenzie et al., 2006; Zhang et al., 2005). Accordingly, the formation of supercomplexes harbouring complexes III and IV is altered in mitochondria lacking Taz1 (Baile et al., 2014;

Brandner et al., 2005) (Fig. 2A, B). To understand better the relevance of BCATs for the rescue of *taz1Δ* growth defect, we investigated whether their overexpression could restore this altered assembly. Upon analysing complexes assembly by blue native (BN)-PAGE, we found that overexpression of neither *BAT1* nor *BAT2* reverted the defects caused by loss of Taz1 to the respiratory chain complexes (Fig. 2A, B). More generally, loss of Taz1 leads to reduced membrane potential ($\Delta\Psi$) by ~30%, as compared to WT mitochondria (Brandner et al., 2005). Overexpression of BCATs did not restore the reduced $\Delta\Psi$ of mitochondria isolated from *taz1Δ* cells, as monitored with the membrane potential-sensitive dye 3,3'-diprophylthiadicarbocyanine iodide ($DiSC_3(5)$) (Fig. 2C).

Next, we measured the oxygen consumption of mitochondria isolated from either control (WT) or *taz1Δ* cells. Interestingly, mitochondria of the mutant cells had higher consumption rate, maybe in an attempt to compensate their compromised function. The overexpression of *BAT1* or *BAT2* in *taz1Δ* cells revert the oxygen consumption to WT levels (Fig. S2A). Hence, *BAT1/2* can affect respiration without correcting the $\Delta\Psi$ and the respiratory chain supercomplexes assembly. As a comparison, deleting the TCA enzyme Fumarase, resulted also in enhanced oxygen consumption whereas, as expected, the absence of the mitochondrial inner membrane insertase *Oxa1* led to highly reduced respiration (Fig. S2B).

We wondered if the capacity to affect the respiration resulted from a rescue in lipid content. A major consequence of the loss of Taz1 function is a decrease in the amounts of CL and accumulation of MLCL species (Xu et al., 2016). Therefore, we investigated by thin layer chromatography (TLC) the effect of *BAT1/2* overexpression on the phospholipid profile of mitochondria isolated from *taz1Δ* cells. As expected, a MLCL accumulation and CL reduction was observed in *taz1Δ* mitochondria. However, *taz1Δ* cells with higher levels of Bat1 or Bat2 did not rescue this altered PLs profile (Fig. 2D). This suggests that recovery of respiration behavior is not through a rescue of lipid homeostasis but through a bypass mechanism. In accordance with this notion, we found that overexpression of *BAT1/2* does not affect the steady state levels of proteins residing in the various mitochondrial sub-compartments (Fig. 2E).

Amino acids supplementation rescues the growth defect of *taz1Δ cells*

Bat1 and Bat2 are branched-chain amino acid aminotransferases that catalyze the conversion of branched-chain amino acids (BCAAs) and α-ketoglutarate into branched chain α-keto acids and glutamate. We next asked whether supplementation of BCAAs to the medium could rescue the growth retardation of *taz1Δ* cells. Indeed, supplementation of valine rescued the growth

defect of *taz1Δ* cells in a dose-dependent manner (Fig. 3A). However, the addition of the two other BCAAs, leucine (Fig. S3A) or isoleucine (Fig. S3D) did not result in improved growth of *taz1Δ* cells. Along the same lines, overexpression of the *LEU2* gene, which encodes a key enzyme in the biosynthesis pathway of leucine, in the mutated cells did not rescue the growth defect (Fig. S3B). Since the BCAT enzymes can catalyze the conversion between keto acids and amino acids in both directions, we also tested whether the corresponding keto acid form of leucine, alpha-ketoisocaproic acid (KIC), might have a beneficiary effect for *taz1Δ* cells. However, addition of this molecule to the solid medium did not improve the growth of the mutated cells (Fig. S3C).

To test whether other amino acids can rescue the defects of Taz1-deficient cells, we supplemented ethanol-containing plates with aspartate. Of note, the growth defect of *taz1Δ* cells was largely rescued upon supplementation with aspartate (Fig. 3B). To investigate if the observed rescue of the growth defect is related to the CL profile of these cells, we analysed the profile of PLs of isolated mitochondria from *taz1Δ* cells grown in the absence or presence of either aspartate or valine (Fig. 3C). Our results revealed that supplementation of *taz1Δ* cells with both amino acids did not restored the defective MLCL/CL ratio characteristic for these mutated cells.

We expanded our analysis also to supplementation with either glutamate or histidine. Whereas the former amino acid only rescues partially the decreased growth of *taz1Δ* cells (Fig. 3D), addition of histidine to the medium could fully restore the growth deficit of *taz1Δ* cells (Fig. 3E). Taken together, these results show that the Bat1/2-mediated rescue of Taz1-depleted cells can be explained by elevated cellular levels of some amino acids. Our findings that elevated levels of BCATs or supplementation of certain amino acids can rescue the growth defect of *taz1Δ* cells led us to investigate whether enhanced transport of amino acids from the vacuole (yeast lysosome) to cytosol can have a similar effect. To that aim, we overexpressed two vacuolar amino acid transporters *AVT1* and *AVT4* in the mutated cells. However, such overexpression did not improve the growth of *taz1Δ* cells (Fig. 3F).

Increased levels of TCA cycle metabolites and amino acids in *taz1Δ* cells with elevated amounts of Bat1

The previous results suggested that overexpression of BCATs or supplementation of amino acids like valine, aspartate, glutamate, or histidine can rescue the growth defects of *taz1Δ* cells. Hence, next we tested whether the levels of these amino acids or metabolites of the TCA cycle

are actually altered in the deletion cells and if the overexpression of BCATs changes their levels. To that end, we grew the cells in 2% ethanol, extracted metabolites from yeast cells and monitored their levels by liquid chromatography coupled with mass spectrometry (LC-MS). The amounts of most of the TCA cycle intermediates were reduced in *taz1Δ* cells (Fig. 4). Yet, we did not observe a restored growth of *taz1Δ* cells upon supplementation of TCA metabolites (Fig. S4). Importantly, we observed that *BAT1* overexpression restores and even greatly increased the levels of most of the TCA metabolites and of the beneficial amino acids like valine and histidine (Fig. 4). In agreement with its reduced rescue capacity, overexpression of *BAT2* did not have a significant effect on the levels of these metabolites (Fig. 4). These results support the notion that reduced levels of certain amino acids can contribute to the cellular defects in *taz1Δ* cells and replenishing these metabolites can rescue the growth retardation of these cells.

Overexpression of mammalian BCATs or valine supplementation enhances the proliferation of *Tafazzin*-deficient mouse embryonic fibroblasts

The aforementioned results were obtained with a yeast model of BTHS. To generalize our hypothesis and substantiate our findings, we turned to mammalian cells. We employed our previously described mouse embryonic fibroblasts (MEFs) where *Tafazzin* was knocked-out (*TAZ*$^{-/-}$) (Chowdhury et al., 2018). We found that the overexpression of the mammalian mitochondrial isoform BCAT2, (Bledsoe et al., 1997), provide a significant increment of proliferation for cells lacking *TAZ* (Fig. 5A). In contrast, elevated levels of the cytosolic form, BCAT1 had only minor effect on the growth of the mutated cells. Of note, overexpressing BCATs in WT cells did not influence the growth of these cells (Fig. 5A). Next, we sought to test the effect of valine supplementation on proliferation of *TAZ*$^{-/-}$ cells and observed a major enhancement already at rather low concentrations of valine supplementation (1 mM) (Fig. 5B). Analysis of growth after 72 hrs revealed that the addition of valine to the growth medium resulted in a 3-fold increase in cell proliferation of the mutant cells whereas that of control cells was increased only slightly. These findings indicate that the ability to rescue the growth of *TAZ* mutant by either overexpression of mitochondrial BCAT or by supplementation of certain amino acids is conserved from yeast to mammalian cells.

Discussion

The deletion of *TAZ1* leads to a severe growth phenotype of yeast cells on synthetic medium using the non-fermentable carbon source ethanol as the sole carbon source. Of note, these mutant cells grow normally on non-fermentable carbon sources like glycerol or acetate suggesting that compromised respiration is not the main problem of these cells. Indeed, our results suggest increased respiration in these cells. The sensitivity of the *taz1Δ* mutant to ethanol is consequential of the decreased CL levels and altered acyl composition of this crucial dimeric PL. As previously reported, ethanol-tolerance of mutants in yeast depends on their lipid composition andunsaturation degree (Chi and Arneborg, 1999). Mitochondrial damage occurs upon ethanol stress via inactivation of some mitochondrial enzymes and increased production of ROS (Costa et al., 1997; Du and Takagi, 2007; Jimenez and Benitez, 1988). In fact, it has been shown that in *taz1Δ* cells grown in ethanol, the carbonylation levels of proteins - an indicative of increased ROS - are double than those of cells grown on glucose (Chen et al., 2008). Thus, the various compromised mitochondrial functions in *taz1Δ* cells aggravate their ethanol sensitivity.

In the current study, we report on BCATs as specific suppressors of the growth defects of both yeast and mammalian cells lacking Taz1 or TAZ, respectively. We identified this new property for Bat1 and Bat2 while searching for high-copy suppressors of the growth phenotype of yeast *taz1Δ* cells. Despite its reasonable growth phenotype suppression capacity, the cytosolic protein Bat2 was not identified in the multi-copy suppressor screen, probably due to incomplete coverage of the used genomic library. Of note, the overexpression of BCATs could not rescue the growth defects of cells lacking CL all together, suggesting that the products of their enzymatic activities cannot complement the absence of this unique PL. Both BCATs were reported previously to affect directly or indirectly several cellular processes. For example, *BAT1*, but not *BAT2*, was identified as a high-copy suppressor of a temperature-sensitive mutation in *ATM1*, encoding a mitochondrial ABC transporter (Kispal et al., 1996). Recently, both yeast BCAT homologs have been implicated to be critical for the activation of TORC1 signalling (Kingsbury et al., 2015). Hence, these aforementioned observations together with our current findings that supplementation of *taz1Δ* cells with amino acids reversed their compromised proliferation, suggest that enhanced metabolism of amino acids might compensate for other cellular dysfunctions.

Overexpression of the BCATs does not restore mitochondrial defects reported for *taz1Δ* cells like altered assembly of respiratory complexes, increased MLCL/CL ratio, or reduced

membrane potential. On the other hand, such overexpression increases the levels of some TCA metabolites. Hence, our findings suggest that the major contribution of BCATs is probably through a compensatory increase in the flux of the TCA cycle. Interestingly, the growth defect rescue in both yeast and mammalian cells with the two different BCAT isoforms was similar. In both cell types, the mitochondrial isoform had a higher rescue capacity. Hence, although the mitochondrial and cytosolic isoforms have overlapping functions in transamination reactions, it appears that their products are required more in mitochondria and that they are not completely free to equilibrate between the matrix of mitochondria and the cytosol.

An interesting question is why only valine among the BCAAs and other amino acids like aspartate or histidine displayed rescue activity on *taz1*Δ cells. Obviously, it is hard to determine how much of the externally added metabolites are actually transported across the cell wall, plasma membrane and into the mitochondrial matrix. Hence, we cannot exclude the obvious possibility that differences in rescue ability reflect (at least partially) variations in the transported amounts (and hence effective concentrations) of the different molecules. An alternative explanation is that in contrast to the two other BCAAs, valine degradation products can be fed directly into the TCA cycle, leading to a faster replenishment of the cellular energy demands.

Currently, despite the obvious link to the TCA cycle, the mechanism by which overexpression of BCATs, and elevated levels of certain amino acids, rescue the growth defects of cells lacking Taz1 is not completely clear. One possibility is that the enhanced levels of either amino acids or TCA metabolites can serve as replenishment for amino acids or metabolites, which formation is compromised in *taz1*Δ cells. An alternative, but not mutual exclusive possibility, is that the backbones of these amino acids, which contain more than two carbons (in contrast to ethanol), are used for general carbon anabolic pathways (like gluconeogenesis).

In addition, beneficial effects of amino acids were reported in several related contexts. For example, dietary supplementation of BCAAs has been implied to protect against ethanol toxicity by reverting structural and functional mitochondrial damages in rodents with alcoholic liver disease (Tedesco et al., 2018). A link between impaired CL remodeling and amino acids metabolism is further supported in a *TAZ* knock-down mouse model in which the increased MLCL/CL ratio led to a substrate shift via *de novo* amino acid biosynthesis as well as amino acid usage by the TCA cycle (Kiebish et al., 2013). Additionally, Bat1 was reported to interact with the TCA cycle enzyme Aconitase. The recent identification of yeast oxodicarboxylate carrier (Odc1) as another factor that can rescue defects of *taz1*Δ cells (de Taffin de Tilques et

al., 2017) further support the link between amino acids metabolism and *taz1*Δ phenotypes. Odc1 is involved in glutamate and lysine biosynthesis by its function as a transporter of several TCA cycle intermediates across the mitochondrial IM (Palmieri et al., 2001). Elevated levels of Odc1 were reported to fully restore the oxidative phosphorylation and growth defects in *taz1*Δ yeast (de Taffin de Tilques et al., 2017).

Furthermore, mutation of BCATs resulted in perturbed TCA-cycle intermediate levels, which in turn led to reduced ATP levels and inhibition of TORC1 (Kingsbury et al., 2015). Another evidence for the potential relevance of CL for the TCA cycle emerges from a recent study showing that yeast cells deleted for CL synthase (*crd1Δ),* and hence are CL-deficient, have decreased acetyl-CoA levels, decreased activity of acetyl-CoA synthetase, and consequently, deficiencies in the TCA cycle. These defects were reflected in decreased growth on medium containing acetate as the sole carbon source (Raja et al., 2017). Interestingly, the *taz1Δ* strain displays no growth defect on acetate media, a phenotype that is characteristic for many yeast mutants bearing disruptions in genes encoding TCA cycle enzymes (Minard and McAlister-Henn, 2009). Thus, although we observed lower levels of some TCA cycle metabolites in *taz1Δ* cells, it is unclear to which extent the TCA cycle is compromised in these cells.

Naturally, one cannot exclude the contribution of peroxisomes in providing new TCA cycle intermediates by β-oxidation or the glyoxylate cycle (Elgersma et al., 1995). Yet, we propose that peroxisomal function is not related to the phenotypes of *taz1Δ* cells since these cells grow normally on medium containing oleic acid as the sole carbon source (data not shown), conditions where yeast cells rely on functional peroxisomes. Collectively, we suggest that elevated levels of certain amino acids can enhance cellular growth either directly upon their conversion to TCA intermediates and increased flux of this pathway or indirectly by their induction of the mTOR signalling pathway. Taken together, we show here that yeast and mammalian cells lacking CL remodeling benefit from the overexpression of BCATs and valine supplementation. As such, this work proposes that the metabolism of amino acids has an important and disease relevant role in such mutated cells and highlights the potential usage of some amino acids as a therapeutic avenue to help alleviate some of the symptoms of patients with Barth syndrome.

Materials and methods

Yeast strains and growth conditions

The wild type *Saccharomyces cerevisiae* W303a/α or BY4741 strains were utilized. Cells were transformed using the Li-acetate method (Gietz and Woods, 2006; Janke et al., 2004; Longtine et al., 1998). Genomic overexpression was performed by homologous recombination replacing the endogenous promoter by the constitutive promoter GPD*pr* (Janke et al., 2004). Primers for these replacements and their validation were designed using the Primers-4-Yeast toolkit (Yofe and Schuldiner, 2014). To delete complete ORFs by homologous recombination, the HIS3MX6 cassette was amplified from the plasmid pFA6a-HIS3MX6 (Wach et al., 1997) with gene-specific primers. Yeast strains used in this study are described in Table S1. Yeast strains were grown in rich YP medium (2% [w/v] bactopeptone, 1% [w/v] yeast extract) containing various carbon sources, in lactate medium (0.3% [wt/vol] yeast extract, 0.5 g/l glucose, 0.5 g/l NaCl, 1 g/l KH2PO4, 1 g/l NH_4Cl, 0.6 g/l $MgCl_2$, 0.5 g/l $CaCl_2$, 2% [vol/vol] lactic acid, pH 5.5), as well as in synthetic (S) medium (0.67% [w/v] bactoyeast nitrogen base without amino acids) with glucose (2% [w/v], D), lactate (2% [w/v], Lac), or ethanol (2% [w/v], E) as carbon source. For drop dilution assays, cells were cultured to logarithmic phase, collected by centrifugation, and resuspended in water to an OD_{600} of 2.0. Cell suspensions were serially diluted fivefold in water and 5 µl of each cell suspension were spotted on the appropriate solid medium followed by incubation at either 30°C or 37°C. In some cases, the indicated concentrations of the specified metabolite were added to SE solid medium.

Recombinant DNA techniques

The open reading frame of *TAZ1* was amplified by PCR from WT yeast genomic DNA and cloned into the plasmid pYX142 using EcoRI and HindIII restriction sites. The construct was verified by DNA sequencing. A list of all plasmids and primers used in this study is included in Table S2.

Multi-copy suppressor screening

Electro-competent yeast cells lacking Taz1 (*taz1Δ*) were transformed with a high-copy-number yeast genomic library in the URA3 2µ plasmid pFL44L (Stettler et al., 1993). To select for transformants, cells were initially grown at 30°C on SD lacking uracil (SD-Ura). Then, clones were replica plated several times on SE medium and further incubated at 30°C. Plasmid DNA was extracted from clones that grew under these conditions and transformed into *E.coli* cells.

Plasmids were obtained from the transformed *E. coli* cells and their capacity to rescue the growth defect of *taz1Δ* cells was confirmed. The DNA inserts of isolated verified plasmids were identified by sequencing.

Biochemical methods

Mitochondria were isolated from yeast cells grown to logarithmic phase in either lactate or S-lactate medium and harvested by differential centrifugation as described (Daum et al., 1982). To analyze the steady state levels of mitochondrial proteins, isolated organelles were subjected to 12.5% or 10% SDS-PAGE and proteins were transferred onto nitrocellulose membranes by semi-dry western blotting. Proteins were immunodecorated with primary antibodies and the detection was performed with horseradish peroxidase-coupled secondary antibody. A list of primary antibodies used in this study is included in Table S3.

Blue Native (BN)-PAGE was performed as described before (Schagger, 2002). Briefly, mitochondria were solubilised in 40 µl buffer containing digitonin (1% digitonin, 20 mM Tris-HCl, 0.1 mM EDTA, 50 mM NaCl, 10% (v/v) glycerol, 1 mM PMSF, pH 7.2). After incubation on ice for 15 min and clarifying spin (30,000g, 15 min, 2°C), 5 µl sample buffer (5% (w/v) Coomassie blue G, 500 mM 6-amino-N-caproic acid, 100 mM Bis-Tris, pH 7.0) was added. The native complexes were analyzed by electrophoresis in a 6-14% gradient of acrylamide BN-PAGE gel. Gels were blotted on polyvinylidene fluoride membranes and proteins were further analyzed by immunodecoration.

Monitoring membrane potential of isolated mitochondria

The membrane potential across the mitochondrial inner membrane ($\Delta\Psi$) was monitored by fluorescence quenching of a $\Delta\Psi$-sensitive dye by adapting a published method (Gartner et al., 1995). Briefly, DiSC3(5) (final concentration of 2 µM) was added to 3 ml buffer containing (0.6 M sorbitol, 0.1% (w/v) fatty acid-free BSA, 0.5 mM EDTA, and 20 mM KPI, pH 7.2. The fluorescence was monitored with excitation at 622 nm and emission at 670 nm, and data points were taken at 2 sec intervals. Once the fluorescence signal was stabilized, 50 µg of isolated mitochondria were added to the cuvette, and the fluorescence intensity was further monitored until a stable signal was obtained. Finally, to completely dissipate the membrane potential, valinomycin (final concentration 1 µM) was added to the mixture, and the increase in the fluorescence intensity was recorded. Membrane potential was assessed as the difference between the fluorescence signal before and after the addition of valinomycin.

Mitochondrial oxygen consumption assay

The rate of oxygen consumption of isolated mitochondria was measured polarographically at 25°C using a Clark-type oxygen electrode connected to a computer-operated Oxygraph control unit (Hansatech Instruments, Germany). Isolated mitochondria (100 µg) suspended in a buffer containing 0.6 M sorbitol, 20 mm Hepes (pH 7.4), 1 mM EDTA and 1 mm $MgCl_2$ were added to the oxygen chamber with continuous stirring. Respiration was initiated by the addition of NADH (final conc. 7 mM) and recorded at sampling intervals of 1 sec (Oxygraph Plus software, Hansatech Instruments).

Extraction and analysis of mitochondrial phospholipids

Lipid extraction of isolated mitochondria was performed according to published method (Bligh and Dyer, 1959). Briefly, a mixture of chloroform:methanol 1:2 (v/v) was added to 600 µg of mitochondria , vortexed, and incubated on ice for 30 min. Then, 1.25 times (v/v) of chloroform and water were added and after vigorous vortex, samples were centrifuged (1000 g, 5 min, RT). The organic phase was collected and solvents were evaporated by speed vac. Then, lipids were resuspended in 40 µL of chloroform:methanol 1:1 (v/v) mixture and either stored at -20°C or immediately used.

Phospholipid (PL) classes from the total lipid extract were separated by thin-layer chromatography (TLC) using glass plates of pre-coated 0.25 mm silica gel with fluorescent indicator UV_{254}. Prior to separation, the silica plates were washed with a mixture of chloroform:methanol 1:1 (v/v) and dried for 15 min. Then, plates were sprayed with a solution of 2.3% (v/v) boric acid in ethanol and dried in an oven at 100°C for 15 min. Next, 40 µL of sample of total lipid extract or 3-5 µL of PL standards were applied to the plate. The spots were air dried and developed in a solvent mixture of chloroform/ethanol/water/trimethylamine (30:35:7:35, v/v/v/v). After complete migration and eluent evaporation, the TLC plates were sprayed with molybdenum blue solution. Identification of the different classes of PLs was performed out by comparison with the migration behavior of PL standards.

Analysis of yeast metabolites by mass spectrometry

Pellets of yeast cells were lyophilized followed by homogenization with a ball mill. Metabolites were first extracted with 400 µl of 80% methanol containing 0.1% formic acid and afterwards re-extracted with 400 µl of 20% methanol containing 0.1% formic acid. Both supernatants were combined and dried in a speed-vac concentrator. Samples were re-dissolved in 120 µl of 20%

methanol containing 0.1% formic acid and 7 µl were injected onto a Waters Acquity HSST3 2.1x100 mm, 1.8 µm ultra-performance liquid chromatography (UPLC) column. Separation was carried out with an isocratic 2 min step of 99% water containing 0.1% formic acid, followed by a linear 10 min gradient to 99% methanol (containing 0.1% formic acid) at a flow rate of 200 µl/min. The analysis was conducted with a Waters Acquity UPLC - SynaptG2 LC/MS system operated in positive and negative electrospray ionization mode with a scan range of 50-2000 m/z at a scan rate of 0.5 sec. For relative quantification of the metabolites, extracted ion traces were generated and integrated.

MEF cell culture, transfection and cellular proliferation measurements

WT and *TAZ*^{KO} MEF cells were cultured at 37°C under a 5% CO_2 humidified atmosphere in Dulbecco's Modified Eagle Medium (DMEM) supplemented with 10% [v/v] fetal bovine serum (FBS) (GIBCO, Invitrogen). Cell growth kinetics was studied under different growth conditions by plating $1x10^5$ cells in media containing 0.9 g/L galactose. Cell counts were performed using a haemocytometer at the interval of 24 hours. In some cases, the indicated concentration of valine was added to the medium.

The transfection ofWT and *TAZ*^{KO} MEF cells ($1x10^7$) was performed by electroporation with 20 µg empty pCDNA5.1 plasmid or pCDNA5.1 containing the cDNA of either BCAT1 or BCAT2 at 1350 V with a single pulse of 30 ms using the Neon Transfection System (Thermo Fisher Scientific). Immediately after the electroporation, the cells were plated in glucose-containing media for 24 hours. Next, $2.5x10^5$ cells of each experimental condition were re-plated in galactose-containing media for cell counts.

Acknowledgments

We thank E. Kracker for excellent technical assistance, Dr. R. Lill for antibodies, and Dr. K.S. Dimmer for helpful discussions. This work was supported by the Barth Syndrome Foundation (D.R. and M.S.), the DFG D.I.P.program (D.R., J.M.H., and M.S.), SFB1002 (TP A06, PR), ERC (ERCAdG No. 339580, PR), MWK FoP 88b (PR), and the Max Planck Society (PR). D.A. was supported by the IMPRS "From Molecules to Organisms".

References

Baile, M.G., M. Sathappa, Y.W. Lu, E. Pryce, K. Whited, J.M. McCaffery, X. Han, N.N. Alder, and S.M. Claypool. 2014. Unremodeled and remodeled cardiolipin are functionally indistinguishable in yeast. *The Journal of biological chemistry*. 289:1768-1778.

Baile, M.G., K. Whited, and S.M. Claypool. 2013. Deacylation on the matrix side of the mitochondrial inner membrane regulates cardiolipin remodeling. *Molecular biology of the cell*. 24:2008-2020.

Bazan, S., E. Mileykovskaya, V.K. Mallampalli, P. Heacock, G.C. Sparagna, and W. Dowhan. 2013. Cardiolipin-dependent reconstitution of respiratory supercomplexes from purified Saccharomyces cerevisiae complexes III and IV. *The Journal of biological chemistry*. 288:401-411.

Bledsoe, R.K., P.A. Dawson, and S.M. Hutson. 1997. Cloning of the rat and human mitochondrial branched chain aminotransferases (BCATm). *Biochimica et biophysica acta*. 1339:9-13.

Bligh, E.G., and W.J. Dyer. 1959. A RAPID METHOD OF TOTAL LIPID EXTRACTION AND PURIFICATION. *Canadian Journal of Biochemistry and Physiology*. 37:911-917.

Brandner, K., D.U. Mick, A.E. Frazier, R.D. Taylor, C. Meisinger, and P. Rehling. 2005. Taz1, an outer mitochondrial membrane protein, affects stability and assembly of inner membrane protein complexes: implications for Barth Syndrome. *Mol Biol Cell*. 16:5202-5214.

Chen, S., Q. He, and M.L. Greenberg. 2008. Loss of tafazzin in yeast leads to increased oxidative stress during respiratory growth. *Molecular microbiology*. 68:1061-1072.

Chi, Z., and N. Arneborg. 1999. Relationship between lipid composition, frequency of ethanol-induced respiratory deficient mutants, and ethanol tolerance in Saccharomyces cerevisiae. *Journal of applied microbiology*. 86:1047-1052.

Chowdhury, A., Aich, A., Jain, G., Wozny, K., Lüchtenborg, C., Hartmann, M., Bernhard, O., Balleiniger, M., Ahmed Alfar, E., Zieseniss, A., Toischer, K., Guan,K., Rizzoli, S., Brügger, B., Fischer, A., Katschinski, D., Rehling, P. Dudek, J. 2018. Mitochondrial ROS activate NF-kB in hypoxia to stimulate HIF-1a expression - a signaling process affected by defective cardiolipin-remodeling in Barth Syndrome. *Cell Reports*, 25:561-570

Claypool, S.M., and C.M. Koehler. 2012. The Complexity of Cardiolipin in Health and Disease. *Trends in Biochemical Sciences*. 37:32-41.

Costa, V., M.A. Amorim, E. Reis, A. Quintanilha, and P. Moradas-Ferreira. 1997. Mitochondrial superoxide dismutase is essential for ethanol tolerance of Saccharomyces cerevisiae in the post-diauxic phase. *Microbiology (Reading, England)*. 143 (Pt 5):1649-1656.

Daum, G., P.C. Bohni, and G. Schatz. 1982. Import of proteins into mitochondria. Cytochrome b2 and cytochrome c peroxidase are located in the intermembrane space of yeast mitochondria. *The Journal of biological chemistry*. 257:13028-13033.

de Taffin de Tilques, M., D. Tribouillard-Tanvier, E. Tétaud, E. Testet, J.-P. di Rago, and J.-P. Lasserre. 2017. Overexpression of mitochondrial oxodicarboxylate carrier (ODC1) preserves oxidative phosphorylation in a yeast model of Barth syndrome. *Disease Models & Mechanisms*. 10:439-450.

Du, X., and H. Takagi. 2007. N-Acetyltransferase Mpr1 confers ethanol tolerance on Saccharomyces cerevisiae by reducing reactive oxygen species. *Applied Microbiology and Biotechnology*. 75:1343-1351.

Elgersma, Y., C.W. van Roermund, R.J. Wanders, and H.F. Tabak. 1995. Peroxisomal and mitochondrial carnitine acetyltransferases of Saccharomyces cerevisiae are encoded by a single gene. *EMBO J*. 14:3472-3479.

Gartner, F., W. Voos, A. Querol, B.R. Miller, E.A. Craig, M.G. Cumsky, and N. Pfanner. 1995. Mitochondrial import of subunit Va of cytochrome c oxidase characterized with yeast mutants. *The Journal of biological chemistry*. 270:3788-3795.

Gebert, N., A.S. Joshi, S. Kutik, T. Becker, M. McKenzie, X.L. Guan, V.P. Mooga, D.A. Stroud, G. Kulkarni, M.R. Wenk, P. Rehling, C. Meisinger, M.T. Ryan, N. Wiedemann, M.L. Greenberg, and N. Pfanner. 2009. Mitochondrial cardiolipin involved in outer-membrane protein biogenesis: implications for Barth syndrome. *Current biology : CB*. 19:2133-2139.

Gietz, R.D., and R.A. Woods. 2006. Yeast transformation by the LiAc/SS Carrier DNA/PEG method. *Methods in molecular biology (Clifton, N.J.)*. 313:107-120.

Gonzalvez, F., M. D'Aurelio, M. Boutant, A. Moustapha, J.P. Puech, T. Landes, L. Arnaune-Pelloquin, G. Vial, N. Taleux, C. Slomianny, R.J. Wanders, R.H. Houtkooper, P. Bellenguer, I.M. Moller, E. Gottlieb, F.M. Vaz, G. Manfredi, and P.X. Petit. 2013. Barth syndrome: cellular compensation of mitochondrial dysfunction and apoptosis inhibition due to changes in cardiolipin remodeling linked to tafazzin (TAZ) gene mutation. *Biochimica et biophysica acta*. 1832:1194-1206.

Gu, Z., F. Valianpour, S. Chen, F.M. Vaz, G.A. Hakkaart, R.J. Wanders, and M.L. Greenberg. 2004. Aberrant cardiolipin metabolism in the yeast taz1 mutant: a model for Barth syndrome. *Mol Microbiol*. 51:149-158.

Ikon, N., and R.O. Ryan. 2017. Barth Syndrome: Connecting Cardiolipin to Cardiomyopathy. *Lipids*. 52:99-108.

Janke, C., M.M. Magiera, N. Rathfelder, C. Taxis, S. Reber, H. Maekawa, A. Moreno-Borchart, G. Doenges, E. Schwob, E. Schiebel, and M. Knop. 2004. A versatile toolbox for PCR-based tagging of yeast genes: new fluorescent proteins, more markers and promoter substitution cassettes. *Yeast*. 21:947-962.

Jimenez, J., and T. Benitez. 1988. Yeast cell viability under conditions of high temperature and ethanol concentrations depends on the mitochondrial genome. *Current genetics*. 13:461-469.

551 Kiebish, M.A., K. Yang, X. Liu, D.J. Mancuso, S. Guan, Z. Zhao, H.F. Sims, R. Cerqua, W.T. Cade, X.
552 Han, and R.W. Gross. 2013. Dysfunctional cardiac mitochondrial bioenergetic, lipidomic, and
553 signaling in a murine model of Barth syndrome. *Journal of Lipid Research*. 54:1312-1325.
554 Kingsbury, J.M., N.D. Sen, and M.E. Cardenas. 2015. Branched-Chain Aminotransferases Control
555 TORC1 Signaling in Saccharomyces cerevisiae. *PLoS Genet*. 11:e1005714.
556 Kispal, G., H. Steiner, D.A. Court, B. Rolinski, and R. Lill. 1996. Mitochondrial and cytosolic branched-
557 chain amino acid transaminases from yeast, homologs of the myc oncogene-regulated Eca39
558 protein. *J Biol Chem*. 271:24458-24464.
559 Longtine, M.S., A. McKenzie, 3rd, D.J. Demarini, N.G. Shah, A. Wach, A. Brachat, P. Philippsen, and
560 J.R. Pringle. 1998. Additional modules for versatile and economical PCR-based gene deletion
561 and modification in Saccharomyces cerevisiae. *Yeast*. 14:953-961.
562 McKenzie, M., M. Lazarou, D.R. Thorburn, and M.T. Ryan. 2006. Mitochondrial respiratory chain
563 supercomplexes are destabilized in Barth Syndrome patients. *Journal of molecular biology*.
564 361:462-469.
565 Minard, K.I., and L. McAlister-Henn. 2009. Redox responses in yeast to acetate as the carbon source.
566 *Archives of biochemistry and biophysics*. 483:136-143.
567 Palmieri, L., G. Agrimi, M.J. Runswick, I.M. Fearnley, F. Palmieri, and J.E. Walker. 2001. Identification
568 in Saccharomyces cerevisiae of two isoforms of a novel mitochondrial transporter for 2-
569 oxoadipate and 2-oxoglutarate. *The Journal of biological chemistry*. 276:1916-1922.
570 Pfeiffer, K., V. Gohil, R.A. Stuart, C. Hunte, U. Brandt, M.L. Greenberg, and H. Schagger. 2003.
571 Cardiolipin stabilizes respiratory chain supercomplexes. *The Journal of biological chemistry*.
572 278:52873-52880.
573 Raja, V., A.S. Joshi, G. Li, K.R. Maddipati, and M.L. Greenberg. 2017. Loss of Cardiolipin Leads to
574 Perturbation of Acetyl-CoA Synthesis. *Journal of Biological Chemistry*. 292:1092-1102.
575 Sauerwald, J., T. Jores, M. Eisenberg-Bord, S.G. Chuartzman, M. Schuldiner, and D. Rapaport. 2015.
576 Genome-Wide Screens in Saccharomyces cerevisiae Highlight a Role for Cardiolipin in
577 Biogenesis of Mitochondrial Outer Membrane Multispan Proteins. *Molecular and cellular*
578 *biology*. 35:3200-3211.
579 Schagger, H. 2002. Respiratory chain supercomplexes of mitochondria and bacteria. *Biochimica et*
580 *biophysica acta*. 1555:154-159.
581 Schlame, M., M. Ren, Y. Xu, M.L. Greenberg, and I. Haller. 2005. Molecular symmetry in
582 mitochondrial cardiolipins. *Chemistry and physics of lipids*. 138:38-49.
583 Schlame, M., J.A. Towbin, P.M. Heerdt, R. Jehle, S. DiMauro, and T.J. Blanck. 2002. Deficiency of
584 tetralinoleoyl-cardiolipin in Barth syndrome. *Annals of neurology*. 51:634-637.

585 Stettler, S., N. Chiannilkulchai, S. Hermann-Le Denmat, D. Lalo, F. Lacroute, A. Sentenac, and P.
586 Thuriaux. 1993. A general suppressor of RNA polymerase I, II and III mutations in
587 Saccharomyces cerevisiae. *Molecular & general genetics : MGG*. 239:169-176.
588 Tan, T., C. Özbalci, B. Brügger, D. Rapaport, and K.S. Dimmer. 2013. Mcp1 and Mcp2, two novel
589 proteins involved in mitochondrial lipid homeostasis. *Journal of Cell Science*. 126:3563-3574.
590 Tedesco, L., G. Corsetti, C. Ruocco, M. Ragni, F. Rossi, M.O. Carruba, A. Valerio, and E. Nisoli. 2018.
591 A specific amino acid formula prevents alcoholic liver disease in rodents. *American journal of*
592 *physiology. Gastrointestinal and liver physiology*.
593 Valianpour, F., R.J. Wanders, H. Overmars, P. Vreken, A.H. Van Gennip, F. Baas, B. Plecko, R. Santer,
594 K. Becker, and P.G. Barth. 2002. Cardiolipin deficiency in X-linked cardioskeletal myopathy
595 and neutropenia (Barth syndrome, MIM 302060): a study in cultured skin fibroblasts. *The*
596 *Journal of pediatrics*. 141:729-733.
597 Vatrinet, R., G. Leone, M. De Luise, G. Girolimetti, M. Vidone, G. Gasparre, and A.M. Porcelli. 2017.
598 The α-ketoglutarate dehydrogenase complex in cancer metabolic plasticity. *Cancer &*
599 *Metabolism*. 5:3.
600 Vreken, P., F. Valianpour, L.G. Nijtmans, L.A. Grivell, B. Plecko, R.J. Wanders, and P.G. Barth. 2000.
601 Defective remodeling of cardiolipin and phosphatidylglycerol in Barth syndrome. *Biochemical*
602 *and biophysical research communications*. 279:378-382.
603 Wach, A., A. Brachat, C. Alberti-Segui, C. Rebischung, and P. Philippsen. 1997. Heterologous HIS3
604 marker and GFP reporter modules for PCR-targeting in Saccharomyces cerevisiae. *Yeast*.
605 13:1065-1075.
606 Xu, Y., C.K. Phoon, B. Berno, K. D'Souza, E. Hoedt, G. Zhang, T.A. Neubert, R.M. Epand, M. Ren,
607 and M. Schlame. 2016. Loss of protein association causes cardiolipin degradation in Barth
608 syndrome. *Nature chemical biology*. 12:641-647.
609 Ye, C., W. Lou, Y. Li, I.A. Chatzispyrou, M. Huttemann, I. Lee, R.H. Houtkooper, F.M. Vaz, S. Chen,
610 and M.L. Greenberg. 2014. Deletion of the cardiolipin-specific phospholipase Cld1 rescues
611 growth and life span defects in the tafazzin mutant: implications for Barth syndrome. *The*
612 *Journal of biological chemistry*. 289:3114-3125.
613 Yofe, I., and M. Schuldiner. 2014. Primers-4-Yeast: a comprehensive web tool for planning primers for
614 Saccharomyces cerevisiae. *Yeast*. 31:77-80.
615 Zhang, M., E. Mileykovskaya, and W. Dowhan. 2005. Cardiolipin is essential for organization of
616 complexes III and IV into a supercomplex in intact yeast mitochondria. *J Biol Chem*. 280:29403-
617 29408.
618
619

Figure legends

Fig. 1. Bat1 and Bat2 are multi-copy suppressors of *taz1Δ* growth defect. (A) WT and *taz1Δ* cells were grown at 30°C in liquid medium and then five-fold serial dilutions were spotted on synthetic medium containing glucose (SD), glycerol (SG), or acetate (SA). WT and *taz1Δ* cells transformed with an empty plasmid (Ø) as well as *taz1Δ* cells expressing plasmid-born Taz1 were cultured as above and spotted on ethanol-containing synthetic medium lacking leucine (SE-Leu). **(B)** *taz1Δ* cells were transformed with the empty plasmid pFL44L, a plasmid encoding *TAZ1* (pYX142-*TAZ1*), or with plasmids of the genomic library isolated from positive candidates of the screen (#13, 15, 16, 29, two colonies each). Cells were analysed by drop dilution assay on SE medium at 30°C. Plasmid #16 harbors *BAT1* and *CRG1* whereas #29 harbors *COX24* and *HMX1*. **(C)** WT and *taz1Δ* cells genomically overexpressing *COX24*, *CRG1* or *HMX1* were analysed at 30°C by drop dilution assay on SE medium. **(D)** WT and *taz1Δ* cells as well as *taz1Δ* cells genomically overexpressing either *BAT1* or *BAT2* were analysed by drop dilution assay at 30°C on SE medium. **(E)** WT, *gep4Δ*, or *crd1Δ* cells as well as *gep4Δ* and *crd1Δ* cells genomically overexpressing either *BAT1* or *BAT2* were analyzed by drop dilution assay at 37°C on YPG medium or at 30°C on YPD medium.

Fig. 2. Overexpression of *BAT1* or *BAT2* does not rescue several defects of *taz1Δ* cells. (A-B) Mitochondria isolated from the indicated strains were lysed with 1% digitonin and subjected to a 6-14% BN-PAGE. Proteins were analysed by immunodetection with an antibody against either Rip1, a subunit of complex III (A) or Cox2, a subunit of complex IV (B). Supercomplexes of the respiratory chain complexes are indicated. **(C)** Membrane potential ($\Delta\Psi$) of mitochondria isolated from the indicated strains was determined by a fluorescence assay. The fluorescence signal of control organelles was set to 100%. Average values ± S.D. bars of three independent experiments are shown. **(D)** Lipids extracted from the mitochondria fraction of the indicated cells were analyzed by TLC and staining with molybdenum blue. The migration behavior of standard phospholipids are indicated. **(E)** The indicated amounts of mitochondria isolated from the specified strains were analysed by SDS-PAGE and immunodecoration with the indicated antibodies.

Fig. 3. Supplementation with some amino acids enhances growth of *taz1Δ* cells. (A-B) The indicated cells were analysed by drop dilution assay at 30°C on SE medium supplemented with the specified concentrations of the amino acids valine (Val) (A) or aspartate (Asp) (B). The

lower panel in A depicts a plate that has a gradient of valine concentration from 0.12 mM to 6.4 mM, whereWT or *taz1Δ* cells were spotted at the indicated OD_{600}.. **(C)** Lipids extracted from mitochondria grown in the absence of presence of 5 mM aspartate (D) or 6.4 mM valine (V) were analyzed by TLC and stained with molybdenum blue . **(D-E)** The indicated cells were analysed by drop dilution assay at 30°C on SE medium supplemented with the indicated concentrations of glutamate (Glu) (D) or histidine (His) (E). **(F)** WT and *taz1Δ* cells as well as *taz1Δ* cells genomically overexpressing either *AVT1* or *AVT4* were analyzed by drop dilution at 30°C on SE medium.

Fig. 4. The levels of some metabolites are altered in *taz1Δ* cells and restored upon overexpression of *BAT1*. The indicated metabolites were extracted from the specified cells grown in ethanol-containing media and were analysed by LC-MS. The relative peak area of each metabolite was determined and the levels in control WT cells were taken as 100%. Mean values ± S.D. of six independent experiments are shown. *, $p < 0.05$; **, $p < 0.01$; ***, $p < 0.001$.

Fig. 5. Overexpression of BCATs or valine supplementation increases cell proliferation of *TAZ*$^{-/-}$ MEF cells. (A) WT and *TAZ*^{KO} MEF cells were transfected with an empty plasmid (MOCK) or with a plasmid overexpressing either BCAT1 or BCAT2. Cells were cultivated in media containing galactose for the indicated time periods before cell counts were performed (± SEM, n=3). **(B)** WT and TAZ^{KO} MEF cells were supplemented with the indicated amounts of valine (Val) and cell count was performed after 72 hours (± SEM, n=3). *, $p < 0.05$; ***, $p < 0.001$.

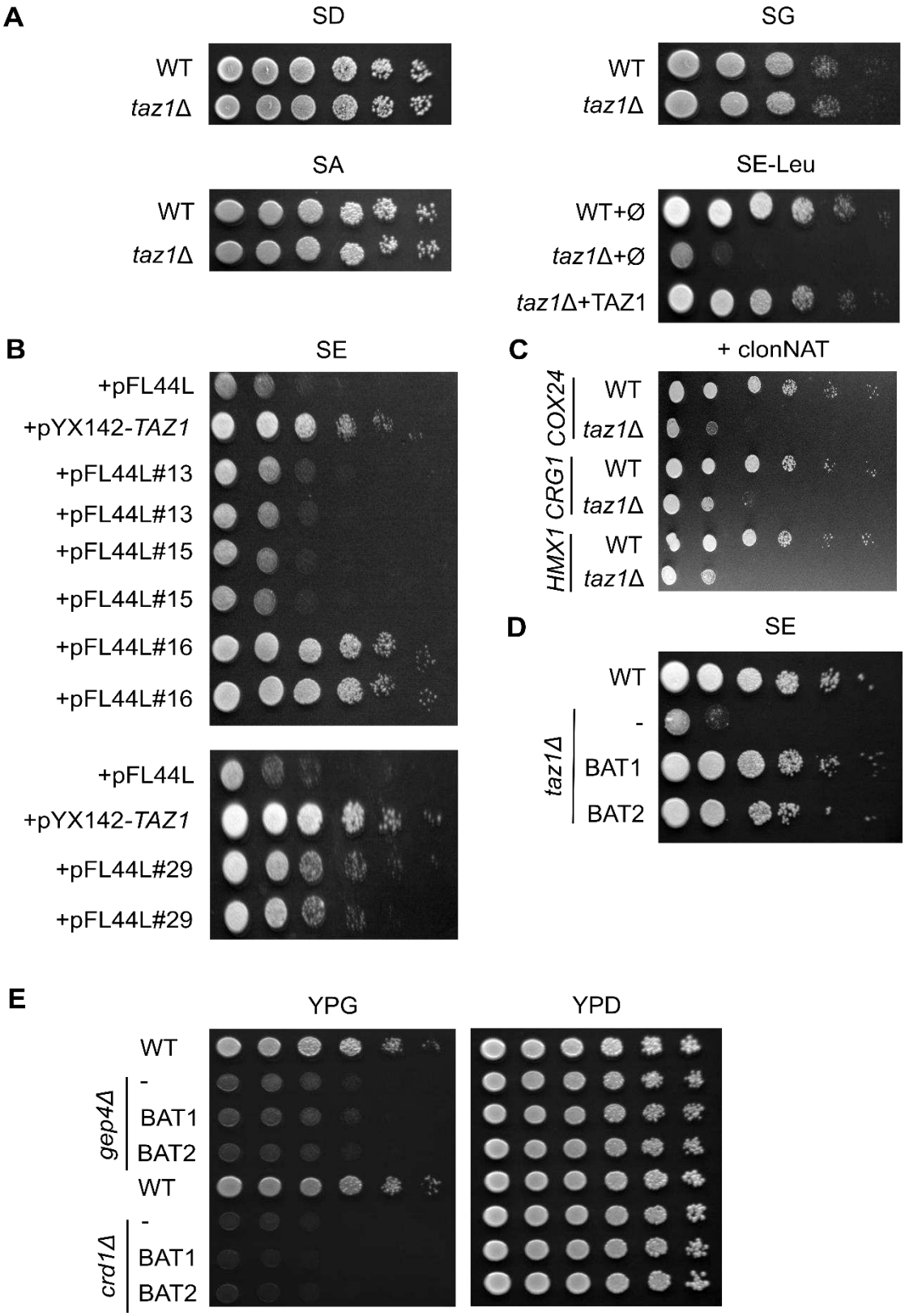

Antunes et al., Fig. 1

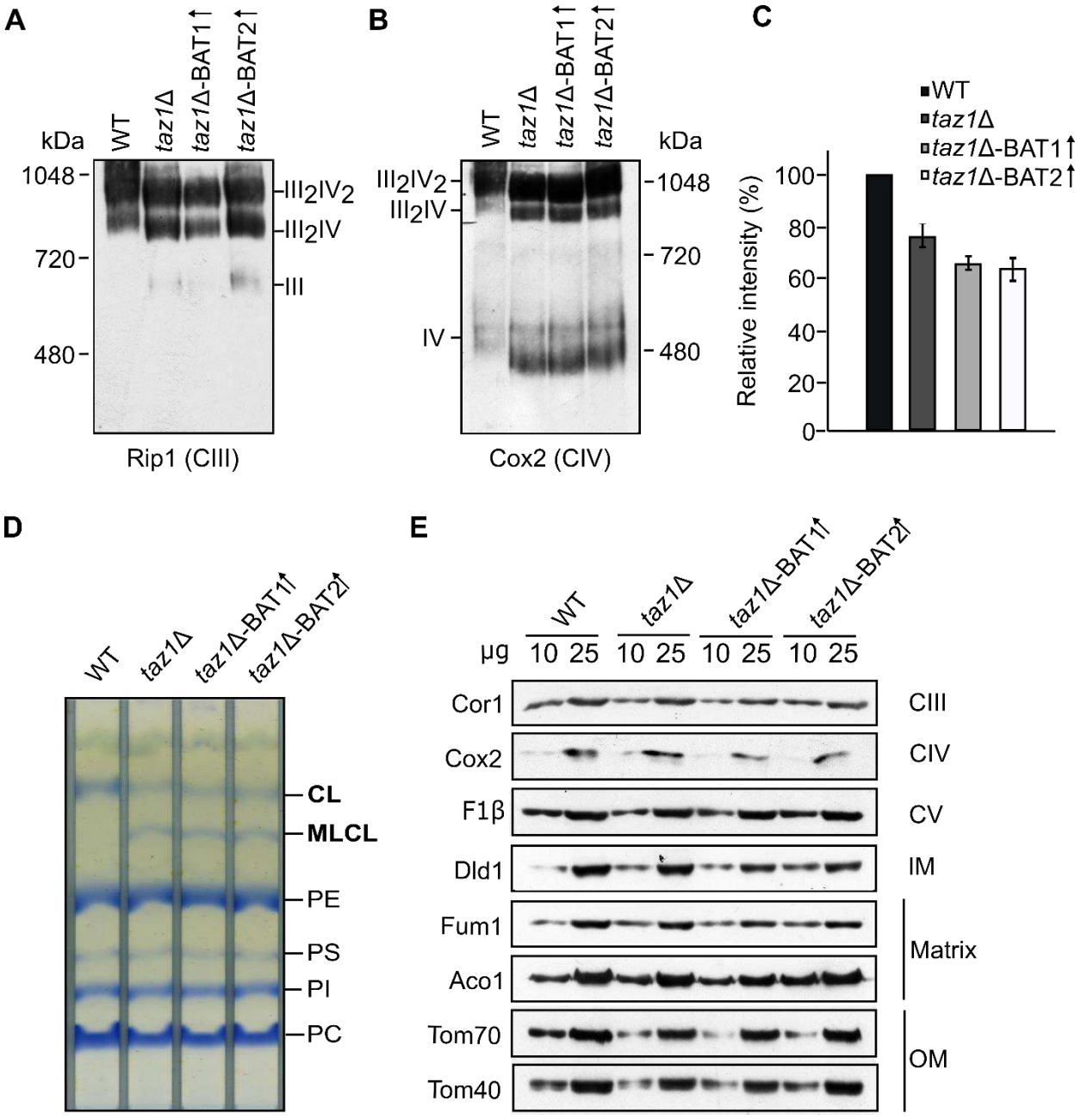

Antunes et al., Fig. 2

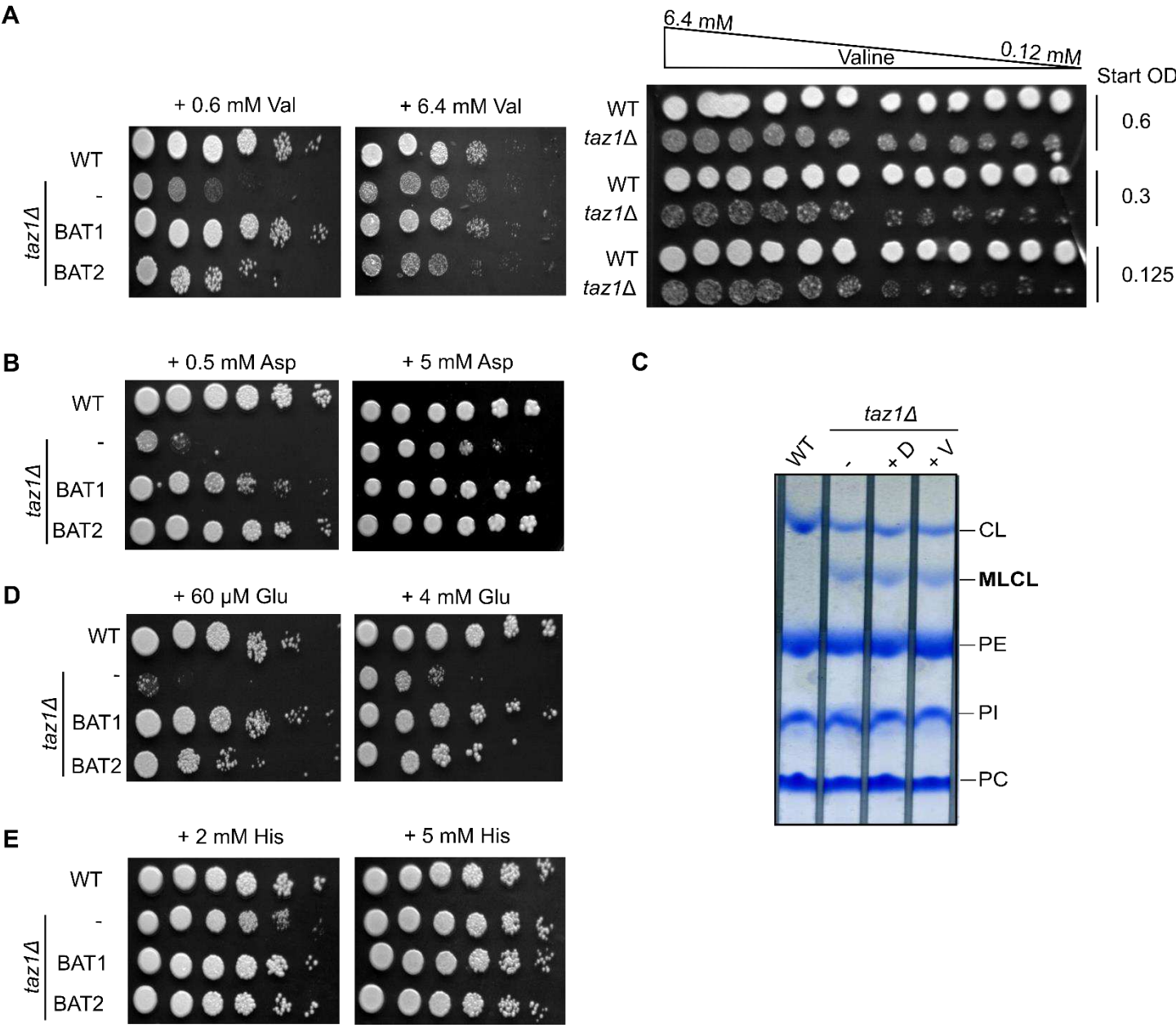

Antunes et al., Fig. 3

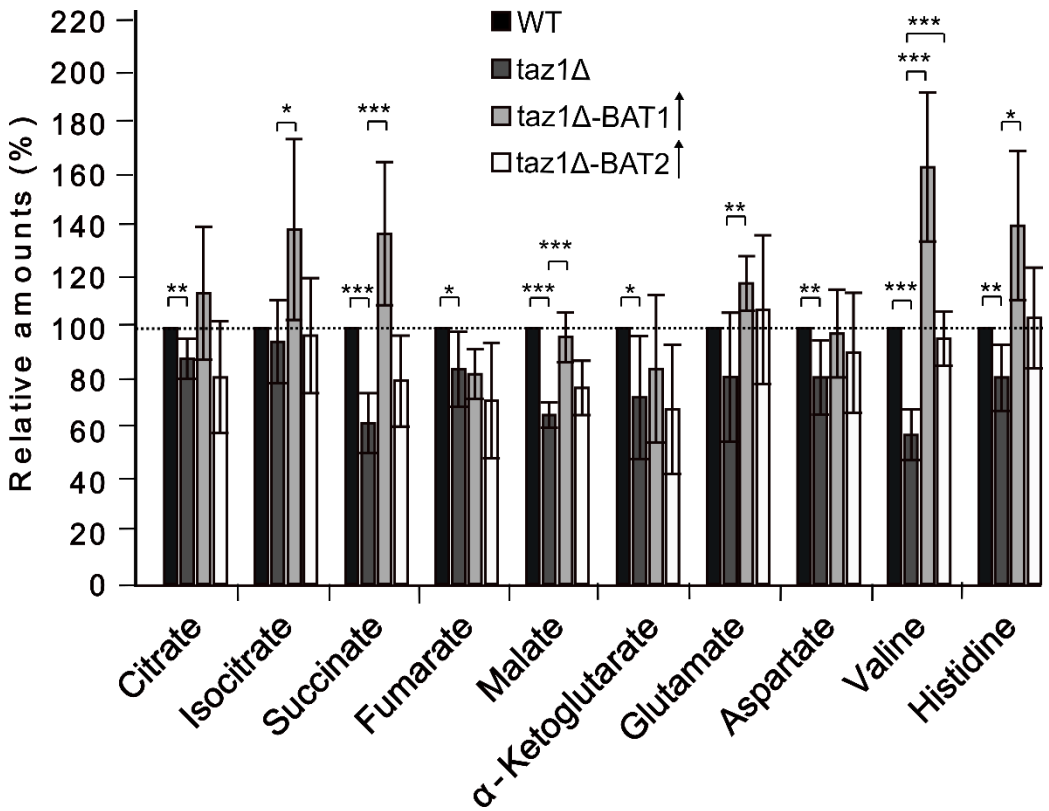

Antunes et al., Fig. 4

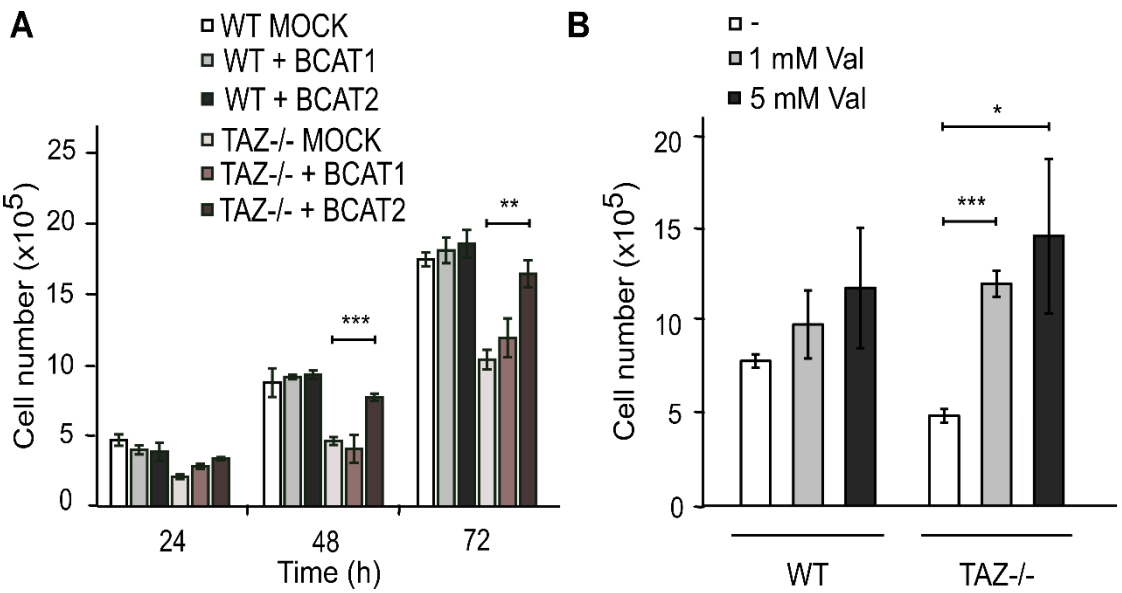

Antunes et al., Fig. 5

Antunes et al.

Overexpression of Branched-Chain Amino Acid Aminotransferases rescues the growth defects of cells lacking the Barth Syndrome related gene *TAZ1*

Supplementary Information

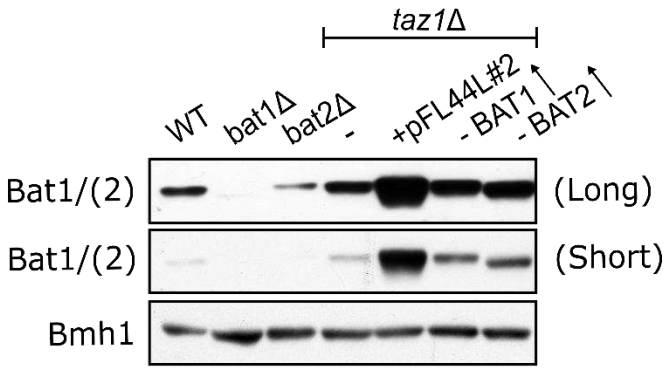

Fig. S1. Steady state levels of Bat1/(2) in relevant cells. Whole cell lysate were obtained from WT, *bat1Δ*, *bat2Δ*, *taz1Δ* transformed with an empty plasmid (-), or with a plasmid isolated from the #2 of the screen or genomically encoding *BAT1* or *BAT2*. Samples were analysed by SDS-PAGE and immunodetection with antibodies against Bat1 (long and short exposition) or the cytosolic marker Bmh1.

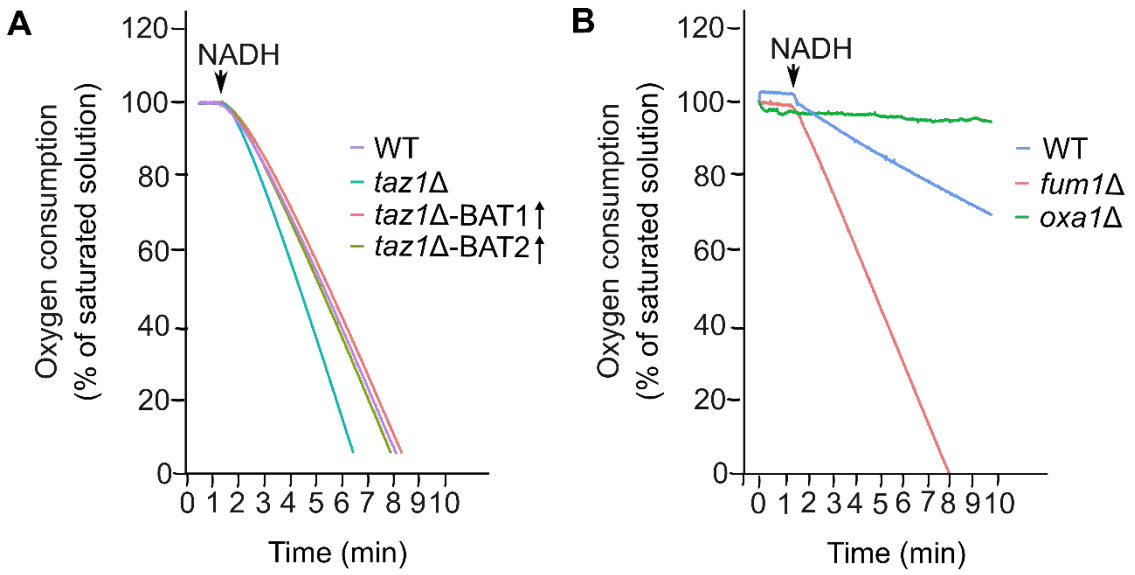

Fig. S2. Overexpression of *BAT1* or *BAT2* restores the altered mitochondrial oxygen consumption in *taz1Δ*. The rate of oxygen consumption of isolated mitochondria of the indicated strains upon NADH addition (7 mM) was measured (A)., Measurement of oxygen consumption on *fum1Δ* or *oxa1Δ* organelles was used as positive and negative control, respectively (B).

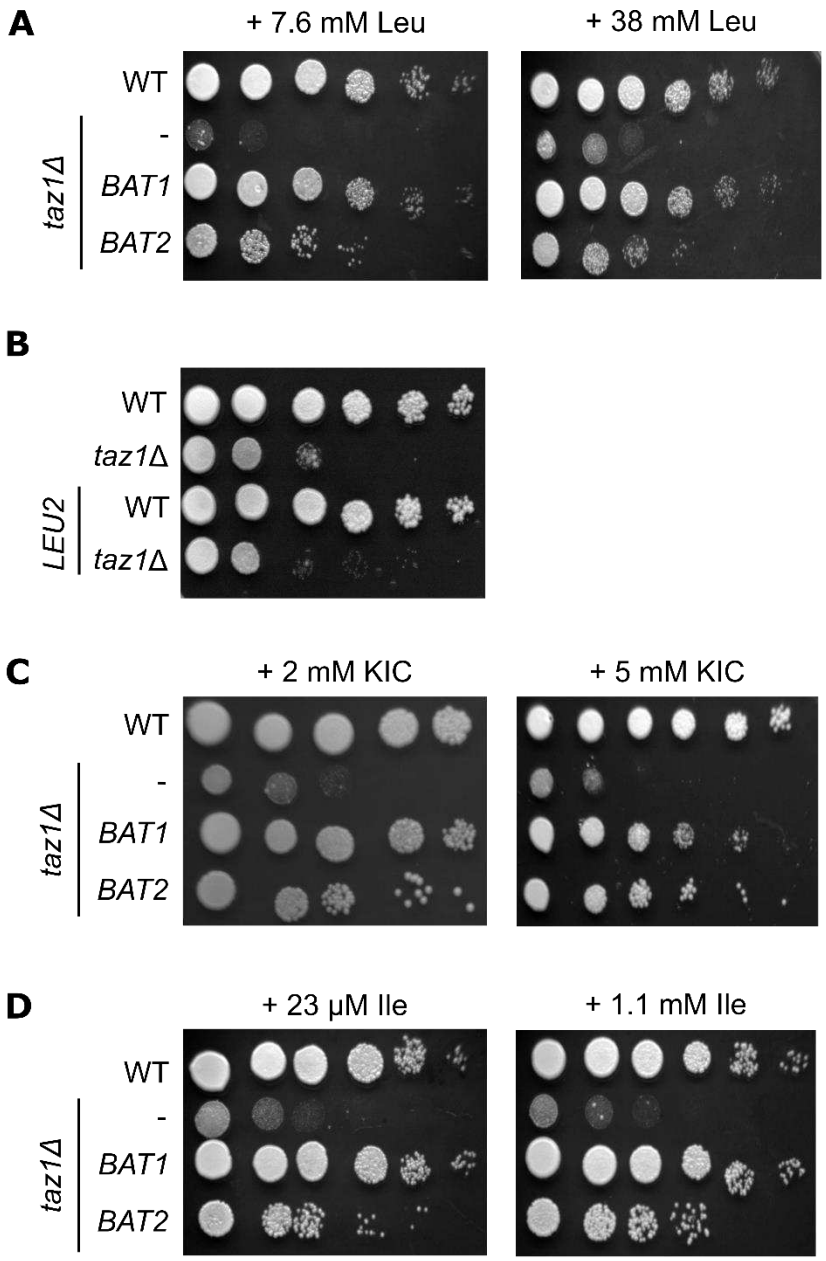

Fig. S3. Supplementation of the branched-chain amino acids leucine and isoleucine has no effect on the growth deffect of *taz1Δ* cells. WT and *taz1Δ* cells with or without the genomic overexpression of the *LEU2* gene were analysed by drop dilution assay at 30°C on SE medium (A). **(B-D)** The indicated cells were analysed by drop dilution assay at 30°C on SE medium supplemented with the specified concentrations of leucine (Leu) (B), α-ketoisocaproic acid (KIC) (C), or isoleucine (Ile) (D).

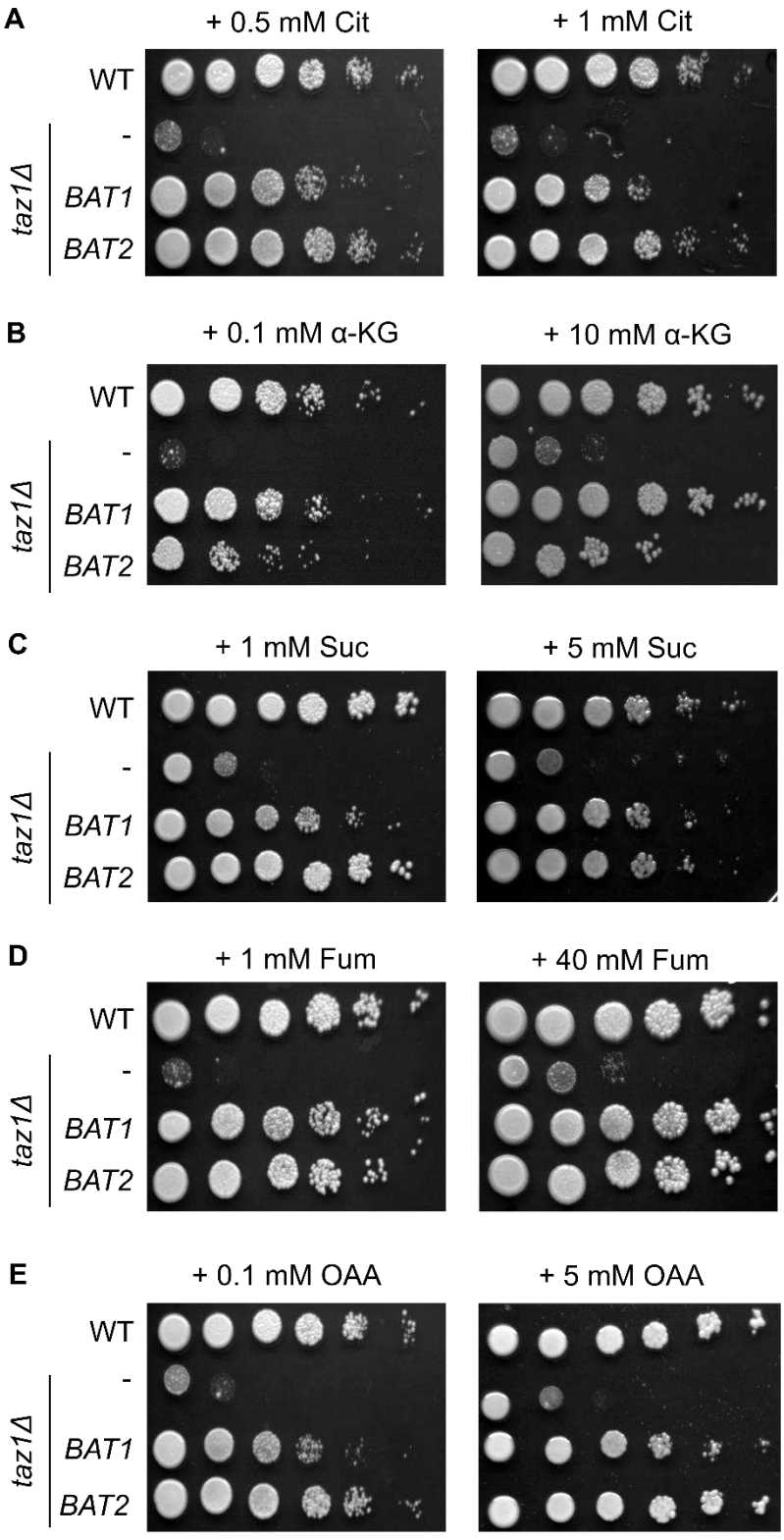

Fig. S4. Supplementation of various TCA cycle metabolites has no effect on growth retardation of *taz1Δ* cells. The specified strains were analysed by drop dilution assay at 30°C on SE medium supplemented with the indicated concentrations of the TCA cycle metabolites citrate (Cit) (A), α-ketoglutarate (α-KG) (B), succinate (Suc) (C), fumarate (Fum) (D), or oxaloacetate (OAA) (E).

Supplementary Table 1. Strains used in this study.

Name	Genotype	Source
WT (W303)	*leu2-3,112 trp1-1 can1-100 ura3-1 ade2-1 his3-11,15*	N/A
WT (BY4741)	*his3-1 leu2-0 met15-0 ura3-0*	N/A
crd1Δ	*BY4741; crd1Δ::HIS3MX6*	current study
gep4Δ	*BY4741; gep4Δ::KANMX4*	(Sauerwald et al., 2015)
crd1Δ-BAT1	*BY4741; crd1Δ::HIS3MX6 BAT1::natNT2-GPDpr-BAT1*	current study
crd1Δ-BAT2	*BY4741; crd1Δ::HIS3MX6 BAT2::natNT2-GPDpr-BAT2*	current study
gep4Δ-BAT1	*BY4741; crd1Δ::KANMX4 BAT1::natNT2-GPDpr-BAT1*	current study
gep4Δ-BAT2	*BY4741; gep4Δ::KANMX4 BAT2::natNT2-GPDpr-BAT2*	current study
WT-LEU2	*W303α LEU2::natNT2-GPDpr-LEU2*	current study
taz1Δ	W303α; *taz1Δ::HIS3MX6*	current study
bat1Δ	W303α; *bat1Δ::HIS3MX6*	current study
bat2Δ	W303α; *bat2Δ::HIS3MX6*	current study
taz1Δ-BAT1	W303α; *taz1Δ::HIS3MX6 BAT1::natNT2-GPDpr-BAT1*	current study
taz1Δ-BAT2	W303α; *taz1Δ::HIS3MX6 BAT2::natNT2-GPDpr-BAT2*	current study
taz1Δ-LEU2	W303α; *taz1Δ::HIS3MX6 LEU2::natNT2-GPDpr-LEU2*	current study
taz1Δ-AVT1	W303α; *taz1Δ::HIS3MX6 AVT1::natNT2-GPDpr-AVT1*	current study
taz1Δ-AVT4	W303α; *taz1Δ::HIS3MX6 AVT4::natNT2-GPDpr-AVT4*	current study

Supplementary Table 2. Plasmids and primers used in this study.

Plasmids	**Promoter**	**Markers**	**Reference**
pFL44L	-	URA3, AmpR	(Stettler et al., 1993)
pYX142-Taz1	TPI	LEU2, AmpR	current study
pYM-N15	GPD	natNT2, AmpR	(Janke et al., 2004)
Primers for deletion by gene-targeting			
DAFwd012	5'-ATA TTT CAT TTT CAA AAA AAA AAA AAG TAA AGT TTT CCC TAT CAA CGT ACG CTG CAG GTC GAC-3'		
DARev011	5'-GAC CTC ATA CAT GCT AGT ATT TAC ACG AAT TTA ATT GCT TAA ATT ATC GAT GAA TTC GAG CTCG-3'		
DAFwd032	5'-CAC CCT ATA AAC GCA AAA TCA GCT AGA ACC TTA GCA TAC TAA AAC CGT ACG CTG CAG GTC GAC-3'		
DARev034	5'-GTT TTT TTT TTT TGG GGG GGG AGG GGA TGT TTA CCT TCA TTA TCA ATC GAT GAA TTC GAG CTCG-3'		
DAFwd033	5'-TTT AGA AAT TTA AGG GAA AGC ATC TCC ACG AGT TTT AAG AAC GAT CGT ACG CTG CAG GTC GAC-3'		
DARev035	5'-TAT TCT TTT TAA CTT TTA ATT ACT TTA CGT AGC AAT AGC GAT ACT ATC GAT GAA TTC GAG CTCG-3'		
DAFwd039	5'-ACA AGC AGG CCT GGT AGC ATA GTT TGG TCC CTA ATA ATT TAG TCA CGT ACG CTG CAG GTC GAC-3'		
DARev042	5'-CAA AAT GAA AAG TCA GGA CCC TTT TCA AAA AGG ATC GCA ATT ATA ATC GAT GAA TTC GAG CTCG-3'		
Primers for introducing open reading frames into pYX plasmids			
DAFwd015	5'-GGG GAA TTC ATG TCT TTT AGG GAT GTC CTA GAA AGA GGA GAT-3'		
DARev014	5'-GGG AAG CTT TCA ATC ATC CTT ACC CTT TGG TTT ACC CTC TGG A-3'		
Primers for genomic N-terminal overexpression			
BAT1 N' tag pYM F	5'-AAA CGC AAA ATC AGC TAG AAC CTT AGC ATA CTA AAA CAT GCG TAC GCT GCA GGT CGA C-3'		
BAT1 N' tag pYM R	5'-TGA TGG AGA ATT TCC CCA ACT TCA AGG AAT GTC TCT GCA ACA TCG ATG AAT TCT CTG TCG-3'		
BAT2 N' tag pYM F	5'-TTT AAG GGA AAG CAT CTC CAC GAG TTT TAA GAA CGA TAT GCG TAC GCT GCA GGT CGA C-3'		
BAT2 N' tag pYM R	5'-TAG TTA TCT TAA CTT TGG AGG CGT CTA GGG GTG CCA AGG TCA TCG ATG AAT TCT CTG TCG-3'		
COX24 N' tag pYM F	5'-CCA AGA CGA GCA CAC ACG ACA CCA GAA CGA GAT AAA CAT GCG TAC GCT GCA GGT CGA C-3'		
COX24 N' tag pYM R	5'-TAG TAA TGC CCA GCC ACC CAG GTC GCA ATG CCC TTC CTA GCA TCG ATG AAT TCT CTG TCG-3'		
CRG1 N' tag pYM F	5'-CTT CAA AGC CAG TCT TCT GTC AAT GGA AGA ATC CAG AAT GCG TAC GCT GCA GGT CGA C-3'		
CRG1 N' tag pYM R	5'-GAG CAG ATT CAA AAT TTT TGT TTA AAT AAC TAG TTT TAG GCA TCG ATG AAT TCT CTG TCG-3'		
HMX1 N' tag pYM F	5'-GCA TAT ATA CAC ACA CAC ACA TAA AAT AAC CGC AAA AAT GCG TAC GCT GC AGG TCG AC-3'		
HMX1 N' tag pYM R	5'-CGT CAG TGG GTG AGG GTA TGA TTG TAT TGC TAC TGT CCT CCA TCG ATG AAT TCT CTG TCG-3'		
DAFwd038	5'-AAT ATA TAT ATA TAT ATT TCA AGG ATA TAC CAT TCT AAT GCG TAC GCT GCA GGT CGA C-3'		

DARev040	5‘-CGT GGT CAC CTG GCA AAA CGA CGA TCT TCT TAG GGG CAG ACA TCG ATG AAT TCT CTG TCG-3‘
DAFwd044	5‘-GAC TTA CGT ATT CTG TAT AAC TGA TTC CGA GAC GCA AAT GCG TAC GCT GCA GGT CGA C-3‘
DARev046	5‘-AGC GCT TAC GGC CAT TGG GAC TCA ATG GTT CTT GCT CAG GCA TCG ATG AAT TCT CTG TCG-3‘
DAFwd045	5‘-TGG AAT CAA CAT AAC AAT ATC CTA GAA CAC ATC ATC AAT GCG TAC GCT GCA GGT CGA C-3‘
DARev047	5‘-TTC GGA TCC CAA GGT GCT CAC CAT CTC CAT TGT TAG TGA CCA TCG ATG AAT TCT CTG TCG-3‘
Primers for screening PCR of gene-targeting	
DAFwd013	5’-CAG TAT TTC TAT TAC GTT ACT CCA G-3’
DARev012	5’-TTA TAT GGT AGT GTT GCC CAA ACT A-3’
DAFwd014	5’-ATG TCT TTT AGG GAT GTC CTA GAA A-3’
DARev013	5’-GGG CGG GGA GTA GGC TTT TTT TAG C-3’
DAFwd034	5‘-GCG GTT GAT ACT TTG TGC AGA TTT C-3‘
DARev036	5‘-ATA CCT TGG CAA CTA AAT TAC AAG C-3‘
DAFwd035	5‘-ATG TTG CAG AGA CAT TCC TTG AAG T-3‘
DARev037	5‘-AGT GCC AAC ACC TAA ACC CTT GGA T-3‘
DAFwd036	5‘-AAT CTG TAG ATC CGA CTC TTT TTC T-3‘
DARev038	5‘-GAG TTG CTT CTA AGG TAT GTA TGG G-3‘
DAFwd037	5‘-ATG ACC TTG GCA CCC CTA GAC GCC T-3‘
DARev039	5‘-GTA ATA AGG ACC CAC AGG GCA GCA A-3‘
DAFwd042	5’-CGA CAG AGA ATT CAT CGA TG-3’
BAT1 N’tag CHK R	5‘-GTT GGC AAA CAA ATT CTA GC-3‘
BAT2 N’tag CHK R	5‘-TAG TGC CGA TTA ATG TAG GC-3‘
COX24 N’tag CHK R	5‘-GCT TTC TTC TTT CTG CCT TC-3‘
CRG1 N’tag CHK R	5‘-GAA TGC AAA AGT TCC ATC AC-3‘
HMX1 N’tag CHK R	5‘-TGT GTA TGT TTT CGT GGA TG-3‘
DARev041	5‘-ACT TCT GGA ACG GTG TAT TG-3‘
DAFwd040	5’-CGT TTG GCA AAC AAT TAC AGG AAG A-3’
DARev043	5’-TGT TAG ACG ATC TGG TAC TAC GAA C-3’
DAFwd041	5’-ATG ATT CAA ATG GTG CCC ATT TAT T-3‘
DARev044	5’-TAT AAA CAA AGC ACT TAT GGC TAG T-3‘
DARev048	5‘-TTGTTGAATTTTGGATGGAC-3‘
DARev049	5‘-CAGCGCTACTCAGGTTAGTC-3‘

.

Supplementary Table 3. Antibodies used in this study.

Antibodies	Dilution	Source
polyclonal rabbit anti-Aco1	1 :7000	Lab stocks
polyclonal rabbit anti-Bmh1	1 :1500	Lab stocks
polyclonal rabbit anti-Bat1	1:3000	Kindly provided by Roland Lill
polyclonal rabbit anti-Cor1	1:2000	Lab stocks
polyclonal rabbit anti-Cox2	1:1000	Lab stocks
polyclonal rabbit anti-Dld1	1:1000	Lab stocks
polyclonal rabbit anti-F1β	1:500	Lab stocks
polyclonal rabbit anti-Fum1	1:10000	Lab stocks
polyclonal rabbit anti-Rip1	1:5000	Lab stocks
polyclonal rabbit anti-Tom40	1:4000	Lab stocks
polyclonal rabbit anti-Tom70	1:2000	Lab stocks

Supplementary References

Janke, C., M.M. Magiera, N. Rathfelder, C. Taxis, S. Reber, H. Maekawa, A. Moreno-Borchart, G. Doenges, E. Schwob, E. Schiebel, and M. Knop. 2004. A versatile toolbox for PCR-based tagging of yeast genes: new fluorescent proteins, more markers and promoter substitution cassettes. *Yeast*. 21:947-962.

Sauerwald, J., T. Jores, M. Eisenberg-Bord, S.G. Chuartzman, M. Schuldiner, and D. Rapaport. 2015. Genome-Wide Screens in Saccharomyces cerevisiae Highlight a Role for Cardiolipin in Biogenesis of Mitochondrial Outer Membrane Multispan Proteins. *Molecular and Cellular Biology*. 35:3200-3211.

Stettler, S., N. Chiannilkulchai, S. Hermann-Le Denmat, D. Lalo, F. Lacroute, A. Sentenac, and P. Thuriaux. 1993. A general suppressor of RNA polymerase I, II and III mutations in Saccharomyces cerevisiae. *Molecular and General Genetics*. 239:169-176.

The ER-Mitochondria contact site coordinates coenzyme Q biosynthesis

Michal Eisenberg-Bord[1]*, Hui S. Tsui[2]*, Diana Antunes[3]*, Lucía Fernández-del-Río[2]*, Michelle C. Bradley[2], Cory D. Dunn[4,5], Doron Rapaport[3#], Catherine F. Clarke[2#] & Maya Schuldiner[1#]

* These authors contributed equally to this work

To whom correspondence should be addressed: cathy@chem.ucla.edu, doron.rapaport@uni-tuebingen.de, maya.schuldiner@weizmann.ac.il

1. Department of Molecular Genetics, Weizmann Institute of Science, Rehovot, Israel 7610001

2. Department of Chemistry and Biochemistry and the Molecular Biology Institute, UCLA, Los Angeles, CA, USA 90095-1569

3. Interfaculty Institute of Biochemistry, University of Tübingen, 72076 Tübingen, Germany

4. Institute of Biotechnology, Helsinki Institute of Life Science, University of Helsinki, 00014 Helsinki, Finland

5. Department of Molecular Biology and Genetics, Koç University, 34450 İstanbul, Turkey

Abstract

Loss of ER-Mitochondria Encounter Structure (ERMES) contact-sites between the yeast endoplasmic reticulum (ER) and mitochondria impairs respiration. However, the molecular reason for this is not known. By analyzing the transcriptional response of ERMES deletion mutants, we find a specific increase in the levels of mRNAs encoding for enzymes involved in the biosynthesis of coenzyme Q_6 (CoQ_6), an essential electron transfer molecule in the respiratory chain. We show that the mega complex of polypeptides involved in CoQ_6 biosynthesis (CoQ synthome) is destabilized in contact-site mutants affecting the levels of CoQ_6 and its intermediates in mitochondria and the whole cell. We suggest that this effect is due to inefficient CoQ_6 biosynthesis and escape of CoQ_6 and intermediates from mitochondria. Fluorescence microscopy shows the enrichment of the CoQ synthome underlying ERMES contact sites. The collaboration between the ER and mitochondria in regulating respiration highlights an additional level of communication between these two organelles.

Introduction

Over the past two decades, our view on the architecture of the eukaryotic cell has been gradually altered. The original view of solitary organelles scattered sparsely in the cytosol has been replaced by an understanding that organelles are arranged within a more complex architecture. In fact, organelles are tightly packed together, and are anything but solitary. All organelles have the capacity to be tethered one to another, by designated structures termed membrane contact sites (Kakimoto et al., 2018; Shai et al., 2018; Valm et al., 2017). Contact sites are areas where the membranes of two organelles come into proximity through the use of tethering molecules. Such areas of close apposition allow the transfer of metabolites and other molecules between the two organelles (Eisenberg-Bord et al., 2016). One of the most studied contact sites forms between the endoplasmic reticulum (ER) and mitochondria. This contact site has an important role in transfer of calcium and phospholipids between the two organelles (Herrera-Cruz and Simmen, 2017).

A major complex promoting association of the ER and mitochondria in the budding yeast *Saccharomyces cerevisiae* (hereafter termed 'yeast') is the ER-Mitochondria Encounter Structure (ERMES) (Kornmann et al., 2009). ERMES is composed of four subunits: two mitochondrial subunits (Mdm10 and Mdm34), an ER subunit (Mmm1) and a soluble subunit (Mdm12). ERMES mutants show severe phenotypes including loss of mitochondrial morphology, increased loss of mitochondrial DNA, and reduced respiration capacity (Berger et al., 1997; Hobbs et al., 2001; Kornmann et al., 2009; Youngman et al., 2004). ERMES was also shown to have a role in mediating mitochondrial dynamics (Friedman et al., 2011; Murley et al., 2013), mitophagy (Böckler et al., 2014), life and death decisions (Smethurst and Cooper, 2016) and iron metabolism (Xue et al., 2017).

One of the most studied roles of the ERMES complex is the transfer of phospholipids. As mitochondria can only partially synthesize the lipids that they require, phospholipids, sterols and ceramide/sphingolipids must be imported from the ER. The ER-mitochondria contact sites accommodate many lipid transfer enzymes and proteins that are involved in lipid metabolism (Dimmer and Rapaport, 2017). Recently it was shown that the Mmm1-Mdm12 complex can mediate phospholipid transfer *in vitro* and that mutations in *MMM1* or *MDM12* lead to impaired phospholipid transfer through the ERMES complex *in vivo* (Kawano et al., 2018). However, ERMES mutants show only a mild decrease in specific phospholipids due to the existence of compensatory mechanisms for phospholipid transfer to mitochondria (Elbaz-Alon et al., 2014, 2015; Hönscher et al., 2014). Despite a

wealth of information on the ERMES complex, why its loss causes respiratory deficiency has not yet been fully elucidated. Hence, we set out to uncover the role of ERMES in regulating respiration.

Here we show that ERMES mutants have increased levels of mRNAs encoding proteins that participate in the coenzyme Q_6 (CoQ_6) biosynthesis pathway. CoQ_6 is a polyisoprenylated benzoquinone lipid that functions in the electron transport chain of the inner mitochondrial membrane of yeast and also acts as a lipophilic antioxidant (Awad et al., 2018; Tran and Clarke, 2007). All the steps required for the assembly of the polyisoprenoid diphosphate tail of CoQ, its ligation to aromatic ring precursors, and modification of the ring precursor, occur within the mitochondria by Coq enzymes associated with the matrix side of the mitochondrial inner membrane (Awad et al., 2018; Bentinger et al., 2010). Many of the Coq polypeptides (Coq3-Coq9 and Coq11) assemble in a mega-complex termed the CoQ synthome (Allan et al., 2015; Belogrudov et al., 2001; He et al., 2014; Marbois et al., 2005, 2009). However, synthesis of the polyisoprenoid tail of CoQ_6 originates from compounds that derive from the mevalonate pathway associated with the ER, suggesting that the ER-mitochondria contact site might promote movement of CoQ_6, its intermediates or precursors, between these two organelles.

Indeed, we show that the CoQ synthome is destabilized in ERMES mutants resulting in inefficient *de novo* CoQ_6 biosynthesis. Such compromised synthesis also results in accumulation of early- and late-stage CoQ_6 intermediates, as well as buildup of CoQ_6 at non-mitochondrial cellular membranes. We further demonstrate that ERMES mutants harbor decreased steady state levels of CoQ_6 and CoQ_6-intermediates within mitochondria. Taken together, the data indicate that the CoQ synthome is possibly involved in stabilizing CoQ_6 and CoQ_6-intermediates and retaining them inside mitochondria. Furthermore, ERMES mediated contacts seem to be localized above specialized matrix niches where the CoQ synthome is enriched, suggesting a spatially regulated process. Collectively, our study provides new insights into the relevance of the ER-mitochondria contact to CoQ_6 homeostasis and, more broadly, to respiration.

Materials and Methods

Yeast strains and plasmids

Saccharomyces cerevisiae strains and plasmids used in this study are listed in Table S1 and Table S2, respectively. Yeast strains were based on the laboratory strain S288C (BY4741) (Baker Brachmann et al., 1998) or W303 (Thomas and Rothstein, 1989). Transformations of PCR fragments into yeast cells were performed using the Li-acetate method (Gietz

and Woods, 2006; Janke et al., 2004; Longtine et al., 1998). Primers were designed using Primers-4-Yeast (Yofe and Schuldiner, 2014).

RNA-Sequencing

S288C (BY4741) cells were grown overnight in a synthetic medium SD (2% [wt/vol] glucose, 0.67% [wt/vol] yeast nitrogen base with ammonium sulfate and amino acid supplements) at 30°C. W303 cells were grown overnight in a synthetic medium SGly (2% [wt/vol] glycerol, 0.67% [wt/vol] yeast nitrogen base with ammonium sulfate and amino acid supplements) at 30°C. In the morning, cells were back-diluted to OD_{600}~0.01 and grown until reaching OD_{600}~ 0.2. Cells were centrifuged (3000 *g*, 3 min), and the pellet was frozen in liquid nitrogen and stored at −80°C until further analysis.

For all samples, RNA was purified as described in (Voichek et al., 2016). Briefly, RNA was extracted according to a protocol of Nucleospin® 96 RNA kit (Machery-Nagel) with two modifications: lysis was performed by adding 450 µl of lysis buffer containing 1 M sorbitol, 100 mM EDTA and 0.45 µl lyticase (10 I U/µl) to cells in a 96 deep-well plate. The plate was then incubated for 30 min at 30°C, centrifuged (3000 *g*, 10 min) and the supernatant was removed. In addition, dithiothreitol was used as a replacement for β-mercaptoethanol.

For S288C cells, RNA was fragmented, poly(A) selected, followed by cDNA preparation, barcoding, and sequencing using Illumina HiSeq 2500, as described (Voichek et al., 2016). For W303 cells, RNA libraries were created by reverse transcription with a barcoded poly(T). DNA-RNA hybrids were pooled, followed by use of a hyperactive variant of the Tn5 transposase (gift from Ido Amit, Weizmann Institute of Science, Israel) for fragmentation. SDS (0.2%) was used to strip Tn5 off the DNA. Following SDS treatment, samples were purified using Solid Phase Reversible Immobilisation (SPRI) (Beckman Coulter) beads. cDNA was then amplified using PCR and sequenced using the Illumina NextSeq 500. Single end reads were then mapped to *S. cerevisiae* genome (R64 in SGD) (Cherry et al., 2012) using bowtie (parameters: --best –a –m 2 –strata -5 10) (Liu et al., 2005). Following alignment, reads mapped to rRNA were excluded. For S288C samples, reads were down sampled to 400,000 reads and normalized for PCR bias using the unique molecular identifier (UMI) (Kivioja et al., 2012). For all samples, expression of each gene was the summary of reads aligned between 400bp upstream and 200bp downstream of the predicted open reading frame. The gene expression summary was normalized to be 1,000,000 and a gene with an expression below 10 was excluded from further analysis (Voichek et al., 2016). Each sample was run twice and values shown are typically the average of the two. However, if only one sample had a value, that value was provided.

Mitochondrial purification from yeast

Yeast wild-type and ERMES mutant cultures were grown in YPGly (1% [wt/vol] Bacto yeast extract, 2% [wt/vol] Bacto peptone, 3% glycerol) at 30°C. Cells were harvested at OD_{600} of < 4.0, and mitochondria were purified with discontinuous Nycodenz as described (Glick and Pon, 1995). Roche Complete EDTA-free protease inhibitor mixture, phosphatase inhibitor cocktail set II (EMD Millipore) and phosphatase inhibitor cocktail set 3 (Sigma-Aldrich) were added to the solutions. Gradient-purified mitochondria were frozen in liquid nitrogen and stored at −80°C until further analysis. Mitochondria from yeast Δ*coq* mutants were purified in the same manner from cultures grown in YPGal medium (1% [wt/vol] Bacto yeast extract, 2% [wt/vol] Bacto peptone, 2% [wt/vol] galactose, 0.1% [wt/vol] dextrose).

SDS-PAGE analysis of steady state levels of Coq polypeptides

Purified mitochondria were resuspended in SDS sample buffer consisting of 50 mM Tris, pH 6.8, 10% glycerol, 2% SDS, 0.1% bromophenol blue, and 1.33% β-mercaptoethanol and proteins were separated by SDS-PAGE on 12% Tris-glycine polyacrylamide gels. An aliquot of 25 μg of purified mitochondria, as measured by the bicinchoninic acid (BCA) assay standardized using bovine serum albumin (BSA), was loaded in each lane.

Two-dimensional BN- and SDS-PAGE analysis of CoQ synthome

Analysis of protein complexes by blue native (BN) gel electrophoresis was performed as previously described (Schagger et al., 1994; Wittig et al., 2006). Briefly, an aliquot of 200 μg protein of purified mitochondria was pelleted by centrifugation (14000 *g*, 10 min) and solubilized at a concentration of 4 mg protein /ml on ice for 1 hr with BN solubilization buffer containing 11 mM HEPES, pH 7.4, 0.33 M sorbitol, 1X NativePAGE sample buffer (Thermo Fisher Scientific), 16 mg/ml digitonin (Biosynth), Roche Complete EDTA-free protease inhibitor mixture, phosphatase inhibitor cocktail set II, and phosphatase inhibitor cocktail set 3. The soluble fraction was obtained by centrifugation (100,000 *g*, 10 min) and the protein concentration in the supernatant was determined by BCA assay. NativePAGE 5% G-250 sample additive (Thermo Fisher Scientific) was added to the supernatant to a final concentration of 0.25%. The first-dimension BN gel electrophoresis was performed using NativePAGE 4-16% Bis-Tris gel 1.0 mm x 10 wells (Thermo Fisher Scientific). First-dimension gel slices were soaked in hot SDS sample buffer for 15 min before loading them onto second dimension 12% Tris-glycine polyacrylamide gels. The high molecular weight standards for first-dimension BN gel electrophoresis were obtained from GE Healthcare (Sigma-Aldrich) [Cat. GE17-0445-01], and the molecular weight standards for second dimension SDS-PAGE were obtained from Bio-Rad [Cat. 1610394].

Immunoblot analyses

Proteins were transferred onto 0.45 μm nitrocellulose membrane (Bio-Rad). Membranes were blocked in 0.5% BSA, 0.1% Tween 20, 0.02% SDS in phosphate-buffered saline. Membranes were probed with primary antibodies (Table S3) in the same blocking buffer at the dilutions listed in Table S3. IRDye 680LT goat anti-rabbit IgG secondary antibody, or IRDye 800CW goat anti-mouse IgG secondary antibody (LiCOR) were used at 1:10,000 dilutions. Blot images were recorded using LiCOR Odyssey Infrared Scanner (LiCOR).

Stable isotope labeling

Cells were grown overnight in 100 ml of YPGly in a shaking incubator (30°C, 250 rpm) and diluted the next morning to an OD_{600} ~0.1 with fresh YPGly. The cultures were incubated as before until they reach an OD_{600} of 0.6 and then 8 μg/ml of the stable isotopes $^{13}C_6$-pABA, $^{13}C_6$-4HB, or ethanol (as vehicle control) were added and the cultures were grown for additional 5 hr. At each time point, triplicates of 10 ml culture were harvested by centrifugation (3000 *g*, 5 min). Cell pellets were stored at −20°C.

Lipid extractions and analysis of CoQ_6 and CoQ_6 intermediates

For lipid extraction, approximately 100 μg of purified mitochondria from each strain were prepared in triplicates, and same amount of internal standard CoQ_4 were added to all samples and standards, followed by addition of 2 ml methanol. Lipids

were extracted twice, each time with 2 ml petroleum ether. Extracted lipids were dried down with N_2 and stored at −20°C. Lipid extraction from isotopically-labeled whole cell was performed in the same way from frozen cell pellets in triplicates.

For lipid analysis, dried lipids were reconstituted in 200 µl of 0.5 mg/ml benzoquinone in order to oxidize hydroquinones to quinones. An aliquot of 20 µl of each sample was injected into a 4000 QTRAP linear MS/MS spectrometer (Applied Biosystems). Applied Biosystems software, Analyst version 1.4.2, was used for data acquisition and processing. The chromatographic separation was carried out using a Luna 5 µm phenyl-hexyl column (100 x 4.6 mm, 5 µm; Phenomenex) and a mobile phase consisted of 95:5 methanol/isopropanol solution with 2.5 mM ammonium formate as solution A and 100% isopropanol solution with 2.5 mM ammonium formate as solution B. The percentage of solution B was increased linearly from 0 to 10% over 7 min, whereby the flow rate was increased from 650 to 800 µl/min. Each sample was analyzed using multiple reaction monitoring mode (MRM). The precursor-to-product ion transitions monitored for each sample are listed in Table S4. The area value of each peak, normalized with the correspondent standard curve and internal standard, was referred to the total mitochondrial protein present in the sample or total OD of cells in each cell pellet. Statistical analysis was performed with GraphPad Prism with one-way ANOVA for mitochondrial lipid analyses, and with two-way ANOVA for whole cell lipid analyses.

Microscopy

Yeast were cultured overnight at 30°C in either SGly for W303 cells or SD for S288C. In the morning, cells were back-diluted to OD_{600}~0.2 and grown until reaching mid-logarithmic phase. Cells were then moved to glass-bottom, 384-well microscope plates (Matrical Bioscience) coated with Concanavalin A. After 20 min incubation at room temperature, the wells were washed with medium. Cells were then imaged at room temperature using a 60X oil lens (NA 1.4) in the VisiScope Confocal Cell Explorer system, which is composed of a Zeiss Yokogawa spinning disk scanning unit (CSU-W1) coupled with an inverted IX83 microscope (Olympus). Single–focal-plane images were taken using a PCO-Edge sCMOS camera, controlled by VisiView software (GFP-488 nm, RFP-561 nm, or BFP-405 nm). Images were reviewed using ImageJ.

Results

Cells lacking ERMES complex subunits up-regulate coenzyme Q biosynthesis transcripts

To investigate how the ERMES complex contributes to the respiratory capacity of the cell, we set out to measure the cellular transcriptional response upon deletion of ERMES subunits. We performed RNA sequencing on ERMES mutants from two different genetic backgrounds: W303 cells that preserve their mitochondrial DNA while being deleted for each of the four ERMES subunits Mmm1, Mdm10, Mdm12 or Mdm34; or S288C (BY4741) cells (who lose their mitochondrial DNA very rapidly) deleted for Mmm1, Mdm10 or Mdm12 (The complete list of mRNA levels in ERMES mutants is in Table S5). When surveying genes required for respiration, we noticed that the mRNA levels of most *COQ* genes involved in the biosynthesis of CoQ_6 were higher relative to those in the respective wild-type control in both genetic backgrounds (Figure 1A for W303 and Figure S1A for S288C), while the mRNA levels of genes encoding subunits of respiration complexes did not show a consistent trend of either up- or down-regulation (Figure S1B).

We therefore tested whether the higher mRNA levels of the *COQ* genes resulted in higher protein levels of those polypeptides in mitochondria purified from W303 cells (Figure 1B). We examined the steady state levels of Coq proteins that have previously been identified as members of the CoQ synthome, as well as Coq10, which is not part of the CoQ synthome but is thought to chaperone CoQ_6 from the synthome to sites of function (Allan et al., 2013; Barros et al., 2005). Surprisingly, we observed that the steady state levels of all Coq proteins in the mutants were either similar or even slightly reduced relative to the control (Figure 1B).

The CoQ synthome is destabilized in the absence of ERMES subunits

As the overall mRNA levels of the *COQ* transcripts were higher in ERMES deletions, but there was no major difference in protein levels, it seems that Coq proteins might be less stable in cells lacking the ERMES complex and that up-regulation of transcription is a compensatory mechanism. Since most of the Coq polypeptides assemble in the CoQ synthome (Belogrudov et al., 2001; He et al., 2014; Marbois et al., 2005, 2009) and proteins may become unstable when not assembled properly into their natural complexes, we examined the CoQ synthome by two-dimensional BN-PAGE (Figure 2). Previously the CoQ synthome was studied when galactose was used as a carbon source (He et al., 2014; Nguyen et al., 2014). However, to prevent loss of mitochondrial DNA (that occurs frequently in these strains) we followed Coq4, Coq5 and Coq9 in mitochondrial lysates from yeast grown on glycerol as the sole carbon source. As expected, in wild-type cells Coq4, Coq5, and Coq9 were detected in one relatively discrete complex greater than 669 kDa. However, in the ERMES mutant strains, a large fraction of the

proteins was found in more rapidly migrating sub-complexes equal to or less than ~440 kDa (Figure 2A, B). Based on this analysis, it appears that the CoQ synthome is destabilized in the absence of the ERMES complex.

ERMES deletion strains show elevated *de novo* synthesis of CoQ_6 and accumulate CoQ_6 and CoQ_6-intermediates in whole cells

To quantify how the biosynthesis of CoQ_6 is affected by destabilization of the synthome in ERMES mutants we measured its rate of synthesis. Yeast cells may utilize either para-aminobenzoic acid (pABA) or 4-hydroxybenzoic acid (4HB) as ring precursors of CoQ_6 (Marbois et al., 2010; Pierrel et al., 2010). Early-stage intermediates, hexaprenyl-aminobenzoic acid (HAB) and hexaprenyl-hydroxybenzoic acid (HHB) are derived from prenylation of pABA or 4HB, respectively. Subsequent modifications of the aromatic ring produce late-stage intermediates demethyl-demethoxy-Q_6H_2 ($DDMQ_6$), and demethoxy-Q_6H_2 (DMQ_6), which eventually lead to production of Q_6H_2 (for a schematic of the pathway see Figure 3A). The amino substituent on the pABA ring is removed by a combination of Arh1, Yah1, Coq6 and Coq9 (He et al., 2015; Ozeir et al., 2015) and 4-imino-demethyl-demethoxy-Q_6H_2 ($IDDMQ_6$) and 4-imino-demethoxy-Q_6H_2 ($IDMQ_6$) likely represent dead-end products.

To determine whether CoQ_6 production was altered in the ERMES deletion strains, we analyzed *de novo* biosynthesis of $^{13}C_6$-CoQ_6 with ^{13}C ring-labeled precursors, namely $^{13}C_6$-pABA and $^{13}C_6$-4HB. Surprisingly, we saw that *Δmdm10*, *Δmdm12*, and *Δmdm34* cells showed enhanced *de novo* synthesis of $^{13}C_6$-CoQ_6 (Figure 3B). These mutants also accumulated CoQ_6-intermediates emanating from $^{13}C_6$-pABA and $^{13}C_6$-4HB (Figure 3C-G), whereas *Δmmm1* cells only contained significantly higher amount of $^{13}C_6$-labeled HAB and HHB, but not of other intermediates (Figure 3C-G). We also measured the levels of non-labeled CoQ_6 (which correspond to the steady state levels) in the same samples, and observed an accumulation of unlabeled CoQ_6 and CoQ_6-intermediates in most of the ERMES deletion mutants, regardless of the presence or absence of ^{13}C-labeled precursor (Figure S2).

The increased rate of production and accumulation of CoQ_6-intermediates in the ERMES deletion mutants suggests a compensatory over-activation of the pathway that occurs when the catalytic efficiency of CoQ_6 biosynthesis is reduced following CoQ synthome destabilization.

ERMES deletion strains show decreased steady state levels of CoQ_6 and CoQ_6-intermediates in isolated mitochondria

Although the biosynthesis of yeast CoQ_6 occurs exclusively within mitochondria, CoQ_6 is present in all

cellular membranes. Thus, to focus on the status of CoQ_6 in mitochondria, we determined the steady state content of CoQ_6 in mitochondria isolated from the ERMES deletion mutants as compared to control strains. Despite the fact that the overall cellular levels of CoQ_6 in these mutants were increased, the steady state level of CoQ_6 was significantly reduced in mitochondria isolated from three of the four ERMES deletion strains namely, Δ*mmm1*, Δ*mdm10* and Δ*mdm12* (Figure 4A). Only strains lacking Mdm34p appeared to have nearly normal levels of CoQ_6. Isolated mitochondria from all of the ERMES deletion strains contained also lower levels of the late-stage intermediates DMQ_6 (Figure 4F) and $IDMQ_6$ (Figure 4E). While the levels of the late-stage intermediate $DDMQ_6$ was reduced in all strains, it was not statistically significant for all (Figure 4D). Our finding of decreased steady state level of CoQ_6 and CoQ_6-intermediates in isolated mitochondria suggests that the accumulation of CoQ_6 and its intermediates as detected in whole cell lipid extracts (Figures 3 and S2) must reside in non mitochondrial membranes.

In the complete absence of the CoQ synthome, strains fail to make CoQ_6 and can only carry out the first two steps of the biosynthetic pathway, producing HAB or HHB from the prenylation reaction of the precursors pABA or 4HB, respectively (He et al., 2014). Indeed, deletion of *COQ7* resulted in a dramatic accumulation of HAB and HHB (Figure 4B, C), as observed previously (Tran and Clarke, 2007). Interestingly, in the strains deleted for ERMES subunits, this accumulation of early CoQ_6-intemediates did not occur, with the exception of HHB slightly accumulating in the *Δmdm34* strain (Figure 4B, C) consistent with a divergent function for Mdm34 (Youngman et al., 2004). The difference in the accumulation phenotypes between the ERMES-deletion strains and Δ*coq7* indicates an additional role for ERMES beside stabilization of the CoQ synthome.

Coq proteins co-localize with ERMES subunits

Strains lacking ERMES subunits show increased levels of cellular CoQ_6 and its intermediates, but decreased levels of mitochondrial CoQ_6 together with a destabilized CoQ synthome. Therefore, we wondered whether the ERMES complex may play a role in organizing the CoQ synthome so that metabolites might be efficiently transferred between mitochondria and the ER. In support of such an assumption, we noticed that some Coq proteins are not distributed evenly throughout the mitochondrial matrix but rather have a more punctate localization, suggesting that there might be distinct areas that are dedicated to the synthesis of CoQ_6 inside the mitochondrial matrix. Tagging Coq6 and Coq9 with GFP, in a strain expressing the ERMES marker Mdm34 tagged with Cherry, in both W303 (Figure 5A) and S288C (Figure S1C), revealed that next to each ERMES complex there was a Coq puncta. This

suggests that the localization of the CoQ synthome is coordinated with the position of the ER-mitochondria contact site.

Discussion

Contact sites play an essential role in shaping the cellular architecture as well as participating in transfer of small molecules between organelles thus enabling tight regulation of biochemical pathways. In this study, we show that the ERMES complex, which acts as an ER-mitochondria contact site tether, also has a fundamental role in regulating CoQ_6 biosynthesis and distribution.

The role of ER-mitochondria contacts in CoQ_6 synthesis seems to reside on two levels. First, absence of the ERMES complex leads to destabilization of the CoQ synthome. This may occur due to even small alterations in phospholipid metabolism occurring in these mutants (Kawano et al., 2008; Elbaz-Alon et al., 2014, 2015; Hönscher et al., 2014) (Figure 5) or may be through another direct, or indirect mechanism. Second, there is a spatial coordination of the ERMES complex with the CoQ synthome. Currently, there is no evidence showing direct interaction of ERMES subunits with known members of the CoQ synthome. Given that ERMES subunits Mdm10 and Mdm34 localize at the mitochondrial outer membrane, and members of CoQ synthome are peripheral mitochondrial inner membrane proteins, the co-localization result raises an intriguing question, how is the CoQ synthome anchored to this location? It was previously shown that Coq4 organizes the CoQ synthome but it probably can not traverse the intra-membrane space (Marbois et al., 2009). Although Coq2 is a transmembrane protein of the inner mitochondrial membrane, so far there is no evidence that it is associated with the CoQ synthome (Awad et al., 2018). Interestingly, in the yeast genome *COQ10* and *MDM12* genes are adjacent and might share a promoter (Cherry et al., 2012). SPELL analysis (Hibbs et al., 2007) demonstrates that these two genes are co-regulated. *COQ10* encodes a membrane spanning putative StART domain protein with a lipid binding pocket for CoQ_6, and late-stage CoQ_6-intermediates. Although Coq10 protein has not been shown to be part of the CoQ synthome, it is necessary for efficient *de novo* CoQ_6 biosynthesis and respiration. As many StART domain proteins are involved in lipid transport, signal transduction and transcriptional regulation, the regulation of the mRNA expression of the *COQ10* and *MDM12* genes might help coordinate the levels of Coq10 polypeptide and the ERMES complex to allow a better positioning of the CoQ synthome next to the ER-mitochondria contact site.

How do CoQ_6 and CoQ_6-intermediates escape from mitochondria and accumulate in non-mitochondrial membranes in the ERMES deletion mutants? Given that many Coq proteins of the CoQ synthome can bind CoQ_6 or CoQ_6-intermediates, one of the possibilities is that the destabilized synthome causes reduced ability to retain these molecules in mitochondria (Figure 6). Catechol quinones, unsubstituted, or partially substituted quinone intermediates, such as $DDMQ_6$ are notorious for their ability to act both as oxidants and electrophiles, rendering oxidative damages to cells (Cavalieri et al., 2002; Waite, 1990). As oxidants, one electron reduction of these quinone compounds generates semiquinone-like reactive oxygen species (ROS) via redox cycling. As electrophiles, these quinone compounds form covalent adducts with proteins and other macromolecules, and cause peroxidation of lipid membranes (Cavalieri et al., 2002). It is likely that the CoQ synthome is involved in sequestering these reactive CoQ_6-intermediates. An alternative option is that in ERMES mutants, there is reduced degradation of CoQ_6 outside mitochondria. Although CoQ_6 degradation has not been studied extensively, it is believed that degradation of the polyisoprene tail of CoQ_6 may be carried out in peroxisomes via both α- and β-oxidation (Wanders, 2014). We have previously shown that Peroxisome-mitochondria (PERMIT) contact sites reside in proximity to ER-mitochondria contact sites (Cohen et al., 2014) and hence loss of ERMES may also affect the capacity to degrade escaped CoQ_6.

We believe that the role of the ER-mitochondria contact site in CoQ_6 regulation is conserved from yeast to mammals. Conditional knock-out mice of mammalian mitofusin 2 (MFN2) show impaired respiration resulting from a decrease in their mitochondrial CoQ_9 and CoQ_{10} levels (the mammalian forms of CoQ_6) (Mourier et al., 2015). It is hypothesized that this is not directly related to the role of MFN2 in mitochondrial fusion, since loss of the homologous MFN1 protein, which shares MFN2's fusion role, does not result in alterations in CoQ biosynthesis. MFN2 is reported to play an additional role as a tether in ER-mitochondria contact sites (de Brito and Scorrano, 2008) suggesting that the loss of the ER-Mitochondria tethering is what leads to the altered levels of CoQ biosynthesis similar to loss of ERMES components in yeast.

Why would interplay between CoQ_6 biosynthesis and the ER-mitochondria contact site evolve? Hmg1 and Hmg2 are two ER transmembrane proteins that catalyze the rate-limiting step of the mevalonate pathway, required for generating the farnesyl pyrophosphate (FPP) utilized as a precursor for CoQ, on the ER membrane (Buhaescu and Izzedine, 2007). In mammalian cells, it was shown that indeed inhibiting the homologous enzymes results in decreased CoQ levels (Maltese and Aprille, 1985). Since the final synthesis steps of CoQ occur in mitochondria, it is clear that a tight communication between the two organelles must be involved. Moreover, FPP serves as a major metabolic junction in the cell as it is a limiting precursor for metabolites that have a role in key cellular processes including the

production of dolichols (required for glycosylation and protein secretion), sterols and farnesylated proteins (required for membrane growth) as well as heme-A, and CoQ (required for respiration) (Goldstein and Brown, 1990). Interestingly, the production of these compounds occurs in different compartments of the cell, including the cytosol, the ER, and mitochondria. This means that in addition to the tight regulation needed to ensure no accumulation of toxic intermediates of the pathway, FPP must be diverted and allocated to specific organelles to control distribution of this precursor and the relative contribution to protein secretion, respiration or membrane growth. How this occurs is still a mystery. Positioning the pathway in areas of organelle-contact suggests a means for spatial regulation of this process.

Recently we have shown that the unfolded protein response (UPR), which coordinates cellular needs and protein folding capacity in the ER, is dependent on the mitochondrial biosynthesis (Cohen et al., 2017). We showed that when mitochondrial function is impaired, and heme is not synthesized properly, the UPR will not activate to its fullest capacity due to limited sterol production. Here, we show that CoQ_6 biosynthesis is also dependent on the cross-talk between the ER and mitochondria. When the physical contact between the ER and mitochondria is impaired, this will affect the formation of CoQ_6 (and probably heme) from mevalonate precursors, increasing its availability for sterol production. Therefore, FPP and Heme may serve as information-rich molecules, each made in one compartment but having a role in the other, allowing coordination of the functional capacity of these two organelles. More broadly these two coordination loops suggest that at any given moment multiple checkpoints are in place to ensure that respiration and secretion are kept in a regulated balance.

Figure legends

Figure 1: Cells lacking ERMES show up-regulation of *COQ* mRNAs

(A) Change in mRNA levels of the indicated *COQ* genes were measured using RNA sequencing in the different W303 strains deleted for ERMES subunits (*Δmmm1, Δmdm10, Δmdm12, and Δmdm34*) relative to a control. The majority of *COQ* biosynthetic genes show an up-regulation of their mRNA levels compared to the WT control. Values are Log2 of ERMES deletion mutant − Log2 of control and are averages of two biological repeats.

(B) Immunoblotting for levels of Coq polypeptides from gradient purified mitochondria of W303 mutants of the ERMES complex *(Δmmm1, Δmdm10, Δmdm12, and Δmdm34)*, *Δcoq* (*Δcoq3- Δcoq10*) and a control, demonstrates that steady state levels of the different Coq polypeptides were not dramatically altered in the ERMES deletion strains. Immunoblotting was performed with antisera against designated yeast Coq polypeptides (Coq3-Coq10), Mdh1 is a mitochondrial marker, and Sec62 is an ER marker. Arrows denote the corresponding protein in their respective blots. Images are representative gels from at least two biological repeats.

Figure 2: The CoQ synthome is destabilized in the absence of ERMES subunits

(A) Two-dimensional blue native/ SDS-PAGE gel electrophoresis analysis of ERMES mutants in W303 background (Δ*mmm1*, Δ*mdm10*, Δ*mdm12*, and Δ*mdm34*) compared to a Δ*coq4* and a wild-type (WT) control strain. Gels were immuno-blotted against Coq4. While in control conditions the Coq synthome appears as one discrete band at >669 kDa (the position of the band is marked by a yellow arrow), in the ΔERMES strains, the signal appears dispersed over a range of smaller molecular weights, indicated by brackets. The red asterisk (*) indicates a discrete non-specific signal observed with the antisera to Coq4.

(B) Two-dimensional Blue Native/ SDS-PAGE gel electrophoresis was performed as described in (A). Δ*coq5* was used as negative control (In this strain Coq9 is destabilized and undetectable). Gels were immuno-blotted against Coq5 and Coq9. The strong Coq5 and Coq9 bands in the higher molecular weight (>669 kDa) in the control conditions (indicated by yellow arrows) weaken in the ΔERMES strains and an additional diffuse signal appears in the lower molecular weights (marked by brackets).

Figure 3: Biosynthesis of CoQ_6 and CoQ_6-intermediates is increased in cells lacking the ERMES complex

(A) Schematic representation of selected steps of the CoQ_6 biosynthesis pathway. CoQ_6-intermediates that were analyzed using mass-spectrometry (MS) are indicated in green text. (B-G) MS-MS analysis for CoQ_6 and CoQ_6-intermediates in whole cell lipid extracts from W303 control, Δ*mmm1*, Δ*mdm10*, Δ*mdm12*, and Δ*mdm34* strains. $^{13}C_6$-CoQ_6 and $^{13}C_6$-CoQ_6-intermediates derived from $^{13}C_6$-pABA are depicted in red, while the $^{13}C_6$-CoQ_6 and $^{13}C_6$-CoQ_6-intermediates derived from $^{13}C_6$-4HB are depicted in blue. $^{13}C_6$-CoQ_6 biosynthesis (B) is increased in Δ*mdm10*, Δ*mdm12*, and Δ*mdm34* strains labeled with $^{13}C_6$-pABA or $^{13}C_6$-4HB. The biosynthesis of $^{13}C_6$-HHB (C) and $^{13}C_6$-HAB (D) is significantly higher in all the ERMES deletion strains. The *de novo* levels of demethyl-demethoxy-Q_6 ($^{13}C_6$-$DDMQ_6$) (E), 4-imino-DMQ_6 ($^{13}C_6$-$IDMQ_6$) (F) and demethoxy-Q_6 ($^{13}C_6$-DMQ_6) (G) are significantly increased in Δ*mdm10*, Δ*mdm12*, and Δ*mdm34* strains, with the exception of $^{13}C_6$-DMQ_6 in Δ*mdm34* that did not change after the labeling with $^{13}C_6$-4HB. Values are means of three repeats. The error bar indicates mean ±SD. Statistically significant differences between control and each of the ERMES mutants are represented by *p<0.05, **p<0.01, ***p<0.001 and ****p<0.0005.

Figure 4: Mitochondria from ERMES mutants show less CoQ_6 and CoQ_6-intermediates

(A-F) Targeted MS-MS analyses for CoQ_6 and CoQ_6-intermediates from purified mitochondria from W303 wild-type (WT) control, Δ*mmm1*, Δ*mdm10*, Δ*mdm12*, and Δ*mdm34* strains. Δ*coq7* was included as a negative control. Levels of (A) CoQ_6 were significantly reduced in all ERMES deletion strains except for Δ*mdm34*. Levels of (B) HHB and (C) HAB were significantly higher in the Δ*coq7* strain, however ERMES deletion strains did not show an accumulation of either HHB or HAB (with the exception of Δ*mdm34* accumulating HHB). Levels of (D) $DDMQ_6$ were not significantly changed. Levels of (E) $IDMQ_6$ and (F) DMQ_6 were significantly reduced in all ERMES deletion strains. Values are means of three biological repeats. The error bar indicates mean +SD. Statistically significant differences between control and each of the ERMES mutants are represented by *p<0.05, **p<0.01, ***p<0.001 and ****p<0.0005. n.d.= not detected.

Figure 5: Members of the CoQ synthome reside in a matrix niche that is underlying the ERMES complex

(A) Yeast cells expressing the indicated GFP-tagged Coq protein, the ERMES protein Mdm34 tagged with Cherry and a Blue Fluorescent Protein (BFP) fused to a mitochondrial targeting sequence (MTS) were imaged using fluorescence microscopy. Arrows indicate Coq foci that underlie the ERMES component on parts of the mitochondrion. Bar = 5µM.
(B) Schematic representation of co-localization of ERMES complex and CoQ synthome. Mdm10 and Mdm34 outer mitochondrial membrane proteins are positioned in close proximity with Coq proteins of the CoQ synthome. Coq6 and Coq9 that were visualized in (A) are highlighted in orange.

Figure 6. Proposed model of how the absence of ERMES affects CoQ synthome and CoQ_6 biosynthesis

(A) Under normal conditions, the CoQ synthome is well assembled and CoQ_6 biosynthesis (represented by red arrow) occurs efficiently in mitochondria. This catalytic efficiency ensures that early- and late-stage CoQ_6-intermediates do not accumulate.
(B) When the ERMES complex is absent, the stability of the CoQ synthome is compromised. A partially destabilized CoQ synthome underlies inefficient CoQ biosynthesis, leading to the accumulation of early- and late-stage CoQ_6-intermediates that fail to be retained within mitochondria. The altered phospholipid metabolism in the ERMES mutants may also indirectly contribute to the destabilized CoQ synthome and inefficient catalysis.

Figure S1: Verification of results on an additional yeast strain genetic background

(A) mRNA levels of the indicated *COQ* genes as were measured using RNA sequencing in control S288C strains as well as in strains deleted for ERMES subunits (*Δmmm1, Δmdm10* and *Δmdm12*). Similar to the W303 background, mRNAs of *COQ* genes show an overall up-regulation of their mRNA levels compared to the wild-type control. Values are Log2 of the designated ERMES deletion mutant – Log2 of control and are averages of two repeats.
(B) mRNA levels of the indicated respiratory genes, as were measured using RNA sequencing in the W303 control and ERMES deletion strains. As opposed to the *COQ* mRNAs, the mRNAs corresponding to genes encoding respiratory complexes were not dramatically or consistently altered when compared to the control. Values are Log2 of deletion mutant – Log2 of control and are averages of two repeats.
(C) S288C Yeast cells expressing the indicated GFP-tagged Coq protein, the ERMES protein Mdm34 tagged with Cherry and a BFP fused to an MTS were imaged using fluorescence microscopy. Arrows indicate Coq foci that underlie the ERMES component on parts of the mitochondrion. Bar = 5µM.

Figure S2. Most of the ERMES mutant strains accumulate unlabeled CoQ_6 and CoQ_6-intermediates.
(A-F) LC-MS/MS analysis for CoQ_6 and CoQ_6-intermediates from whole cells of W303 control, Δ*mmm1*, Δ*mdm10*, Δ*mdm12*, and Δ*mdm34* strains. Cells were harvested after 5 hours labeling using $^{13}C_6$-pABA, $^{13}C_6$-4HB or ethanol. $^{13}C_6$-CoQ_6 and ^{12}C-CoQ_6 are depicted in the stacked bar graph in panel (A), and both accumulate in most of the ERMES deletion mutant strains. For simplicity, only unlabeled CoQ_6-intermediates (hence steady state levels of these metabolites) are depicted in panels B-F. Similar results were observed for HHB (B) and HAB (C), but the increase is more drastic in the absence of $^{13}C_6$-labeled precursors (see EtOH control). Levels of $DDMQ_6$ (D), $IDMQ_6$ (E) and DMQ_6 (F) are significantly increased in Δ*mdm10*, Δ*mdm12*, and Δ*mdm34* strains in all the conditions. Values are means of three repeats. The error bar indicates mean +SD. Statistically significant differences between control and each of the ERMES mutants are represented by *p<0.05, **p<0.01, ***p<0.001 and ****p<0.0005.

Acknowledgements

We thank Christian Ungermann and Naama Barkai for plasmids and Ido Amit for the transposase required for the sequencing. We thank Yoav Voichek and Yulia Gordon for producing and analyzing the RNA-sequencing data. We thank Dr. Alexander Brandis and Tevi Mehlman from the Targeted Metabolomics unit of the Life Sciences Core Facilities of the Weizmann Institute for Mass-Spectrometry analysis.
CDD acknowledges funding from an EMBO Installation Grant (2138) and from an ERC Starting Grant (RevMito 637649). MEB is grateful to the Azrieli Foundation for the award of an Azrieli Fellowship. This work was supported by the Deutsche Forschungsgemeinschaft (DIP to MS and DR), and the IMPRS "From Molecules to Organisms" (D.A.) Work in the Schuldiner lab is additionally supported by an SFB1190 from the DFG as well as a “Life” grant from the Volkswagen foundation. MS is an incumbent of the Dr. Gilbert Omenn and Martha Darling Professorial Chair in Molecular Genetics. This work is supported by the National Science Foundation Grant MCB-1330803 (to CFC) and by the National Institutes of Health Grant T32 GM 008496 to HST and MCB.

Supplemental material

References

Allan, C.M., Hill, S., Morvaridi, S., Saiki, R., Johnson, J.S., Liau, W.-S., Hirano, K., Kawashima, T., Ji, Z., Loo, J.A., et al. (2013). A conserved START domain coenzyme Q-binding polypeptide is required for efficient Q biosynthesis, respiratory electron transport, and antioxidant function in Saccharomyces cerevisiae. Biochim. Biophys. Acta - Mol. Cell Biol. Lipids *1831*, 776–791.

Allan, C.M., Awad, A.M., Johnson, J.S., Shirasaki, D.I., Wang, C., Blaby-Haas, C.E., Merchant, S.S., Loo, J.A., and Clarke, C.F. (2015). Identification of Coq11, a new coenzyme Q biosynthetic protein in the CoQ-synthome in Saccharomyces cerevisiae. J. Biol. Chem. *290*, 7517–7534.

Awad, A.M., Bradley, M.C., Fernández-Del-Río, L., Nag, A., Tsui, H.S., and Clarke, C.F. (2018). Coenzyme Q10 deficiencies: pathways in yeast and humans. Essays Biochem. EBC20170106.

Baker Brachmann, C., Davies, A., Cost, G.J., Caputo, E., Li, J., Hieter, P., Boeke, J.D., Brachmann, C.B., Davies, A., Cost, G.J., et al. (1998). Designer deletion strains derived fromSaccharomyces cerevisiae S288C: A useful set of strains and plasmids for PCR-mediated gene disruption and other applications. Yeast *14*, 115–132.

Barros, M.H., Johnson, A., Gin, P., Marbois, B.N., Clarke, C.F., and Tzagoloff, A. (2005). The Saccharomyces cerevisiae COQ10 gene encodes a START domain protein required for function of coenzyme Q in respiration. J. Biol. Chem. *280*, 42627–42635.

Belogrudov, G.I., Lee, P.T., Jonassen, T., Hsu, A.Y., Gin, P., and Clarke, C.F. (2001). Yeast COQ4 Encodes a Mitochondrial Protein Required for Coenzyme Q Synthesis. Arch. Biochem. Biophys. *392*, 48–58.

Bentinger, M., Tekle, M., and Dallner, G. (2010). Coenzyme Q – Biosynthesis and functions. Biochem. Biophys. Res. Commun. *396*, 74–79.

Berger, K.H., Sogo, L.F., and Yaffe, M.P. (1997). Mdm12p, a component required for mitochondrial inheritance that is conserved between budding and fission yeast. J. Cell Biol. *136*, 545–553.

Böckler, S., Westermann, B., Brito, O.M. de, Scorrano, L., Dimmer, K.S., Jakobs, S., Vogel, F., Altmann, K., Westermann, B., Giaever, G., et al. (2014). Mitochondrial ER contacts are crucial for mitophagy in yeast. Dev. Cell *28*, 450–458.

de Brito, O.M., and Scorrano, L. (2008). Mitofusin 2 tethers endoplasmic reticulum to mitochondria. Nature *456*, 605–610.

Buhaescu, I., and Izzedine, H. (2007). Mevalonate pathway: A review of clinical and therapeutical implications. Clin. Biochem. *40*, 575–584.

Cavalieri, E.L., Li, K.-M., Balu, N., Saeed, M., Devanesan, P., Higginbotham, S., Zhao, J., Gross, M.L., and Rogan, E.G. (2002). Catechol ortho-quinones: the electrophilic compounds that form depurinating DNA adducts and could initiate cancer and other diseases. Carcinogenesis *23*, 1071–1077.

Cherry, J.M., Hong, E.L., Amundsen, C., Balakrishnan, R., Binkley, G., Chan, E.T., Christie, K.R., Costanzo, M.C., Dwight, S.S., Engel, S.R., et al. (2012). Saccharomyces Genome Database: the genomics resource of budding yeast. Nucleic Acids Res. *40*, D700-5.

Cohen, N., Breker, M., Bakunts, A., Pesek, K., Chas, A., Argemí, J., Orsi, A., Gal, L., Chuartzman, S., Wigelman, Y., et al. (2017). Iron affects Ire1 clustering propensity and the amplitude of endoplasmic reticulum stress signaling. J. Cell Sci. *130*, 3222–3233.

Cohen, Y., Klug, Y.A., Dimitrov, L., Erez, Z., Chuartzman, S.G., Elinger, D., Yofe, I., Soliman, K., Gärtner, J., Thoms, S., et al. (2014). Peroxisomes are juxtaposed to strategic sites on mitochondria. Mol. Biosyst. *10*, 1742–1748.

Dimmer, K.S., and Rapaport, D. (2017). Mitochondrial contact sites as platforms for phospholipid exchange. Biochim. Biophys. Acta - Mol. Cell Biol. Lipids *1862*, 69–80.

Eisenberg-Bord, M., Shai, N., Schuldiner, M., and Bohnert, M. (2016). A Tether Is a Tether Is a Tether: Tethering at Membrane Contact Sites. Dev. Cell *39*, 395–409.

Elbaz-Alon, Y., Rosenfeld-Gur, E., Shinder, V., Futerman, A.H., Geiger, T., and Schuldiner, M. (2014). A Dynamic Interface between Vacuoles and Mitochondria in Yeast. Dev. Cell *30*, 95–102.

Elbaz-Alon, Y., Eisenberg-Bord, M., Shinder, V., Stiller, S.B., Shimoni, E., Wiedemann, N., Geiger, T., and Schuldiner, M. (2015). Lam6 Regulates the Extent of Contacts between Organelles. Cell Rep. *12*, 7–14.

Friedman, J.R., Lackner, L.L., West, M., DiBenedetto, J.R., Nunnari, J., and Voeltz, G.K. (2011). ER tubules mark sites of mitochondrial division. Science *334*, 358–362.

Gietz, R.D., and Woods, R.A. (2006). Yeast transformation by the LiAc/SS Carrier DNA/PEG method. Methods Mol. Biol. *313*, 107–120.

Glick, B.S., and Pon, L.A. (1995). [14] Isolation of highly purified mitochondria from Saccharomyces cerevisiae. Methods Enzymol. *260*, 213–223.

Goldstein, J.L., and Brown, M.S. (1990). Regulation of the mevalonate pathway. Nature *343*, 425–430.

He, C.H., Xie, L.X., Allan, C.M., Tran, U.C., and Clarke, C.F. (2014). Coenzyme Q supplementation or over-expression of the yeast Coq8 putative kinase stabilizes multi-subunit Coq polypeptide complexes in yeast coq null mutants. Biochim. Biophys. Acta - Mol. Cell Biol. Lipids *1841*, 630–644.

He, C.H., Black, D.S., Nguyen, T.P.T., Wang, C., Srinivasan, C., and Clarke, C.F. (2015). Yeast Coq9 controls deamination of coenzyme Q intermediates that derive from para-aminobenzoic acid. Biochim. Biophys. Acta *1851*, 1227–1239.

Herrera-Cruz, M.S., and Simmen, T. (2017). Of yeast, mice and men: MAMs come in two flavors. Biol. Direct *12*, 3.

Hibbs, M.A., Hess, D.C., Myers, C.L., Huttenhower, C., Li, K., and Troyanskaya, O.G. (2007). Exploring the functional landscape of gene expression: directed search of large microarray compendia. Bioinformatics *23*, 2692–2699.

Hobbs, A.E., Srinivasan, M., McCaffery, J.M., and Jensen, R.E. (2001). Mmm1p, a mitochondrial outer membrane protein, is connected to mitochondrial DNA (mtDNA) nucleoids and required for mtDNA stability. J. Cell Biol. *152*, 401–410.

Hönscher, C., Mari, M., Auffarth, K., Bohnert, M., Griffith, J., Geerts, W., van der Laan, M., Cabrera, M., Reggiori, F., and Ungermann, C. (2014). Cellular Metabolism Regulates Contact Sites between Vacuoles and Mitochondria. Dev. Cell *30*, 86–94.

Janke, C., Magiera, M.M., Rathfelder, N., Taxis, C., Reber, S., Maekawa, H., Moreno-Borchart, A., Doenges, G., Schwob, E., Schiebel, E., et al. (2004). A versatile toolbox for PCR-based tagging of yeast genes: new fluorescent proteins, more markers and promoter substitution cassettes. Yeast *21*, 947–962.

Kakimoto, Y., Tashiro, S., Kojima, R., Morozumi, Y., Endo, T., and Tamura, Y. (2018). Visualizing multiple inter-organelle contact sites using the organelle-targeted split-GFP system. Sci. Rep. *8*, 6175.

Kawano, S., Tamura, Y., Kojima, R., Bala, S., Asai, E., Michel, A.H., Kornmann, B., Riezman, I., Riezman, H., Sakae, Y., et al. (2018). Structure – function insights into direct lipid transfer between membranes by Mmm1 – Mdm12 of ERM ES. J. Cell Biol. *217*, 1–22.

Kivioja, T., Vähärautio, A., Karlsson, K., Bonke, M., Enge, M., Linnarsson, S., and Taipale, J. (2012). Counting absolute numbers of molecules using unique molecular identifiers. Nat. Methods *9*, 72–74.

Kornmann, B., Currie, E., Collins, S.R., Schuldiner, M., Nunnari, J., Weissman, J.S., and Walter, P. (2009). An ER-mitochondria tethering complex revealed by a synthetic biology screen. Science *325*, 477–481.

Liu, C.L., Kaplan, T., Kim, M., Buratowski, S., Schreiber, S.L., Friedman, N., and Rando, O.J. (2005). Single-Nucleosome Mapping of Histone Modifications in S. cerevisiae. PLoS Biol. *3*, e328.

Longtine, M.S., McKenzie, A., Demarini, D.J., Shah, N.G., Wach, A., Brachat, A., Philippsen, P., and Pringle, J.R. (1998). Additional modules for versatile and economical PCR-based gene deletion and modification in Saccharomyces cerevisiae. Yeast *14*, 953–961.

Maltese, W.A., and Aprille, J.R. (1985). Relation of mevalonate synthesis to mitochondrial ubiquinone content and respiratory function in cultured neuroblastoma cells. J. Biol. Chem. *260*, 11524–11529.

Marbois, B., Gin, P., Faull, K.F., Poon, W.W., Lee, P.T., Strahan, J., Shepherd, J.N., and Clarke, C.F. (2005). Coq3 and Coq4 define a polypeptide complex in yeast mitochondria for the biosynthesis of coenzyme Q. J. Biol. Chem. *280*, 20231–20238.

Marbois, B., Gin, P., Gulmezian, M., and Clarke, C.F. (2009). The yeast Coq4 polypeptide organizes a mitochondrial protein complex essential for coenzyme Q biosynthesis. Biochim. Biophys. Acta - Mol. Cell Biol. Lipids *1791*, 69–75.

Marbois, B., Xie, L.X., Choi, S., Hirano, K., Hyman, K., and Clarke, C.F. (2010). para-aminobenzoic acid is a precursor in coenzyme Q6 biosynthesis in Saccharomyces cerevisiae. J. Biol. Chem. *285*, 27827–27838.

Mourier, A., Motori, E., Brandt, T., Lagouge, M., Atanassov, I., Galinier, A., Rappl, G., Brodesser, S., Hultenby, K., Dieterich, C., et al. (2015). Mitofusin 2 is required to maintain mitochondrial coenzyme Q levels. J. Cell Biol. *208*, 429–442.

Murley, A., Lackner, L.L., Osman, C., West, M., Voeltz, G.K., Walter, P., and Nunnari, J. (2013). ER-associated mitochondrial division links the distribution of mitochondria and mitochondrial DNA in yeast. Elife *2*, e00422.

Nguyen, T.P.T., Casarin, A., Desbats, M.A., Doimo, M., Trevisson, E., Santos-Ocaña, C., Navas, P., Clarke, C.F., and Salviati, L. (2014). Molecular characterization of the human COQ5 C-methyltransferase in coenzyme Q10 biosynthesis. Biochim. Biophys. Acta - Mol. Cell Biol. Lipids *1841*, 1628–1638.

Ozeir, M., Pelosi, L., Ismail, A., Mellot-Draznieks, C., Fontecave, M., and Pierrel, F. (2015). Coq6 is responsible for the C4-deamination reaction in coenzyme Q biosynthesis in Saccharomyces cerevisiae. J. Biol. Chem. *290*, 24140–24151.

Pierrel, F., Hamelin, O., Douki, T., Kieffer-Jaquinod, S., Mühlenhoff, U., Ozeir, M., Lill, R., and Fontecave, M. (2010). Involvement of mitochondrial ferredoxin and para-aminobenzoic acid in yeast coenzyme Q biosynthesis. Chem. Biol. *17*, 449–459.

Schagger, H., Cramer, W.A., and Vonjagow, G. (1994). Analysis of Molecular Masses and Oligomeric States of Protein Complexes by Blue Native Electrophoresis and Isolation of Membrane Protein Complexes by Two-Dimensional Native Electrophoresis. Anal. Biochem. *217*, 220–230.

Shai, N., Yifrach, E., van Roermund, C.W.T., Cohen, N., Bibi, C., IJlst, L., Cavellini, L., Meurisse, J., Schuster, R., Zada, L., et al. (2018). Systematic mapping of contact sites reveals tethers and a function for the peroxisome-mitochondria contact. Nat. Commun. *9*, 1761.

Smethurst, D.G.J., and Cooper, K.F. (2016). ER fatalities-The role of ER-mitochondrial contact sites in yeast life and death decisions. Mech. Ageing Dev. *161*, 225–233.

Thomas, B.J., and Rothstein, R. (1989). Elevated recombination rates in transcriptionally active DNA. Cell *56*, 619–630.

Tran, U.C., and Clarke, C.F. (2007). Endogenous synthesis of coenzyme Q in eukaryotes. Mitochondrion *7 Suppl*, S62-71.

Valm, A.M., Cohen, S., Legant, W.R., Melunis, J., Hershberg, U., Wait, E., Cohen, A.R., Davidson, M.W., Betzig, E., and Lippincott-Schwartz, J. (2017). Applying systems-level spectral imaging and analysis to reveal the organelle interactome. Nature *546*, 162–167.

Voichek, Y., Bar-Ziv, R., and Barkai, N. (2016). Expression homeostasis during DNA replication. Science *351*, 1087–1090.

Waite, J.H. (1990). The phylogeny and chemical diversity of quinone-tanned glues and varnishes. Comp. Biochem. Physiol. B. *97*, 19–29.

Wanders, R.J.A. (2014). Metabolic functions of peroxisomes in health and disease. Biochimie *98*, 36–44.

Wittig, I., Braun, H.-P., and Schägger, H. (2006). Blue native PAGE. Nat. Protoc. *1*, 418–428.

Xue, Y., Schmollinger, S., Attar, N., Campos, O.A., Vogelauer, M., Carey, M.F., Merchant, S.S., and Kurdistani, S.K. (2017). Endoplasmic reticulum–mitochondria junction is required for iron homeostasis. J. Biol. Chem. *292*, 13197–13204.

Yofe, I., and Schuldiner, M. (2014). Primers-4-Yeast: a comprehensive web tool for planning primers for *Saccharomyces cerevisiae*. Yeast *31*, 77–80.

Youngman, M.J., Hobbs, A.E.A., Burgess, S.M., Srinivasan, M., and Jensen, R.E. (2004). Mmm2p, a mitochondrial outer membrane protein required for yeast mitochondrial shape and maintenance of mtDNA nucleoids. J. Cell Biol. *164*, 677–688.

Figure 1

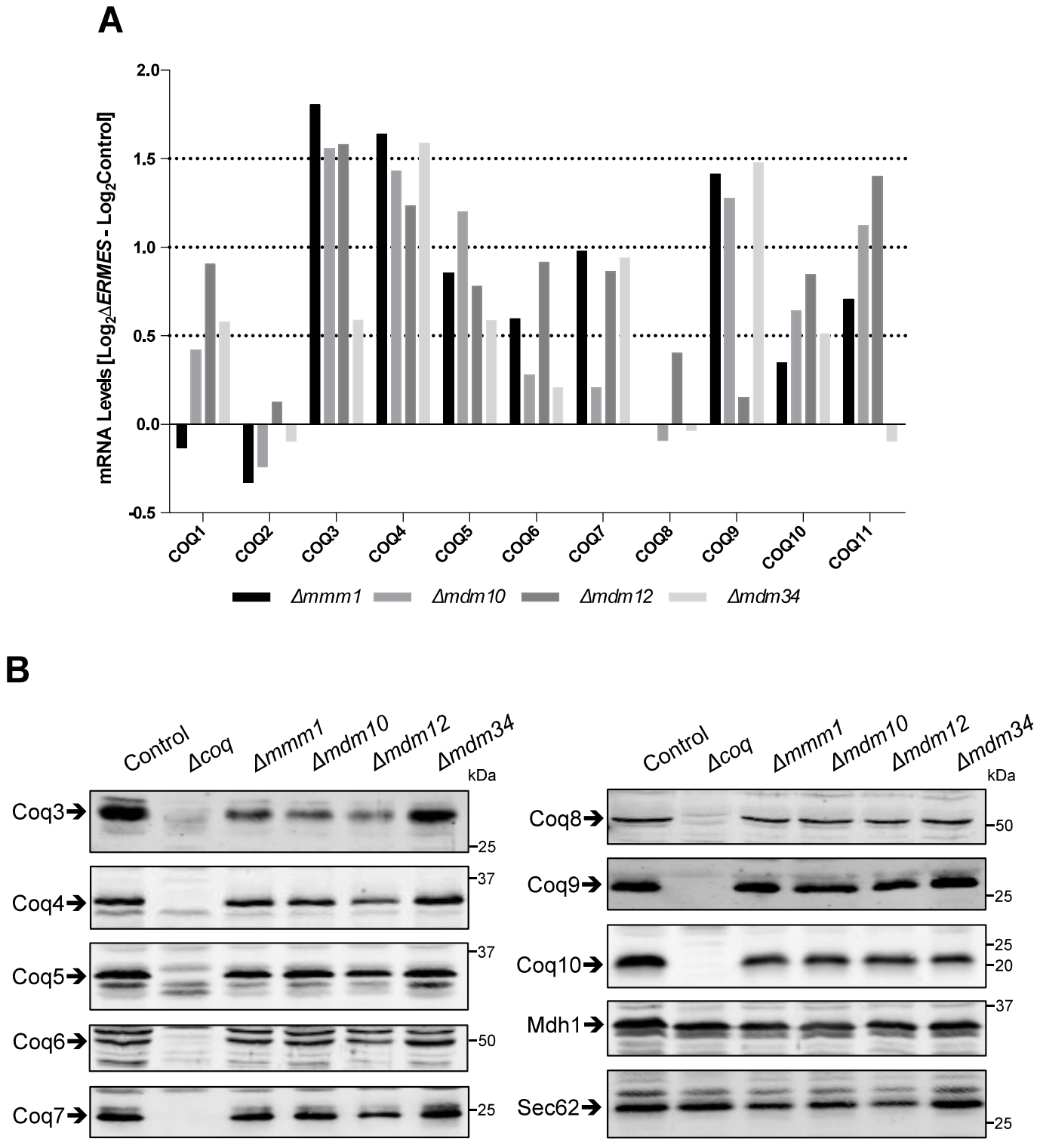
A
mRNA Levels [Log2ΔERMES - Log2Control]
2.0
1.5
1.0
0.5
0.0
-0.5
COQ1
COQ2
COQ3
COQ4
COQ5
COQ6
COQ7
COQ8
COQ9
COQ10
COQ11
Δmmm1
Δmdm10
Δmdm12
Δmdm34
B
Control
Δcoq
Δmmm1
Δmdm10
Δmdm12
Δmdm34
kDa
Coq3
Coq4
Coq5
Coq6
Coq7
25
37
37
50
25
Coq8
Coq9
Coq10
Mdh1
Sec62
50
25
25
20
37
25

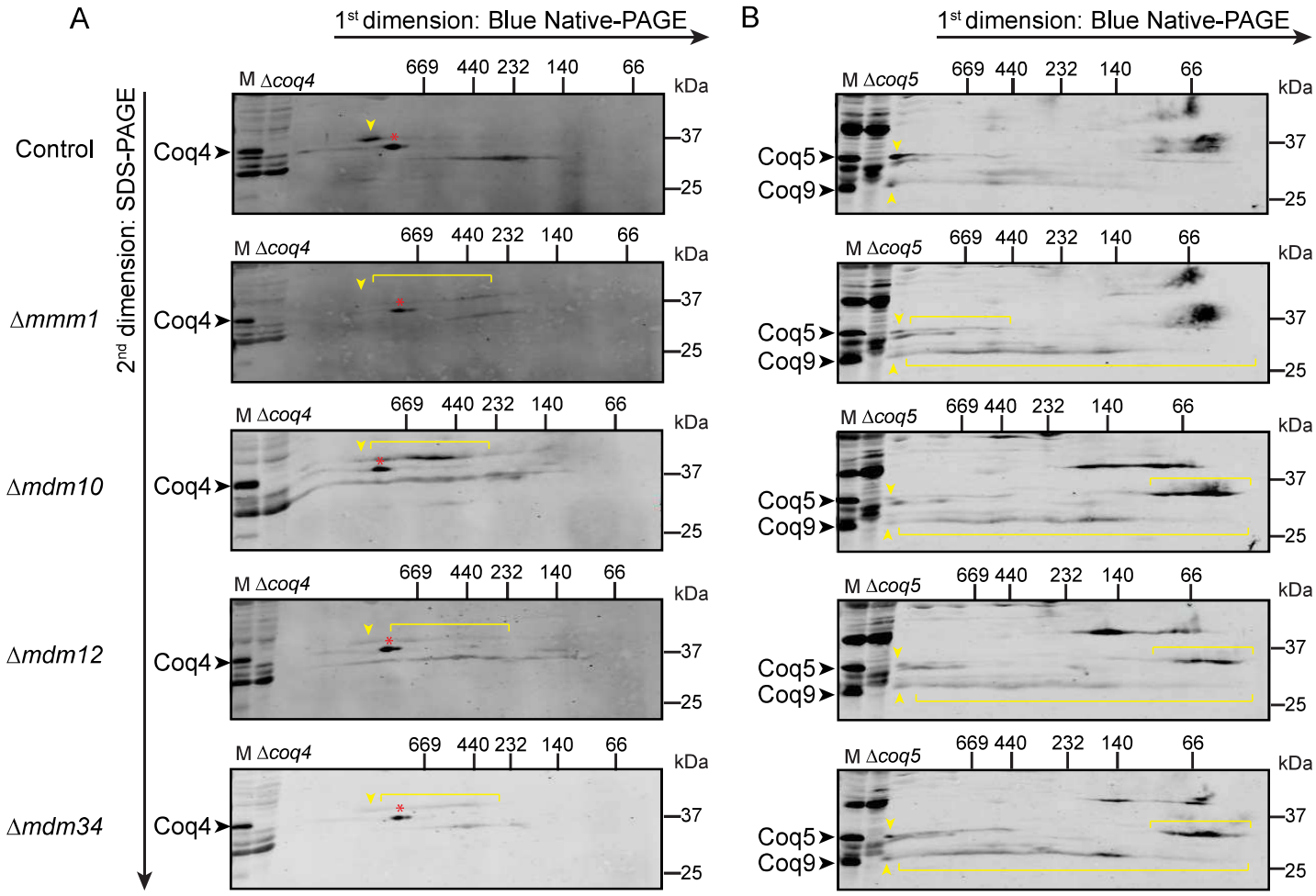

Eisenberg-Bord & Tsui et al., Figure 2

Figure 3

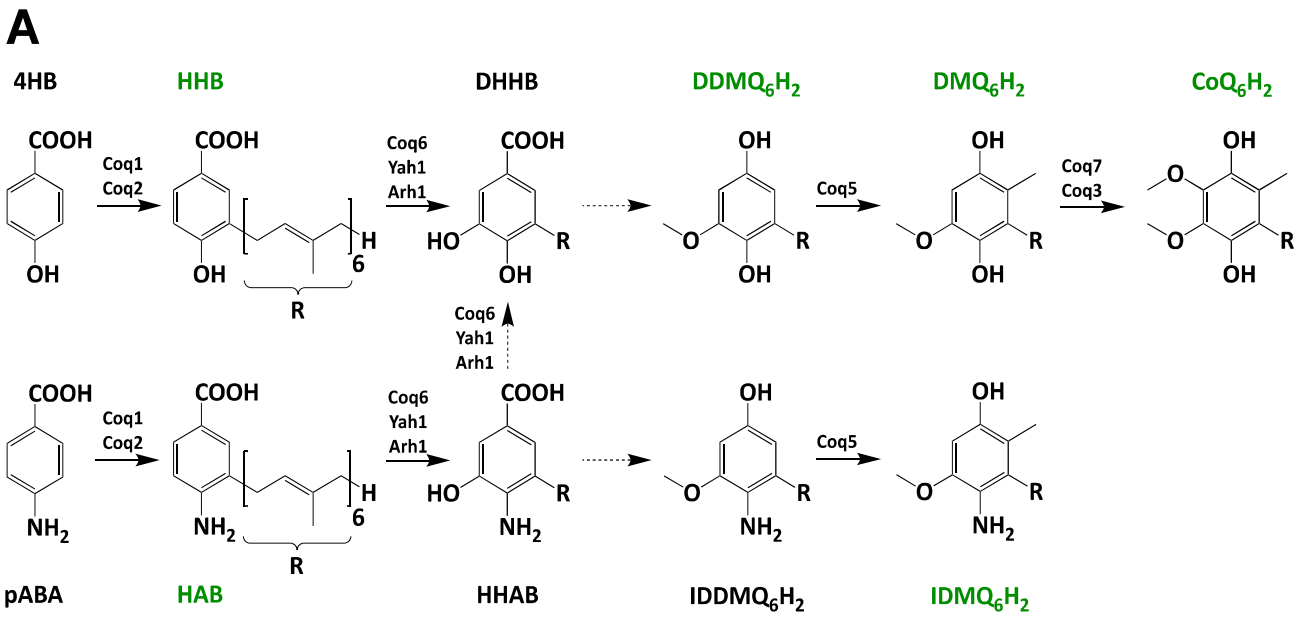
A
4HB
HHB
DHHB
DDMQ6H2
DMQ6H2
CoQ6H2
Coq1
Coq2
Coq6
Yah1
Arh1
Coq5
Coq7
Coq3
pABA
HAB
HHAB
IDDMQ6H2
IDMQ6H2

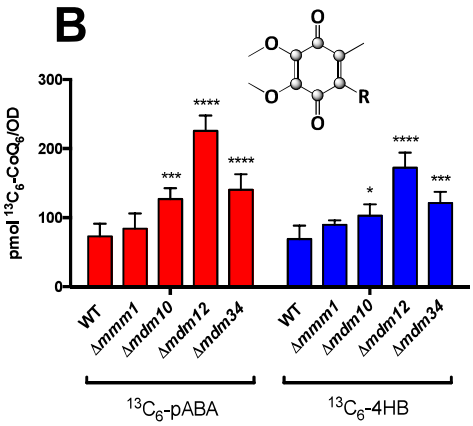
B
pmol 13C6-CoQ6/OD
WT
Δmmm1
Δmdm10
Δmdm12
Δmdm34
13C6-pABA
13C6-4HB

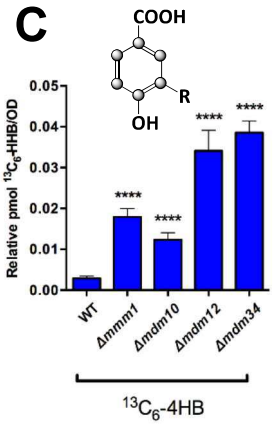
C
Relative pmol 13C6-HHB/OD
13C6-4HB

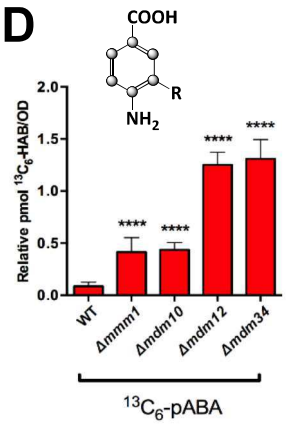
D
Relative pmol 13C6-HAB/OD
13C6-pABA

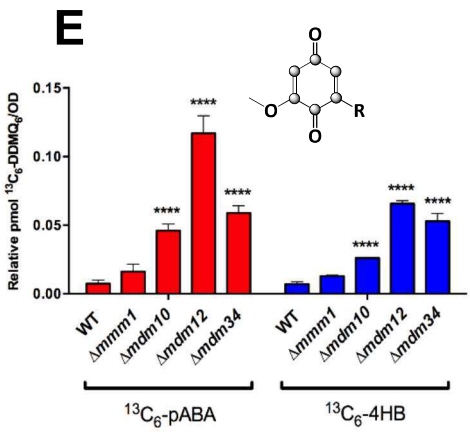
E
Relative pmol 13C6-DDMQ6/OD
13C6-pABA
13C6-4HB

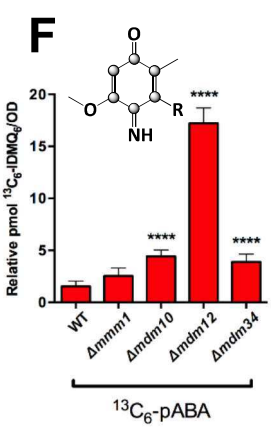
F
Relative pmol 13C6-IDMQ6/OD
13C6-pABA

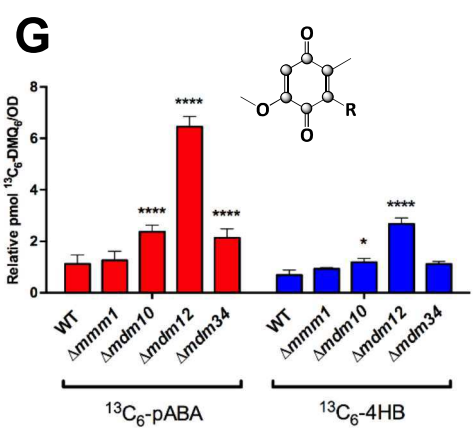
G
Relative pmol 13C6-DMQ6/OD
13C6-pABA
13C6-4HB

Figure 4

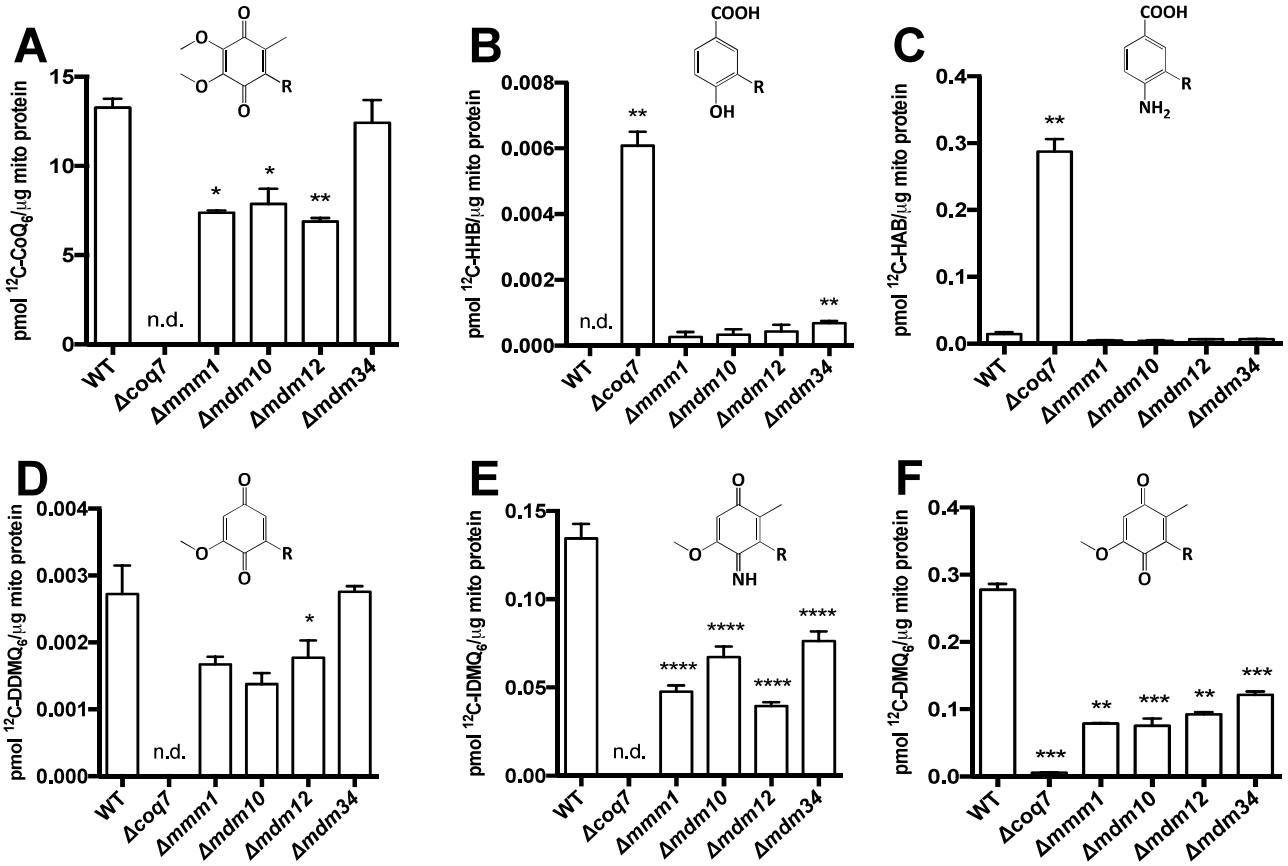
A
pmol 12C-CoQ6/µg mito protein
15
10
5
0
n.d.
*
*
**
WT
Δcoq7
Δmmm1
Δmdm10
Δmdm12
Δmdm34
B
pmol 12C-HHB/µg mito protein
0.008
0.006
0.004
0.002
0.000
COOH
OH
R
**
n.d.
**
C
pmol 12C-HAB/µg mito protein
0.4
0.3
0.2
0.1
0.0
COOH
NH2
R
**
D
pmol 12C-DDMQ6/µg mito protein
0.004
0.003
0.002
0.001
0.000
n.d.
*
E
pmol 12C-IDMQ6/µg mito protein
0.15
0.10
0.05
0.00
NH
n.d.
****
****
****
****
F
pmol 12C-DMQ6/µg mito protein
0.4
0.3
0.2
0.1
0.0
***
**
***
**
***

Figure 5

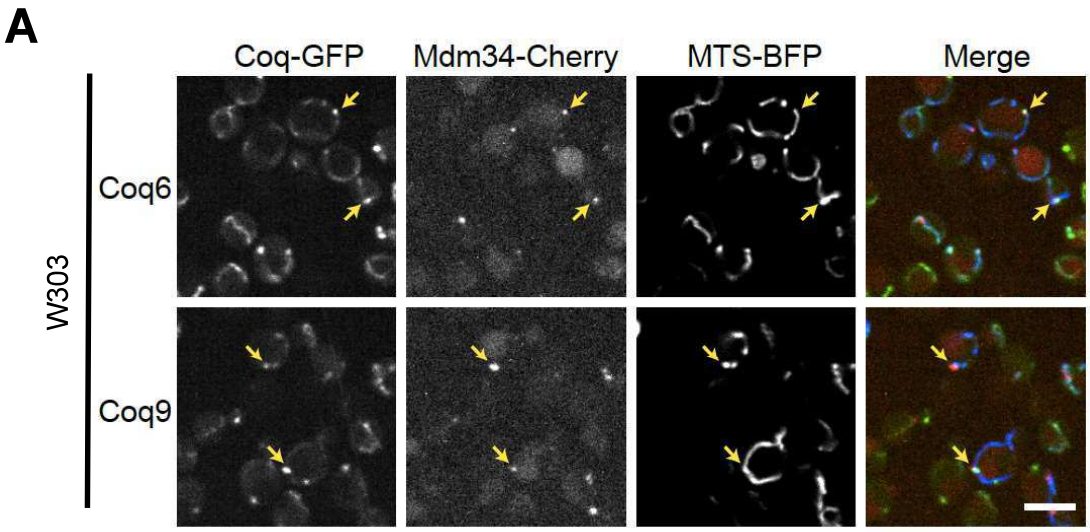
A
Coq-GFP
Mdm34-Cherry
MTS-BFP
Merge
W303
Coq6
Coq9

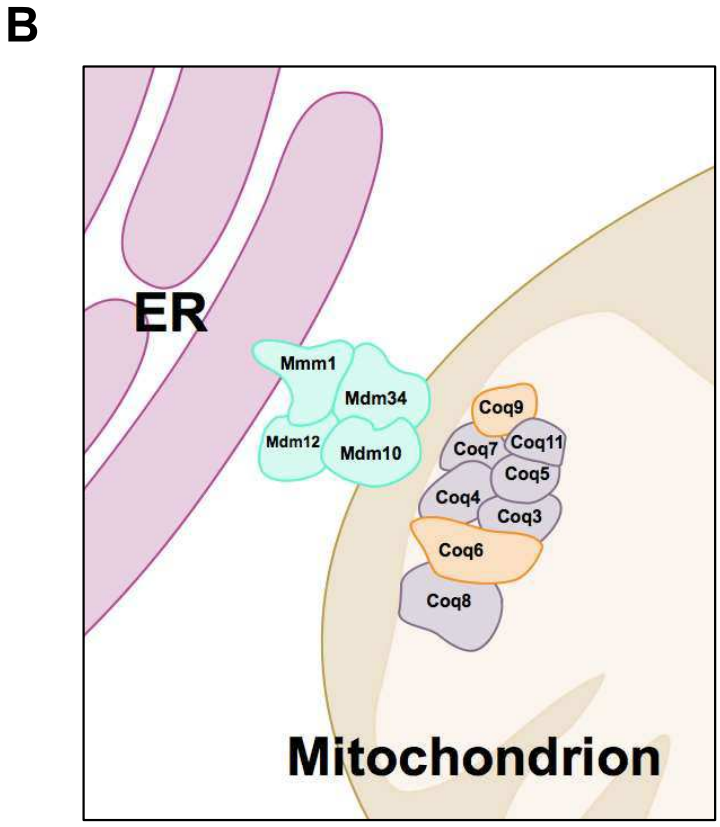
B
ER
Mmm1
Mdm34
Mdm12
Mdm10
Coq9
Coq7
Coq11
Coq5
Coq4
Coq3
Coq6
Coq8
Mitochondrion

Figure 6

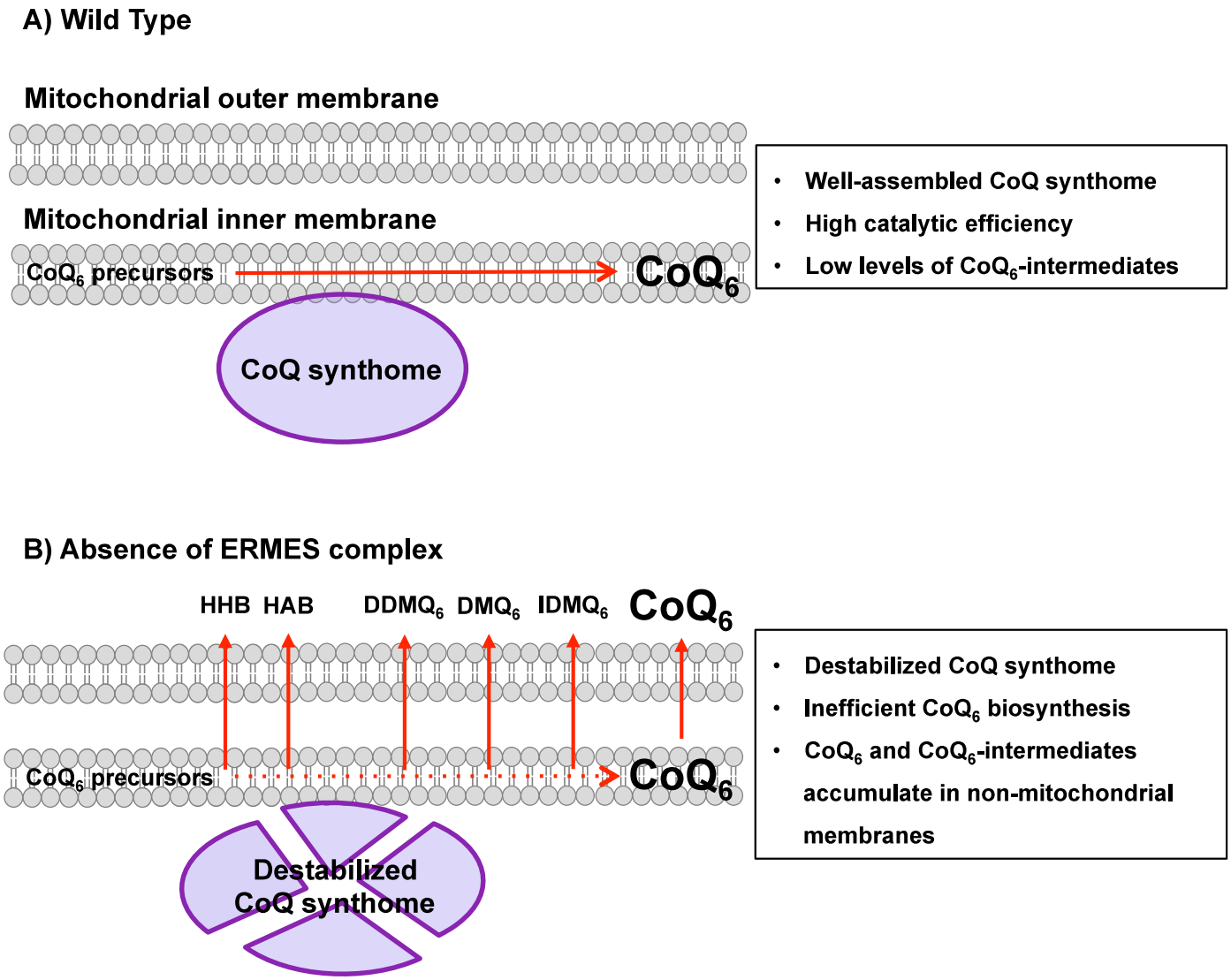
A) Wild Type
Mitochondrial outer membrane
Mitochondrial inner membrane
CoQ6 precursors
CoQ6
CoQ synthome
• Well-assembled CoQ synthome
• High catalytic efficiency
• Low levels of CoQ6-intermediates
B) Absence of ERMES complex
HHB HAB
DDMQ6 DMQ6 IDMQ6
CoQ6
CoQ6 precursors
CoQ6
Destabilized
CoQ synthome
• Destabilized CoQ synthome
• Inefficient CoQ6 biosynthesis
• CoQ6 and CoQ6-intermediates accumulate in non-mitochondrial membranes

Figure S1A

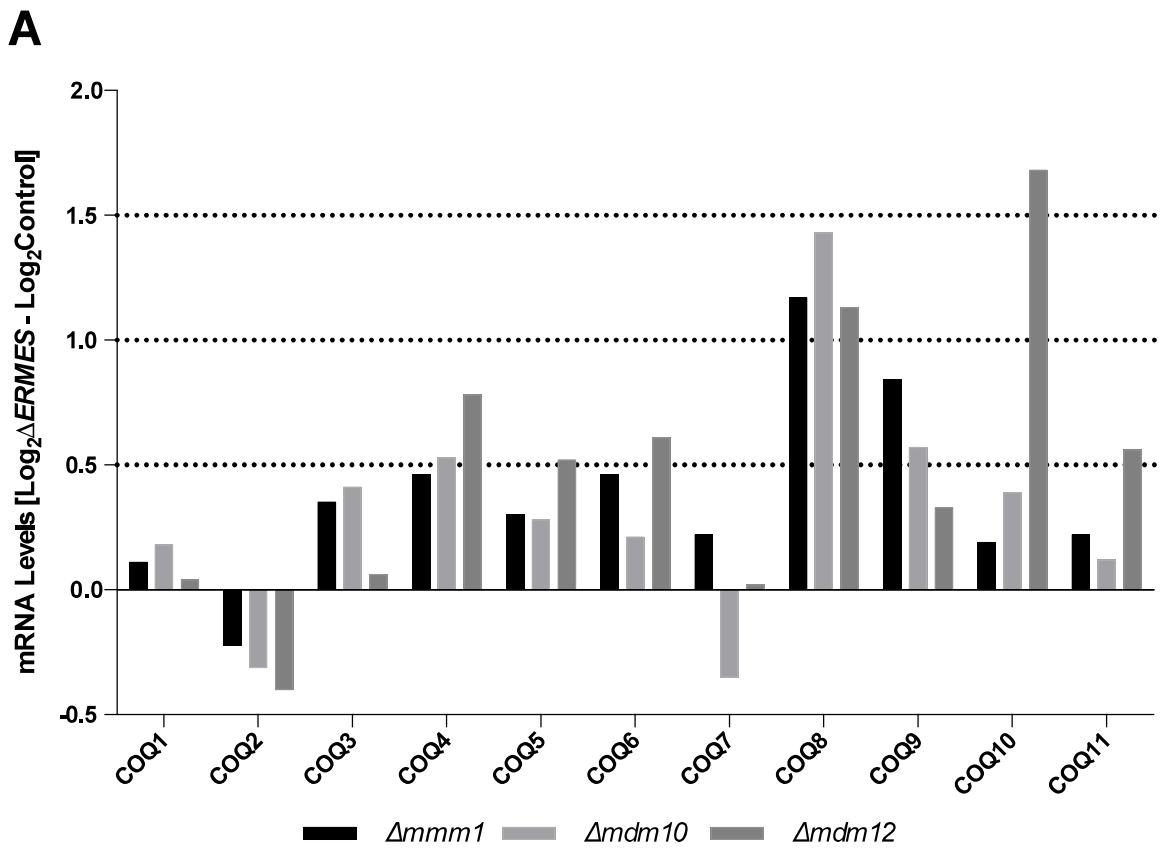
A
2.0
1.5
1.0
0.5
0.0
-0.5
mRNA Levels [Log2ΔERMES - Log2Control]
COQ1
COQ2
COQ3
COQ4
COQ5
COQ6
COQ7
COQ8
COQ9
COQ10
COQ11
Δmmm1
Δmdm10
Δmdm12

Figure S1B

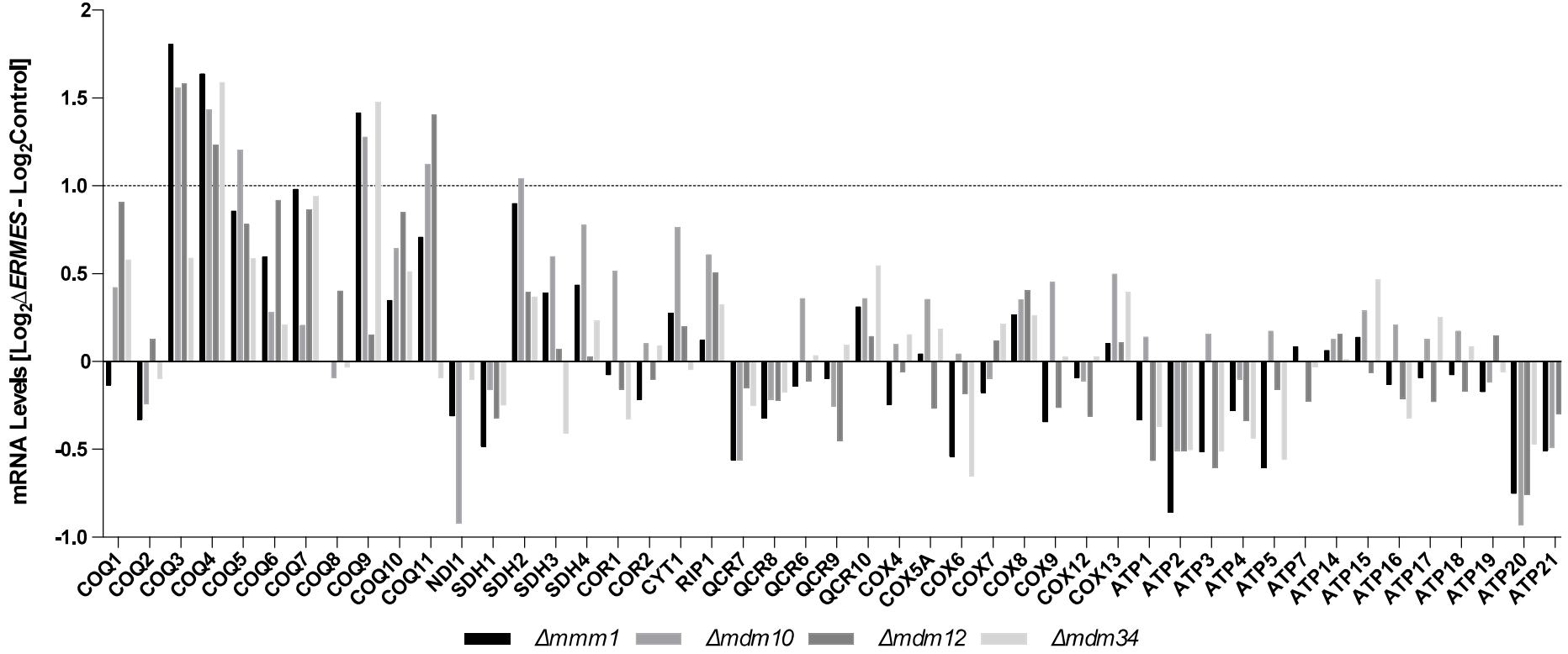
mRNA Levels [Log2ΔERMES - Log2Control]
2
1.5
1.0
0.5
0
-0.5
-1.0
COQ1 COQ2 COQ3 COQ4 COQ5 COQ6 COQ7 COQ8 COQ9 COQ10 COQ11 NDI1 SDH1 SDH2 SDH3 SDH4 COR1 COR2 CYT1 RIP1 QCR7 QCR8 QCR6 QCR9 QCR10 COX4 COX5A COX6 COX7 COX8 COX9 COX12 COX13 ATP1 ATP2 ATP3 ATP4 ATP5 ATP7 ATP14 ATP15 ATP16 ATP17 ATP18 ATP19 ATP20 ATP21
Δmmm1
Δmdm10
Δmdm12
Δmdm34

Figure S1C

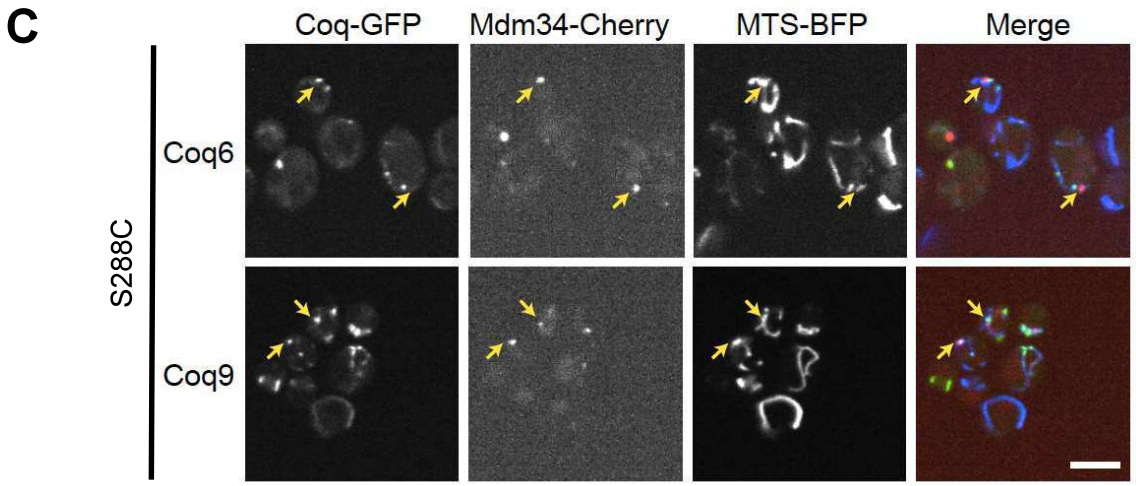

Figure S2

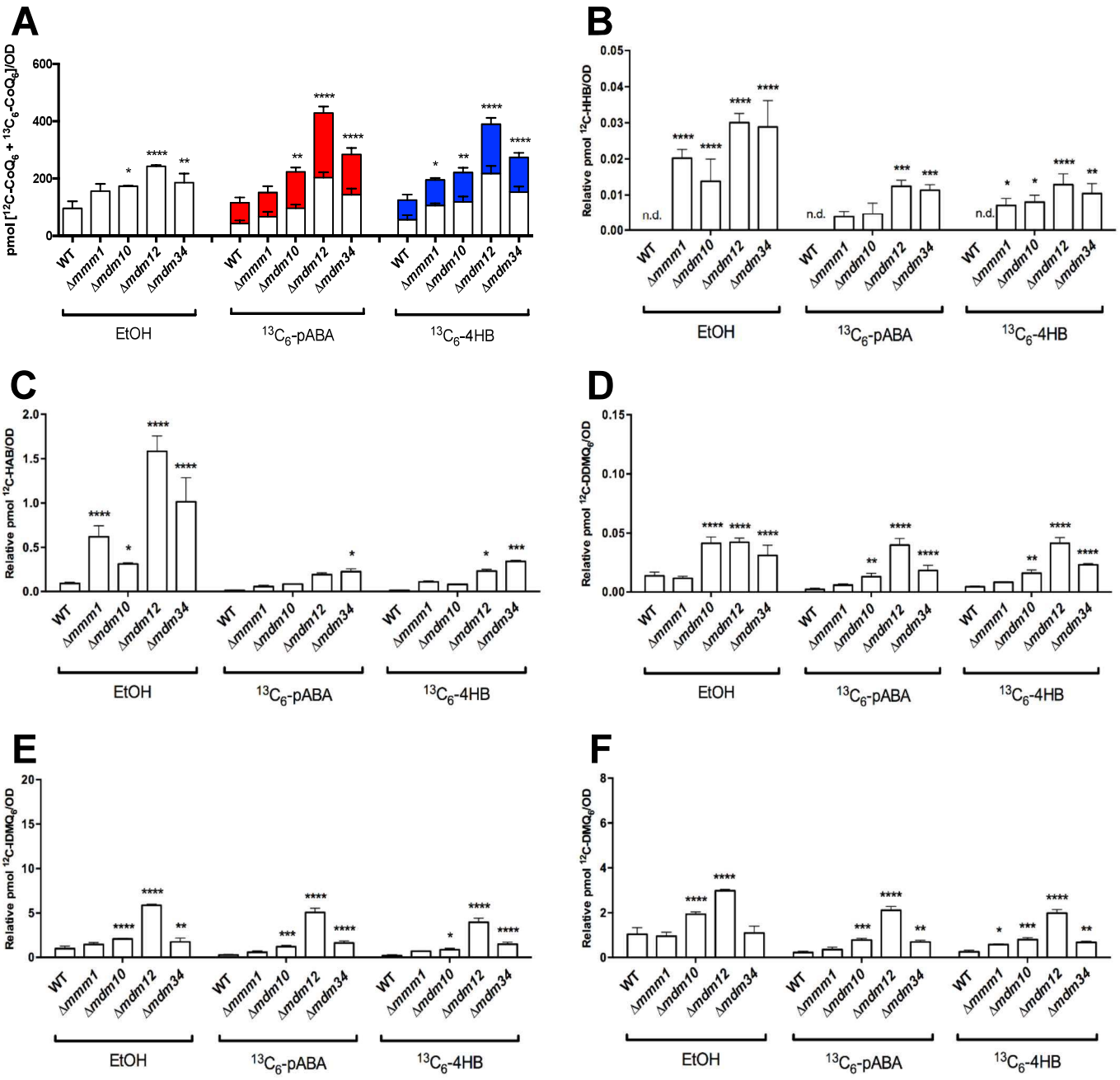
A
pmol [12C-CoQ6 + 13C6-CoQ6]/OD
B
Relative pmol 12C-HHB/OD
n.d.
C
Relative pmol 12C-HAB/OD
D
Relative pmol 12C-DDMQ6/OD
E
Relative pmol 12C-IDMQ6/OD
F
Relative pmol 12C-DMQ6/OD
WT
Δmmm1
Δmdm10
Δmdm12
Δmdm34
EtOH
13C6-pABA
13C6-4HB